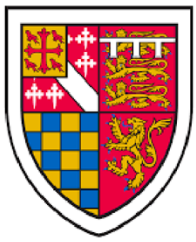
Structural insights into the $GABA_A$ receptor gating cycle

Daniel Mihaylov

This thesis is submitted for the degree of

Doctor of Philosophy

March 2024







MRC Laboratory of Molecular Biology

and

St. Edmund's College, University of Cambridge

Declaration

This thesis is the result of my own work and includes nothing which is the outcome of work done in collaboration except where explicitly specified in the relevant chapters. It is not substantially the same as any work that has already been submitted for any degree or other qualification. It does not exceed the prescribed word limit for the Biology Degree Committee.

Daniel Mihaylov

31 March 2024

Abstract

$GABA_A$ receptors are pentameric ligand-gated ion channels (pLGICs) that control multiple aspects of animal physiology, including the rapid inhibitory neurotransmission within the vertebrate central nervous system. They activate and desensitize in a few milliseconds, which is a crucial requirement for accurate synaptic signalling. Such fast conformational transitions, however, have proven impervious to investigation via conventional structural biology methods. Moreover, $GABA_A$ receptors operate in cellular membranes with diverse lipid compositions and biophysical properties. These are thought to play essential modulatory functions, however, a molecular understanding of such impacts is lacking. As a result, the mechanisms of GABA-ergic signalling, in physiologically meaningful environments and time scales, remain among the most important unknowns in molecular neuroscience.

To address these issues, I first sought to identify optimal reconstitution environments for recombinantly expressed β3 homomeric and synaptic α1β3γ2L $GABA_A$ receptors by testing multiple nanodisc scaffolds and lipid compositions. Subsequently, with the optimal condition established, I proceeded to investigate a series of $GABA_A$ receptor structures bound to β-lactam antibiotics that are postulated to act as open channel pore blockers. Surprisingly, complexes with the penicillin derivative nafcillin suggested that the $GABA_A$ receptor gating motions might include conformations that diverge considerably from the pseudo-symmetric arrangements observed previously.

To test whether the asymmetry observed is physiologically meaningful, and to achieve a comprehensive characterisation of the $GABA_A$ receptor gating cycle, I employed a time-resolved cryo-EM strategy that enables millisecond-scale time delays between agonist application and sample freezing. This approach allowed the visualization of novel and complex asymmetric gating motions involved in the activation and desensitization of the receptor, ranging from side chain to major secondary structure rearrangements. Remarkably, the asymmetric gating cycle is conserved among homomeric and heteromeric $GABA_A$ receptors, with lipids such as cholesterol playing a crucial role in stabilizing the newly formed interfaces. Moreover, these results have further revealed a novel inhibitory mechanism driven by the lipid PIP_2, which directly controls the opening of α1β3 and α1β3γ2L receptors. Lastly, I will also demonstrate how positive allosteric modulators alter

the gating landscape and how the general anaesthetic propofol can directly activate the receptor.

This work provides a new structural and mechanistic framework to explore and interpret the action of pharmacological modulators and to design novel molecules with improved therapeutic properties.

Acknowledgments

First and foremost, I extend my heartfelt gratitude to Radu Aricescu for his unwavering support and countless ideas throughout my PhD journey. Radu's huge passion for science and his pursuit of the unknown have been instrumental in shaping this work.

My special gratitude goes to Nigel Unwin, whose guidance and discussions on pLGICs and lipid environments have been enlightening. I am especially thankful for his introduction to his groundbreaking time-resolved plunger, which forms the cornerstone of this thesis.

I am also grateful to the entire LMB community, particularly my second supervisor, Chris Russo, whose mentorship and encouragement have been invaluable. I am grateful to my university supervisor, Paul Miller, for his insightful scientific discussions and contributions with DNA constructs.

My sincere appreciation extends to all past and present group members: Veronica Chang, Kuni Suzuki, Christos Papantoniou, Anirudh Sharma, Nicolas Kjaer-Jensen, Milena Timcenko and specifically to Vikram Kasaragod, Jonas Miehling and Andrija Sente. Your friendship, scientific insights, shared laughter and shared ‘TC media’ beverages stored in the cold room have made this journey truly memorable. A special mention goes to my dear friend and fellow Bulgarian, Katerina Naydenova, for her unwavering support both in and out of the lab. I am grateful to Ingo Greger for engaging scientific discussions and to Teru Nakagawa for insightful conversations on time-resolved cryo-EM.

Lastly, but most importantly, I express my deepest gratitude to my family –Maia, Bobi, Viki and Lili - for their unwavering support and love. Their presence has been my anchor throughout this journey, and I am forever grateful for their compassion and encouragement.

Table of Contents

Declaration ..... *I*

Abstract ..... *II*

Acknowledgments ..... *IV*

Chapter I - Introduction *1*

1.1 Historic overview and architecture of the pentameric ligand-gated ion channels **3**

1.2 The diversity of human $GABA_A$ receptors **5**

1.3 The gating cycle of non-$GABA_A$ pLGIC family members **6**

1.4 Current overview of the $GABA_A$ receptor gating cycle **9**

1.5 Pharmacological modulation of the $GABA_A$ receptor **11**

1.6 Aims of this thesis **13**

Chapter II - Materials and Methods *15*

2.1 Molecular biology **17**

2.2 Protein production and purification **17**

2.2.2 Mammalian protein production in cell pools 17

2.2.3 Transient mammalian protein production 18

2.2.4 MSP2N2 purification 18

2.2.5 Saposin A purification 19

2.2.6 Generation of 1D4 beads 19

2.2.7 $GABA_A$ receptor purification and reconstitution into lipid nanodisc 20

2.2.8 Megabody (Mb) and nanobody (Nb) purification 21

2.3 Lipid solubilization and extraction **22**

2.3.1 Lipid solubilization 22

2.3.2 Extraction of lipids from nanodisc samples 22

2.3.3 Cholesterol content measurement 23

2.3.4 Mass spectrometry analysis of the nanodisc lipids 23

2.4 Electron Microscopy **23**

2.4.1 Cryo-EM sample preparation using commercial plungers 23

2.4.2 Cryo-EM sample preparation with a time-resolved plunger 24

2.4.3 Cryo-EM data collection 24

2.4.4 Cryo-EM image processing 24

2.4.5 Model building and refinement 25

Chapter III - The environment of the reconstituted $GABA_A$ receptor *27*

3.1 Introduction **29**

3.2 The functional impact of nanobody-derived fiducials **29**

3.3 The structural impact of nanodisc scaffolds **32**

3.3.1 The Saposin A scaffold 32

3.3.2 The $GABA_A$ receptor in SMA lipid nanodiscs 34
3.4 The impact of nanodisc thickness 36
3.5 The influence of cholesterol on the nanodisc 38
3.6 Discussion 43
Chapter IV - Inhibition of synaptic $GABA_A$ receptors by β-lactam antibiotics 45
4.1 Introduction 47
4.2 Mechanism of $GABA_A$ receptor inhibition by PenG and PenV co-applied with GABA 49
4.3 Differential blocking properties of piperacillin 50
4.4 Nafcillin is a multi-site allosteric modulator of the α1β3γ2L $GABA_A$ receptor 51
4.5 Discussion 54
Chapter V - Structural dynamics of $GABA_A$ receptor gating on the millisecond timescale 59
5.1 Introduction 61
5.2 Experimental setup and considerations 63
5.3 The β3 homomeric $GABA_A$ receptor gates through asymmetric short-lived intermediate states 66
5.4 The β3γ2 diheteromer gating motion 73
5.5 PIP_2 controls the opening of full-length α1β3 and α1β3γ2 receptors 76
5.6 α1β3 receptors gate via two branches 81
5.7 Positive allosteric modulators and general anaesthetics may tune α1β3 $GABA_A$ receptors by branch selection 90
Chapter VI - Conclusion and outlook 93
6.1 Conclusion 95
6.2 Outlook and future directions 98
6.2.1 The gating cycle of triheteromeric receptors 98
6.2.2 Allosteric modulation of triheteromeric receptors 99
6.2.3 The mechanism of $GABA_A$ receptor deactivation 101
6.2.4 Updated model for $GABA_A$ receptor gating 103
References 105
Appendix 123

Chapter I

Introduction

1.1 Historic overview and architecture of the pentameric ligand-gated ion channels

The central nervous system (CNS) operates through a delicate balance between excitatory and inhibitory neurotransmission. In vertebrates, synaptic γ-aminobutyric acid type A receptors ($GABA_A$ receptors) mediate the vast majority of inhibitory signalling on the millisecond timescale. Upon binding the neurotransmitter GABA, these receptors open chloride-permeable channels, inducing neuronal hyperpolarization and diminishing the impact of excitatory signals (Mody and Pearce, 2004, Sieghart, 2006). Additionally, $GABA_A$ receptors extend beyond the confines of the synapse and can also be found in the extrasynaptic space. There, they facilitate tonic inhibition and regulate neuronal activity through sustained background GABA signalling resulting from agonist spillover from the synaptic cleft (Hannan et al., 2020). In the CNS, $GABA_A$ receptors play a crucial role in information processing and memory formation. It has been shown that the miniature inhibitory postsynaptic currents (mIPSC) amplitude rapidly increases after training, indicating that during memory encoding the $GABA_A$ receptor inhibitory synapse is strengthened (Sakimoto et al., 2019). The molecular mechanism for this has been shown to stem from prolonged exposure of the receptor to agonist which desensitizes it. This in turn leads to an increase in receptor density on the postsynaptic membrane and this recruitment is induced by the phosphorylation of the receptor's intracellular domain after desensitization (Field et al., 2021). Interestingly, $GABA_A$ receptors are also expressed outside the CNS. For example, the receptor can also be found in the endocrine pancreas (Rorsman et al., 1989) where GABA signalling induces membrane hyperpolarization of the α cells that suppresses glucagon secretion (Xu et al., 2006), and membrane depolarization in β cells that increases insulin secretion (Soltani et al., 2011). Furthermore, $GABA_A$ receptors can also be found on the membranes of $CD8^+$ T killer cells and activation of the receptor obstructs the T cell response (Zhang et al., 2021a). Hence, these receptors embody a widely distributed signalling mechanism that controls multiple physiological processes.

$GABA_A$ receptors belong to the pentameric ligand-gated ion channels (pLGICs). Generally, pLGICs can be categorized into two classes—cation-selective or anion-selective. Cation-selective channels, permeable to Na^+ or Ca^{2+} ions play a crucial role in depolarizing i.e. exciting neurons. The vertebrate family includes nACh receptors (Unwin, 2005), 5-hydroxytryptamine receptors (Pithadia and Jain, 2009), and zinc-activated cation channels (Davies et al., 2003). Conversely, anion-selective channels hyperpolarize the neurons by the influx of Cl^- down their electrochemical gradient, with $GABA_A$ receptors and glycine

receptors being members of the vertebrate family (Grenningloh et al., 1987). Unlike their cationic counterparts, $GABA_A$ receptors are less selective for the ion that flows upon opening. For example, $GABA_A$ receptors are also permeable to HCO_3^- with a permeability ratio of HCO_3^-/Cl^- in the range of 0.2 to 0.4 (Kaila et al., 1997).

What is more, pLGICs are present in different organisms. In insects, the $GABA_A$ receptor homologue RDL is expressed in the mushroom bodies and plays a critical role in memory acquisition and stability (Liu et al., 2007). Additionally, pLGICs can be found in prokaryotes, exemplified by the *Erwinia* ligand-gated ion channel (ELIC) and the *Gloebacter* ligand-gated ion channel (GLIC) (Miller and Smart, 2010). Nematodes also feature family members, such as the *Caenorhabditis elegans* glutamate-activated chloride channel (GluCl) which controls locomotion and feeding (Bidaut, 1980, Wolstenholme, 2012).

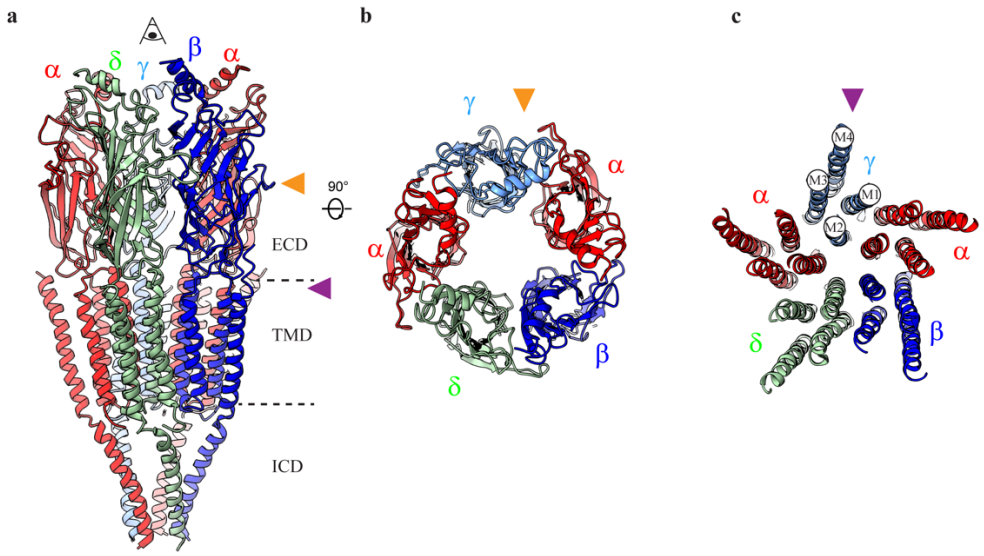


Figure 1.1 – Overall architecture of the pLGIC family

a) *Overall architecture of the receptor highlighting the immunoglobulin-like β-sandwich fold of the ECD, the alpha-helical TMD as well as the intracellular domain.* ***b)*** *The ECD domain viewed from above highlighting the pseudo five-fold symmetry of the channel.* ***c)*** *The TMD bundles form the pore with the M2 residues lining the lumen. Four helices named M1-M4 comprise the domain of one subunit. The figures were generate from PDB: 2BG9 (Unwin, 2005).*

From a structural perspective, the *Torpedo* nACh receptor is the prototypical family member and pioneering studies revealed the channel's overall architecture. The agonist binding site is located 30Å away from the membrane whereas clearly identifiable rods assigned as transmembrane helix 2 span the lipid bilayer forming the wall that lines the pore (Unwin,

1993, Unwin, 1996). Later on in 2005, the first high resolution structure of the *Torpedo* nACh receptor was reported (Unwin, 2005). This study revealed that pLGICs are comprised of five subunits arranged pseudo-symmetrically around a central pore. Each subunit consists of three domains - an extracellular domain (ECD) made of a short N-terminal α helix absent in prokaryotic receptors followed by a ten-strand β sandwich core (Fig. 1.1a-b), a transmembrane domain (TMD) composed of four transmembrane segments (M1-M4) that fold into alpha helices, organized in a conserved bundle, with M2 crucial for the formation of the pore (Fig. 1.1a,c) as well as an intracellular domain (ICD), which is absent in prokaryotic pLGICs (Fig. 1.1a) .

This architecture was later confirmed to be conserved among other family members when crystal structures of ELIC, GLIC, and GluCl emerged (Hilf and Dutzler, 2008, Bocquet et al., 2009, Hibbs and Gouaux, 2011). In 2014, the first crystal structure of the β3 homomeric $GABA_A$ receptor provided additional evidence for the conserved structural features across the family (Miller and Aricescu, 2014).

1.2 The diversity of human $GABA_A$ receptors

The human genome encodes 19 different $GABA_A$ receptors subunits – namely α1-6, β1-3, γ1-3, δ, ε, θ, π, ρ1-3 (Fig. 1.2) (Sigel and Steinmann, 2012). Receptor ensembles containing different subunit types have distinct kinetic properties, pharmacology and cellular locations. In general, neuronal $GABA_A$ receptors can be divided broadly into two classes – synaptic i.e. those that are localized at inhibitory synapses and extrasynaptic that can be found in somatic, dendritic and axonic regions. For example, receptors containing α1-3, β2-3 and γ2 subunits are clustered on post-synaptic membranes thus directly facing the neurotransmitter release sites (Nusser et al., 1998). Such receptors have low GABA affinity but activate much quicker than their extrasynaptic counterparts which are mostly composed of α4, α6, β3 and δ subunits (Wisden et al., 1992, Farrant and Nusser, 2005). Moreover, α1β3 and α1β3δ receptors are also considered to be extrasynaptic (Smart, 1992, Brickley and Mody, 2012) highlighting the importance of the γ subunit for synaptic localization. The mechanism of synaptic anchoring was recently identified and is mediated by the interaction between γ2 subunits and the auxiliary protein GARLH4 (LH4) (Han et al., 2021). LH4 in turn binds to Neuroligin-2 whose extracellular domain binds the presynaptic neurexins thus forming a trans-synaptic nanocolumn (Craig and Kang, 2007). Moreover, α1-2 subunits also contribute to synaptic anchoring by interacting with the cytoskeletal proteins gephyrin and

collybistin, albeit to a lesser extent due to the low binding affinity between these proteins (Papadopoulos and Soykan, 2011). Historically, heteromeric receptors were believed to assemble from two α subunits, two β subunits and a fifth subunit usually γ or δ (Sigel and Steinmann, 2012). Recently, however, several studies have shown that the combination of receptor subunits in the mouse brain that can be part of the obligatory pentamer can be much higher than anticipated with different α subunits forming tetraheteromers (Sun et al., 2023) or different numbers of β subunits ranging from two to four being incorporated in the heteropentamer *in vitro* (Sente et al., 2022). This is dictated by the relative subunit amounts available during assembly as well as the strength of the interfaces between the subunits present. Crucially, most neuron types express a considerable number of subunits which suggests the possibility that neuronal surfaces may simultaneously display a diverse population of receptors. What is more, $GABA_A$ receptor-specific chaperons such as Clptm1 also play a critical role in the assembly pathways (Ge et al., 2018). Such complex networks may therefore be important for the evolution of neuronal circuits and be determinants of behaviour.

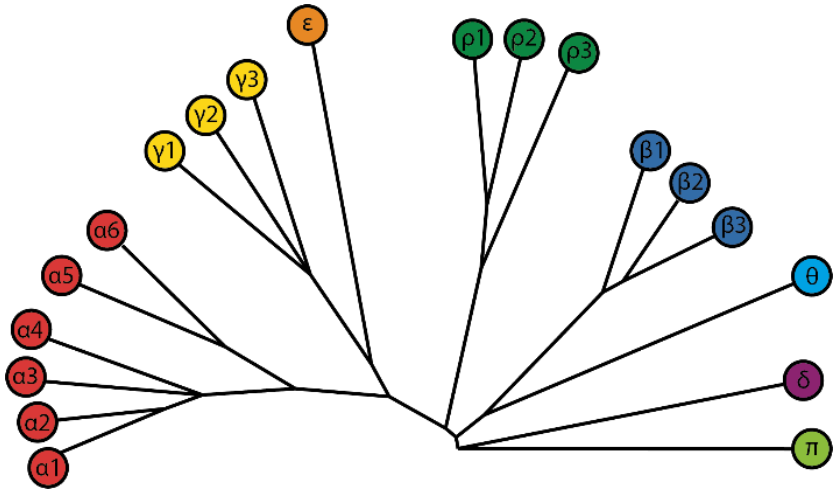


Figure 1.2 – Phylogenetic tree of the 19 different $GABA_A$ receptor subunit types

The phylogenetic tree of the 19 different $GABA_A$ subunits. Adapted from (Sigel and Steinmann, 2012)

1.3 The gating cycle of non-$GABA_A$ pLGIC family members

The intrinsic characteristic shared by all pLGICs is their fast activation upon agonist binding, coupled with a rapid desensitization. The speed of such transitions is pivotal for precise synaptic signalling and effective information processing. The entire sequence of motions from resting to open to desensitized is collectively termed gating and typically unfolds

within the millisecond to second range, depending on the specific agonists and receptor subtypes involved.

For example, the α7 nAChR desensitizes in just 90ms (McCormack et al., 2010), while the GlyR takes approximately 500 milliseconds to desensitize (Yu et al., 2021, Legendre et al., 2002). In contrast, the bacterial GLIC desensitizes a little bit slower in roughly 1 s (Gonzalez-Gutierrez et al., 2017, Velisetty and Chakrapani, 2012), while ELIC is the slowest member of the family and desensitizes in approximately 4 s (Laha et al., 2013). Following desensitization, only small fractions of the receptors open to generate steady-state currents.

Therefore, it is unrealistic to expect a large proportion of the receptors to be in an active (i.e., open) state after prolonged ligand incubations that are several orders of magnitude longer than the time required for desensitization to occur. Surprisingly, however, structural studies on the same receptors have shown marked disparities when compared to the electrophysiology recordings. For example, GLIC and GluCl have been crystallized in supposedly open conformations despite the fact that agonists were applied to the receptor for days during crystallization (Hilf and Dutzler, 2009, Bocquet et al., 2009, Hibbs and Gouaux, 2011). For the α7 nAChR, which is the fastest member of the family, an open state has been postulated when ligand application was performed on the hour timescale (Noviello et al., 2021). For the homomeric GlyR, a more time-controlled approach was undertaken where ligand application was limited to 10s (Yu et al., 2021). This, however, is still 20 times longer than the rate of desensitization. In this cryo-EM study, roughly half of the receptors were reported in an apparent open state, with only 20% in a desensitized state. Moreover, an expanded open state was observed in 25% of all particles, deemed non-physiological by the authors.

Taken together, a distinct discrepancy emerges between the structural and functional aspects of the gating cycle in pLGICs. This disparity can be attributed to the non-physiological conditions imposed on the receptors during the aforementioned structural studies. Notably, the structural elucidation of GLIC and ELIC involved the use of detergent micelles, a methodology prone to introducing artifacts and disrupting the coupling between the extracellular and transmembrane domains. This is highlighted in two crystal structures of ELIC in the absence and presence of agonist (Gonzalez-Gutierrez et al., 2012, Zimmermann and Dutzler, 2011). While electron density indicative of agonist was present in the ELIC agonist binding pockets, no structural rearrangements were observed in the TMD. This

finding suggests that while agonist interaction occurs, it does not lead to significant alterations in the structural configuration of the TMD pore suggesting that ECD and TMD are uncoupled in this environment. Similar artifacts induced by detergents have also been observed in the reconstitution of the $GABA_A$ receptor within detergent micelles, resulting in the collapse of the entire transmembrane domain (Phulera et al., 2018, Zhu et al., 2018). This challenge was successfully addressed through the utilization of nanodiscs, which create a native-like lipid environment surrounding the receptor's TMD (Laverty et al., 2019, Masiulis et al., 2019, Kim et al., 2020).

The decoupling of the receptor can be attributed to the loss of crucial lipids during the solubilization process. As demonstrated in the case of nAChR, optimal membrane fluidity, measured by the steady-state anisotropy of membrane probes, is essential for the transition between resting and agonist-bound states (Fong and McNamee, 1986, Criado et al., 1982). Notably, studies have revealed that receptors reconstituted in membranes containing both cholesterol and negatively charged phospholipids exhibit gating motions. In contrast, receptors in membranes lacking cholesterol, although capable of binding agonist, fail to gate (Hamouda et al., 2006). This underscores the pivotal role of the membrane environment in governing the gating dynamics of the receptor.

Moreover, the α7 nAChR and homomeric GlyR supposed open states were investigated in the context of Saposin A nanodiscs and SMALPs, which mimic the physiological environment more closely than the harsh detergent micelles and suggest that the open state is symmetric (Dörr et al., 2016, Flayhan et al., 2018, Sigel and Steinmann, 2012, Noviello et al., 2021, Yu et al., 2021). Significantly, it is worth noting that other pLGICs including the heteromeric Gly receptor in detergent micelles and the 5HT3a receptor in Saposin A nanodiscs, have been proposed to undergo asymmetric gating in contrast to the aforementioned studies (Liu and Wang, 2023, Zhang et al., 2021b). Nevertheless, it is crucial to highlight that the emergence of these symmetric and asymmetric intermediate states occurs on the hour timescale, likely not faithfully representing the dynamics within an *in vivo* context. Taken together, the gating kinetics of all these studies are inconsistent with electrophysiological recordings. I will demonstrate that these environments do not adequately support the faithful representation of receptor gating dynamics, leading to the collapse of the receptor's transmembrane region, and discuss the most optimal method for reconstituting the receptor in a physiologically meaningful context.

Insights from single-channel electrophysiology recordings have unveiled the existence of multiple short-lived closed, open and desensitized states of different duration during a receptor's gating cycle (Elenes and Auerbach, 2002, Mortensen et al., 2004, Kasaragod et al., 2022, Bianchi et al., 2007). A complete structural overview of these transitions, however, is currently lacking due to the fast nature of gating. Nonetheless, several studies conducted in a native environment while also mirroring *in vivo* agonist stimulation timescales, have unveiled a remarkable phenomenon. Despite the symmetric or pseudo-symmetric nature of pLGICs in their resting states, gating appears to proceed through asymmetric motions. In pioneering investigations, it was revealed that the *Torpedo* nAChR, upon exposure to a 5-ms ligand application, triggers the β subunit to move away from the pore, thereby perturbing the symmetry of the channel leading to the emergence of an asymmetric intermediate (Unwin and Fujiyoshi, 2012, Unwin, 1995). This observation also appears to extend to the homopentameric ELIC. ^{19}F-NMR on the millisecond to second timescale has suggested that the channel exhibits multiple conformations within a given functional state, and the transitions between these functional states are orchestrated through asymmetry (Kinde et al., 2015).

1.4 Current overview of the $GABA_A$ receptor gating cycle

Virtually all pentameric ligand-gated ion channels initiate their gating cycle through a common motion—the binding of the agonist to the extracellular orthosteric binding site. This holds true even for the soluble AChBP, where agonist binding triggers the closure of loop C and the capping of the bound ligand (Hansen et al., 2005, Brejc et al., 2001). Similar mechanisms of agonist binding are observed in the structures of other pLGICs, including the Gly and nACh receptors, and this pattern extends to the $GABA_A$ receptors as well.

In the case of $GABA_A$, only two states of the gating cycle have been structurally characterized thus far—the resting-like state with the antagonist bicuculine and the desensitized state bound to GABA or a combination of GABA and general anaesthetics or benzodiazepines (Laverty et al., 2019, Masiulis et al., 2019, Kim et al., 2020). Structural studies on both the canonical resting state and the canonical desensitized state with GABA alone, undertaken by me, revealed consistent overall quaternary motion with the antagonist-bound resting state and the desensitized state.

In the deep desensitized state i.e. the long-lived desensitized state, densities for GABA can be identified below loop C at the $\beta3^+/\alpha1^-$ interfaces. The closure of loop C results in an

overall counter-clockwise rotation of the entire extracellular domain as viewed from the extracellular region, forming an iris-like constriction as it transitions into the deep-desensitized, a motion termed ‘unblooming’ (Fig. 1.3a,d) (Changeux, 2014). The structural impact of GABA binding extends to the transmembrane domain, with conformational changes in the ECD transmitted through the M2-M3 loop—a critical element in the conformational wave of all pLGICs (Fig. 1.3e) (Bouzat, 2012, Bera et al., 2002, Lee et al., 2009, Changeux, 2014, Grosman et al., 2000). Consequently, the TMD subunits rotate clockwise and drift outward, significantly affecting the activation gate where all 9’ Leu turn clockwise away from the pore and towards the inter-subunit space (Fig. 1.3b). This rearrangement is reflected in the pore profile, with the 9’ gate widely open in the desensitized state, the -2’ gate closing further, with the entire pore constricting to form a shallower slope (Fig. 1.3c).

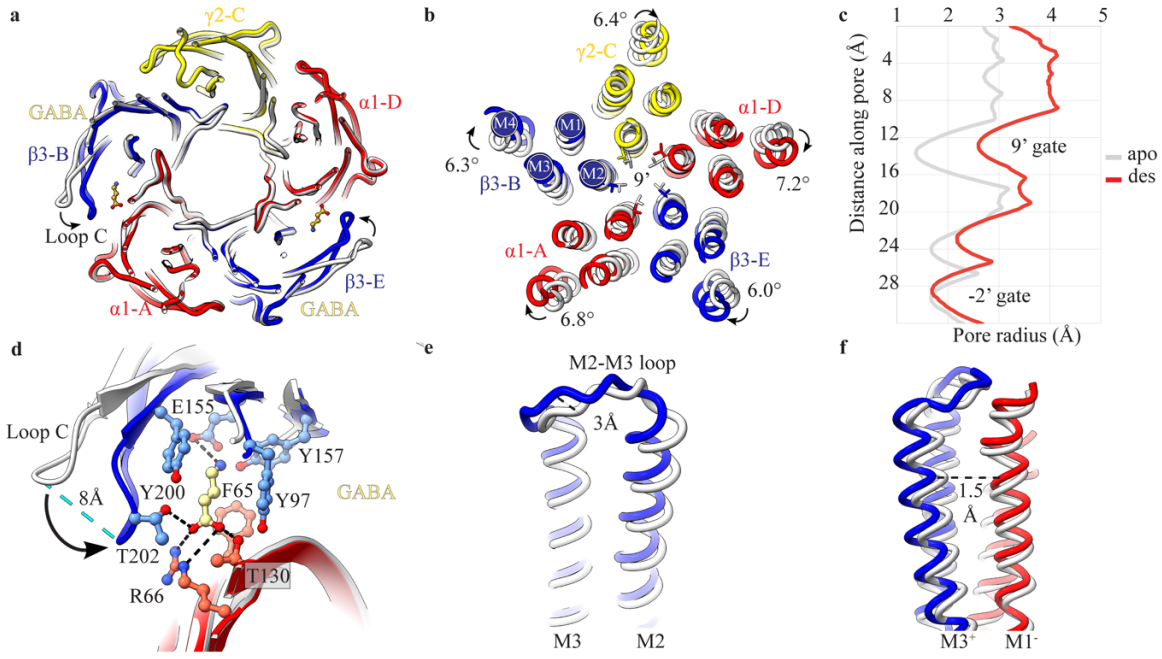


Figure 1.3 – Resting versus desensitized states of the GABA$_A$ receptor

The structural rearrangement in the ECD of the apo (grey) and desensitized (coloured) state. ***a)*** *GABA binding under loop C leads to the closure of the ECD and an overall anti-clockwise motion.* ***b)*** *The conformational change in the TMD, where 9’ Leucine gate rotates away from the pore and an overall clockwise motion takes place.* ***c)*** *Pore profile comparing the apo and desensitized state highlighting the opening of the 9’ activation gate during desensitization. Conformational change upon GABA binding in* ***d)*** *loop C,* ***e)*** *M2-M3 loop and* ***f)*** *the TMD subunit interface.*

Comparing the apo versus the deep desensitized states reveals distinct differences. GABA binding initiates the closure of loop C and the unblooming of the ECD (Fig. 1.3d), translating

these changes to the TMD region. Notably, loop C moves by 8Å upon GABA binding. Loop C is a flexible region of the receptor and can adopt many different conformations in the resting state. Thus, the presence of GABA only stabilizes one of the conformations of the loop by binding in an aromatic cage as well as by forming a critical hydrogen bond network (Fig. 1.3d). The M2-M3 loop on the other hand plays a pivotal role in stabilizing both the resting and desensitized states and in facilitating communication between the ECD and TMD (Fig. 1.3e). The distances between adjacent subunit TMD interfaces also increases by roughly 1.5Å after desensitization and the TMD bundles of the individual subunits all rotate clockwise by 6 to 7 degrees (Fig. 1.3f). However, these states represent only the endpoints of the gating cycle, with no available structural information on the mechanisms underlying receptor activation and desensitization. The reason for this is that $GABA_A$ receptors, just like the other members of the family, desensitize quickly. Depending on the assembly of choice, the rate at which the receptor will desensitize will differ – for example the $\alpha1\beta2\gamma2$ and $\alpha1\beta3\gamma2$ triheteromer will desensitize in roughly 200ms whereas the $\alpha3\beta2\gamma2$ subtype in 650ms (Barberis et al., 2007). Nevertheless, this is still much faster than what can be captured by conventional structural biology techniques. For this to be overcome, a time-resolved structural approach on the millisecond timescale is required.

1.5 Pharmacological modulation of the $GABA_A$ receptor

$GABA_A$ receptors serve as targets for a diverse array of allosteric modulators. Positive allosteric modulators (PAMs) like the classical benzodiazepines (BZDs), including diazepam (Valium) and alprazolam (Xanax), are effective in treating conditions such as anxiety, epilepsy, and sleep disorders (Sieghart and Savić, 2018). BZDs modulate synaptic $GABA_A$ receptors by binding to the α^+/γ^- extracellular domain interface below loop C (Masiulis et al., 2019). Crucially, only the synaptic α1-3,5 subunits at the principal position with a γ2 subunit in the complementary position are susceptible to classical BZD targeting (Lüscher et al., 2012). This specificity is facilitated by a conserved His residue contributed by the α subunit (in the case of the human α1 His102), crucial for ligand stabilization (Masiulis et al., 2019, Wieland et al., 1992). Notably, the α4 and α6 subunits feature a substituted Arg in place of this conserved His, rendering them impervious to classic BZD binding (Rudolph and Möhler, 2004). The γ subunit is also critical for the specificity of BZD binding as $\alpha1\beta3\delta$ receptors are not modulated by classical BZDs (Sigel and Steinmann, 2012).

Interestingly BZDs can also function as negative allosteric modulators. One such example is the partial inverse agonist Ro15-4513 which shifts the GABA EC_{50} to the right (Sente et al., 2022). This ligand binds the same pocket as diazepam; however, has a contrasting effect on the receptor. Furthermore, flumazenil is a benzodiazepine pocket neutral antagonist i.e. has no effect on GABA EC_{50} and can be used for the treatment of benzodiazepine overdose. Interestingly, flumazenil also binds the benzodiazepine pocket with a similar mode to that of Valium or Xanax but notably has a different function. Flumazenil binding, however, does not lead to any major conformational changes in the receptor compared to the desensitized state with e.g. GABA and alprazolam (Phulera et al., 2018, Masiulis et al., 2019, Kim et al., 2020, Kasaragod et al., 2023). It is therefore unclear how these ligands can bind to the same pocket with a similar pose but have contrasting effects on the receptor and GABA action. A plausible explanation is that they can interfere with the receptor during its gating cycle and stabilize or destabilize particular conformations.

Additional PAMs have been identified to engage with other receptor ensembles as well. For instance, histamine (HSM) binds to the $\beta3^{+}/\beta3^{-}$ interface and potentiates the $\alpha1\beta3$ diheteromer and $\alpha4\beta3\delta$ triheteromer (Kasaragod et al., 2022, Sente et al., 2022). Co-application of HSM with GABA results in an increase in current amplitude. However, no discernible conformational changes have been established between the histamine-bound and histamine-free desensitized states. Consequently, the precise structural mechanism by which histamine modulates the receptor remains unclear.

Another important class of modulators are the general anaesthetics, which can function as both potent allosteric modulators as well as agonists (Martin and Lowery, 2018, Thompson et al., 1996). For example, in the case of propofol, several major effects on the receptor can be observed – firstly, low levels of propofol can potentiate the opening of the receptor at 3μM GABA concentration which is less than the concentration of GABA during synaptic vesicle release (Orser et al., 1998). Secondly, propofol at higher concentration can directly activate the receptor without the need for GABA to be present (Orser et al., 1998, Mozrzymas et al., 2003b). This is also true for other general anaesthetics such as etomidate (Guitchounts et al., 2012, Liao et al., 2019). Thus, general anaesthetics can serve a dual role of both agonists and PAMs. Lastly, the desensitization and deactivation of the receptor are also slowed down (Bai et al., 1999b). Recent structural studies have elucidated the binding sites of propofol and etomidate, however, the study was performed on receptors pre-incubated with GABA thus only showing how anaesthetics bind the deep-desensitized state

(Kim et al., 2020). Therefore, how anaesthetics structurally modulate the receptor and are capable of directly activating it is as of yet unclear.

The expansive allosteric landscape within the $GABA_A$ receptor family, however, renders it a potent off-target for noncompetitive antagonists, a characteristic that may introduce undesired and unpredictable side effects (Olsen, 2018, Cascio, 2006). Among such antagonists are the β-lactam antibiotics, a class of molecules linked to myoclonic jerks and seizures in clinical studies (Meyer, 2014, Sugimoto et al., 2003, Man and Fu, 2015). While the neurotoxicity of β-lactam antibiotics has been known for close to a century, a comprehensive structural understanding of the mechanisms behind these adverse side effects is currently missing (Walker et al., 1945). Nevertheless, it has been shown that penicillin G, a member of the β-lactam antibiotics, competes with picrotoxin for binding inside the channel's pore therefore likely playing the role of a pore blocker (Krishek et al., 1996, Bali and Akabas, 2007). The exact mechanism for this block, however, remains unclear.

1.6 Aims of this thesis

In this thesis I will describe my attempts to address the unknowns mentioned above.

Aim 1 – The optimal environment for reconstituting recombinant $GABA_A$ receptors

Our current understanding of the structure of pLGICs has increased exponentially following several breakthroughs, including the structure of the *Torpedo* nAChR in its native membrane and exposed to ligand in physiologically meaningful timescales (Unwin, 2005, Unwin and Fujiyoshi, 2012). This in part was facilitated by the abundance of the receptor in the electrical organ of the stingray. $GABA_A$ receptors lack tissue sources with abundant protein expression, thus studying them requires purification and *in vitro* reconstitution. However, this approach involves detergent-solubilization, which, as demonstrated in GLIC, ELIC, and GluCl, can damage the receptor and lead to the uncoupling of the TMD and ECD. Recent efforts have involved reconstituting pLGICs into nanodiscs to better mimic the physiological membrane. Despite these advancements, the obtained structures of the GlyR in SMALPs and the α7 nAChR in Saposin A nanodiscs diverged from the established gating kinetics observed through electrophysiological recordings (Noviello et al., 2021, Yu et al., 2021). Establishing an *in vitro* reconstitution method that authentically replicates the native membrane is therefore crucial. My investigation will focus on determining a physiologically relevant environment for reconstituting $GABA_A$ receptors.

Aim 2 – The mechanism of inhibition of synaptic $GABA_A$ receptors by β-lactam antibiotics

After establishing the *in vitro* environment that most closely mimics the physiological membrane, my investigation will delve deeper into elucidating the mechanism of neurotoxicity of β-lactam antibiotics. I aim to provide detailed insights into the binding modes of these antibiotics within the pore of the channel and to address how these molecules can interfere with the gating of the receptor.

Aim 3 – Illuminating the millisecond structural dynamics of $GABA_A$ receptor gating

The $GABA_A$ receptor undergoes activation and desensitization within a few milliseconds, a critical requirement for precise synaptic signalling. However, these rapid conformational transitions have proven challenging to investigate using conventional structural biology methods. To address this issue, I will employ the time-resolved cryo-EM strategy introduced by Berriman and Unwin in 1994 (Berriman and Unwin, 1994). Through this methodology, I aim to characterize the dynamic motions involved in the activation and desensitization of homomeric and heteromeric receptors with a temporal resolution of less than 10 milliseconds. I will also aim to demonstrate how positive allosteric modulators such as histamine alter the structural landscape of gating and how the general anaesthetic propofol can directly activate the receptor.

Chapter II

Materials and Methods

2.1 Molecular biology

All $GABA_A$ constructs used in this thesis, except those used by collaborators to generate stable cell lines, were synthesized as double-stranded cDNAs at Integrated DNA Technologies (https://eu.idtdna.com/). The genes were digested with the restriction enzyme of choice and cloned into the pHL vector for transient expression or pHR vector for lentiviral transduction, respectively (Aricescu et al., 2006, Elegheert et al., 2018). The translated sequences of all cDNA constructs used for this work are listed in the Appendix.

2.2 Protein production and purification

2.2.1 Protein production in stable HEK293S cell lines

The full-length human $GABA_A$ receptor variants α1β3γ2L and α1β3 were produced by using previously published cell lines provided by Keith Miller, Harvard Medical School (Dostalova et al., 2014, Dostalova et al., 2010). The cells were grown and proteins produced as described previously (Laverty et al., 2019, Masiulis et al., 2019). Briefly, the cells were grown in suspension at 37°C, 160 rpm, 8% CO_2 in FreeStyle 293 media (Gibco), supplemented with 1% FBS (Invitrogen), 1% L-Glutamine (Gibco) and 1% non-essential amino acids (Gibco). The appropriate antibiotics to select for the desired subunit were added to the following concentration: 200 μg/mL Geneticin (for γ2L), 50 μg/mL hygromycin-B3 (for β3), 250 μg/mL zeocin (for α1) and 5μg/mL blasticidin (for the TetR repressor). Gene expression was induced by the addition of 2μg/mL doxycycline at cell density of 2 million/mL. Kifunesine at 1μg/L (Toronto Research Chemicals) was added to ensure a uniform, high-mannose composition of N-glycans ($Man_9GlcNAc_2$), representative for neuronal receptors. Afterwards, the cell cultures were grown for 24h and harvested by centrifugation. Cell pellets were snap frozen in LN_2 and stored at -80°C until further use.

2.2.2 Mammalian protein production in cell pools

Full length human β3 homomerirc receptors were produced in HEK293S GntI$^-$ cell pools generated upon lentiviral transduction, as described before (Elegheert et al., 2018). Truncated α1β3γ2 receptors were produced in a cell pool generated by transduction with a lentivirus mix encoding $GABA_A$ subunits in the following ratio - truncated α1-SBP tag : truncated β3-SBP tag : truncated γ2-1D4 tag = 1:1:0.8 and purification was carried out by pulling on the γ2-1D4 tag as described in sections 2.2.6 and 2.2.7. The plasmids for truncated

α1-SBP tag and truncated γ2-1D4 tag were provided by Paul Miller (University of Cambridge) and the cell pool was generated by Veronica Chang (MRC LMB).

The cells were then grown under the same conditions as previously published protocols (Laverty et al., 2019, Masiulis et al., 2019). No antibiotics were added to the media except 5μg/mL blasticidin, necessary to keep selective pressure on the TetR gene. Gene expression was induced by the addition of 2μg/mL doxycycline at a cell density of 2 million/mL. The cultures were then grown for additional 24h and harvested by centrifugation. The pellets were snap frozen in LN_2 and stored at -80°C until further use.

2.2.3 Transient mammalian protein production

The truncated α1β3 heterodimer and truncated β3 homomer receptors were cloned into the pHL vector and produced by transient transfection following published procedures (Miller and Aricescu, 2014). For 1L of Expi293F cells (Thermo Fisher Scientific), 1.1 mg of the required DNA was mixed with 33mL of Expi expression media (Gibco). In the case of the truncated α1β3 I used plasmid mix containing a 5:1 ratio of α1:β3 vectors to favour the presence of two α1 subunits in the pentameric $GABA_A$ receptor assembly. The solution was mixed with 33mL of media supplemented with 3mL (1mg/mL) of PEI 'MAX' (PolySciences). After a 15min incubation at room temperature, the DNA+PEI mixture was added to the cell suspension at cell density of 2 million/mL. The cultures were then grown for 24h and harvested by centrifugation. The pellets were snap frozen in LN_2 and stored at -80°C until further use.

2.2.4 MSP2N2 purification

The pET28a vector containing the MSP2N2 gene was acquired from Addgene and was transformed into BL21(DE3) *E. coli* cells. Three liters of cells were grown in terrific broth (TB) media to OD_{600nm}=3 and the MSP2N2 gene expression was induced upon the addition of 1mM Isopropyl β- d-1-thiogalactopyranoside (IPTG) for 4 h at 28°C. Cells were collected by centrifugation and the pellets were resuspended in 200mL 50mM Tris, 300mM NaCl pH=8 supplemented with cOmplete protease inhibitor tablets (Roche). Next, the cells were homogenized with a cell disruptor at pressure of 38,000 psi, and the lysate was centrifuged at 30,000×g for 30 min at 4°C. The supernatant was incubated with 2.5mL of Ni-nitrilotriacetic acid (Ni-NTA) resin (Thermo Fisher Scientific) for 2h at 11°C in batch mode and kept in suspension by 111rpm rotation. The beads were collected onto a gravity flow column (Bio-RadLaboratories) and were washed sequentially with:

1) 10 column volumes (CVs) 40mM Tris/HCl, 0.3 M NaCl, 1% Triton pH=8.0
2) 5 CVs 40mM Tris/HCl, 0.3 M NaCl, 50mM cholate pH=8.0
3) 10 CVs 40mM Tris/HCl, 0.3 M NaCl pH=8.0
4) 20 CV 40mM Tris/HCl, 0.3 M NaCl, 20mM imidazole pH=8.0.

MSP2N2 was eluted with 40mM Tris/HCl, 0.3 M NaCl, 0.3 M imidazole pH=8.0, concentrated and applied on a S200 16/60 gel filtration column equilibrated in 40mM Tris/HCl, 150mM NaCl pH=7.5. Fractions containing MSP2N2 were pooled and concentrated to 5 mg/mL.

2.2.5 Saposin A purification

The pET45 vector containing the Saposin A gene was acquired from Addgene and was transformed into Rosetta(DE3) *E.coli* cells (Sigma). Three liters of cells were grown in TB media to OD_{600nm}=1 and the Saposin A gene expression was induced with 1mM IPTG for 4 h at 28°C. Cells were collected by centrifugation and the pellets were resuspended in 20mM HEPES, 150mM NaCl pH=7.6 supplemented with a cOmplete protease inhibitor tablet. Next, the cells were homogenized with a cell disruptor at pressure of 38,000 psi, and the lysate was centrifuged at 30,000×g for 30 min at 4°C. The supernatant was collected and heated to 85°C for 10mins and centrifuged again at 30,000×g for 30 min at 4°C.

The supernatant after heating was applied on a HisTrap™ High Performance (Cytiva) 5mL column, washed and eluted with the following buffers:

1) Wash 1: 15CVs of 20mM imidazole, 20mM HEPES, 150mM NaCl pH=7.6
2) Wash 2: 15CVs of 40mM imidazole, 20mM HEPES, 150mM NaCl pH=7.6
3) Elution: 5CVs of 500mM imidazole, 20mM HEPES, 150mM NaCl pH=7.6

The eluate was dialyzed overnight in SnakeSkin 3.5kDa MW cutoff dialysis tubing (Thermo Fisher Scientific) against buffer containing 20mM HEPES, 150mM NaCl pH=7.6. 3C protease was added to Saposin A in a 1:100 molar ratio to cleave the His_6-tag during the dialysis step. The sample was then purified with reverse nickel chromatography. The flowthrough was collected, concentrated to 9mg/mL, snap frozen in LN_2 and stored at -80°C until further use.

2.2.6 Generation of 1D4 beads

1g of CnBr-activated Sepharose 4B (GE Healthcare, Cat. Number 17-0430-31) were incubated at room temperature with 50mL of 1mM HCl for 15 minutes until the beads were swollen. The beads were applied on a gravity column (Bio-Rad Laboratories) and washed

with further 50mL of 1mM HCl followed by a wash with 50mL of 500mM NaCl, 100mM $NaHCO_3$ pH=8.5. 14mg of the monoclonal Rho-1D4 (University of British Columbia) was diluted in 10mL of PBS pH=7.4 and incubated with the beads overnight while rotating at 4°C. On the next day the excess liquid was removed by gravity flow and the efficient coupling of the antibody determined by measuring the A_{280nm} absorption of the flowthrough. The beads were then washed with 50mL of 200mM Glycine pH=8 and incubated with further 50mL of 200mM Glycine pH=8 at room temperature while rotating for 2h. The beads were then washed with the following buffers:

1) 50mL of 500mM NaCl, 100mM $NaHCO_3$ pH=8.5
2) 50mL of 500mM NaCl, 100mM NaOAc pH=4
3) 50mL of 500mM NaCl, 100mM $NaHCO_3$ pH=8.5
4) 50mL of PBS pH=7.4

After the final washing step, the beads were resuspended in 15mL of PBS pH=7.4 and stored at 4°C.

2.2.7 $GABA_A$ receptor purification and reconstitution into lipid nanodisc

Cell pellets were resuspended in PBS pH=7.4 supplemented with cOmplete protease inhibitor tablet (Roche). For nanodisc reconstitution, a 10% (w/v) solution of lauryl maltose neopentyl glycol (LMNG, Anatrace) was prepared in water and added at 1% (w/v) to the cell suspension. Cells were solubilized for 1h at 4°C, and cell debris and other insoluble material were removed by centrifugation (15,000×g, 15 min). The supernatant from 1L of cells was incubated with 300µL of the desired affinity resin (1D4 beads (generated in house as described in section 2.2.6) for the full-length α1β3γ2L and truncated α1β3, Streptavidin agarose (Thermo Fisher) for the truncated β3 homomer, FLAG M2 monoclonal antibody affinity gel (Sigma) for the full-length α1β3 and Strep-Tactin Sepharose resin (IBA) for the full-length β3 homomer) and gently mixed at 4°C for about 2 h.

The resin was recovered by centrifugation at 300×g, 4°C and washed 3 times with 50mL PBS pH=7.4 containing 0.1% (v/v) LMNG. The beads were then collected by centrifugation at 300×g, 4°C and incubated for 30min with 45µg of phosphatidylcholine (POPC, Avanti) and bovine brain lipid (BBE) extract (type I, Folch fraction I, Sigma-Aldrich) mixture (POPC:BBE = 70:30 w/w). In the case where different lipids other than POPC (listed in chapter 2.3.1) were used to generate the lipid environment, the desired lipid of choice was mixed with the BBE at the same ratio. For the cholesterol enrichment experiments performed

during disc formation, the desired concentration (1.6mM to 13mM) of MβCD-cholesterol (Sigma) was added together with the lipids. 100µL MSP2N2 (5mg/mL) was then added to the beads and further incubated for 30min. Next, Bio-beads SM-2 (Bio-Rad) equilibrated in PBS were incubated with the resin for 90 minutes. The beads were then washed 6 times with 1mL of PBS pH=7.4 and eluted overnight with the respective buffer for the resin of choice (5mM 1D4 peptide, PBS pH=7.4 for 1D4 resin, 100µg/mL FLAG peptide, PBS pH=7.4 for FLAG resin and 2.5mM Biotin, PBS pH=7.4 for Streptavidin and Streptactin resins). When cholesterol enrichment was performed after disc formation, 4mM MβCD-cholesterol was added after the washes and further incubated for 2h followed by 6 more washes and overnight elution.

For Saposin A reconstitution I used the same protocol as for MSP2N2 described above.

The procedure for reconstituting the receptor in SMALPs is similar to the one in nanodisc but with the following differences. After the cells were resuspended, they were passed twice through a cell disruptor at 25,000 psi and spun at 15,000×g for 15 minutes to remove cell debris. The supernatant was collected and ultracentrifuged at 195,000×g for 1 hour at 4°C to collect the membrane fraction. The membrane pellet was then resuspended in TBS (20mM Tris pH=8, 150mM NaCl) and dissociated using a Dounce homogenizer. The membranes were diluted to a final concentration of 80mg/mL. 1% (*w/v*) Xiran 30100 (from a 20% (w/v) Xiran 30100 stock) was then added to the solution and incubated for 2 hours at 4°C. Cell debris and insoluble material were removed by centrifugation (15,000×g, 15 min). The supernatant was then incubated for 2h with 1D4-affinity resin, washed 3 times with 50mL TBS pH=8 and eluted with 5mM 1D4 peptide, TBS pH=8 overnight at 4°C.

2.2.8 Megabody (Mb) and nanobody (Nb) purification

Mb25 and Mb38 used in this thesis were generated and described previously (Laverty et al., 2019, Masiulis et al., 2019, Uchański et al., 2021) and were a generous gift from Jan Steyaert's group (VIB-VUB Center for Structural Biology, VIB, Brussels, Belgium). The proteins were stored as 300µM stock solutions in 10mM Tris, 140mM NaCl at -80°C.

In the case of Nb38, the nanobody was cloned into the pMESD22c7 plasmid for periplasmic expression and transformed into WK6 *E. coli* cells. Bacterial cell cultures (1 L) were grown in TB media containing 100 µg/mL ampicillin, 0.1% Glucose and 2mM $MgCl_2$. Gene expression was induced by 1mM IPTG and the temperature adjusted to 28°C for 16 h. Cells were collected by centrifugation at 6,000×g for 15mins at 4°C, resuspended in 200mM Tris,

0.5mM EDTA, 500mM Sucrose pH=8 containing a protease inhibitor tablet (Roche) and incubated for 2h at 4°C while rotating. Cell debris were removed by centrifugation for 30 min at 35,000×g and 4°C. The supernatant containing the periplasmic fraction was collected and incubated with 2mL Ni-nitrilotriacetic acid (Ni-NTA) resin (Thermo Fisher Scientific) for 1h at room temperature while inverting. The lysate containing the Ni-NTA resin was transferred into a gravity flow column (Bio-Rad laboratories). The resin was washed with 15 CVs 100mM Tris, 500mM NaCl, 25mM imidazole pH=8. The protein was eluted with 5 CV 100mM Tris, 500mM NaCl, 500mM imidazole pH=8 and was concentrated with a 10 kDa filter unit (Millipore). The eluate was then applied to a S200 16/60 size exclusion column (GE Healthcare) equilibrated in 10mM Tris, 140mM NaCl pH=8. Fractions containing Nb38 were collected and concentrated with a 10 kDa filter unit to 5mg/mL. Aliquots were flash frozen in liquid nitrogen and stored at -80°C.

2.3 Lipid solubilization and extraction

2.3.1 Lipid solubilization

All lipids were purchased from Avanti – either already in chloroform or as powder in which case they were solubilized in chloroform. The solubilized lipids were moved to a glass container and the chloroform was evaporated under nitrogen gas to reduce oxidation rates with continuous vortexing. Once the chloroform was completely evaporated, the lipids were washed with pentane to remove any residual chloroform and left under nitrogen gas overnight. On the next day, PBS pH=7.4 was added to the lipids and vortexed extensively followed by bath sonication (30s on, 30s off) until all lipids were in suspension. The lipids were then transferred to a 15mL Falcon tube and LMNG was added to a final concentration of 3% (w/w) from a 10% (w/w) stock in PBS pH=7.4. The lipids were then vortexed and sonicated until the solution became transparent. For POPC, di20:1PC and di22:1PC the concentration of lipids was 10mg/mL. For di24:1PC and Sphingomyelin (d18:1/24:0) the concentration was 2.5mg/mL

2.3.2 Extraction of lipids from nanodisc samples

To analyse the lipid composition of the nanodiscs used for $GABA_A$ receptor reconstitution, 20µL samples were mixed with 200µl ice-cold MeOH, vortexed and sonicated in an ice bath for 15 min. Then 400µL chloroform was added, and the sample was again vortexed and sonicated for further 15 min. Next, 150µL ice-cold MilliQ Water was added, followed by

vortexing and sonication for 15 min. The sample was then spun at 16,000×g for 15 min and the organic layer (lower layer containing the lipids) was carefully removed. Another 400µL of chloroform was added to re-extract the lipids, followed by vortexing, sonication and a second 16,000×g, 15 min centrifugation. The 800µL sample was evaporated in a vacuum desiccator at 45°C. The dried lipids were stored at -20°C until further use.

2.3.3 Cholesterol content measurement

The cholesterol concentration was measured with the Sigma cholesterol assay kit (CS0005) following the manufacturer protocol. Samples were measured in triplicates and the cholesterol concentration measured fluorometrically.

2.3.4 Mass spectrometry analysis of the nanodisc lipids

Prior to drying the lipids, SPLASH LIPIDOMIX Mass Spec Standard (Sigma) was added to the samples as per the manufacturer's protocol to serve as an internal control for the experiment. The SPLASH LIPIDOMIX was also analysed by itself. Dried down sample extracts were reconstituted in 50µL IPA, vortexed and sonicated for 10 minutes. The mass spectrometry experiment was performed by Samantha Ferries and Nyasha Munjoma (Waters Corp), as described previously (Munjoma et al., 2022).

2.4 Electron Microscopy

2.4.1 Cryo-EM sample preparation using commercial plungers

Prior to vitrification on EM grids, purified $GABA_A$ receptor samples were pre-incubated with 2µM Mb38 or 3µM Mb25 for 30 min. All samples described in chapters III and IV were vitrified using a Leica EM GP2 plunger (Leica Microsystems; 99% humidity, 14 °C) or a Vitrobot Mark IV System (Thermo Fisher Scientific; 100% humidity, 14 °C). Samples (3.5 µL) were applied to a freshly glow-discharged (PELCO easiGlow, 30 mA for 120s) gold R1.2/1.3 300 mesh UltraAuFoil grid (Quantifoil) and blotted for 2.5s before plunge-freezing in liquid ethane. For the fast application approach discussed in chapter III, the ligand was added directly to the grid just before blotting resulting in a 10s exposure to the drug. For the samples described in chapter IV, the β-lactams were mixed with GABA and incubated with the receptors for 2 minutes on ice prior vitrification. The final concentrations of β-lactams used were 10mM (for Penicillin G, Penicillin V and Piperacillin) or 3mM (for Nafcillin). The final GABA concentration used was 50 µM. Grids were then stored in liquid nitrogen before imaging.

2.4.2 Cryo-EM sample preparation with a time-resolved plunger

The plunger used for the results presented in Chapter V was essentially the same as previously described (Berriman and Unwin, 1994). Quantifoil 1.2/1.3 grids were manually plunged in liquid ethane at ~8°C and ~95% humidity. The total ligand exposure time was limited to ~10ms. $GABA_A$ receptor samples were sprayed as follows: full-length α1β3γ2L was sprayed with 100mM GABA + 7mM ETM, 2mg/mL Ferritin (Sigma) in PBS; the full-length α1β3 was sprayed with 300mM GABA + 300mM HSM, 2mg/mL Ferritin in PBS; the truncated β3 homomer was sprayed with 150mM HSM, 2mg/mL Ferritin in PBS; the truncated α1β3-Mb25 complex with either 300mM GABA, 2mg/mL Ferritin in PBS; 300mM GABA + 300mM HSM, 2mg/mL Ferritin in PBS or 200mM PPF in MeOH.

2.4.3 Cryo-EM data collection

Cryo-EM datasets were collected on a Titan Krios G2 microscope at the MRC LMB equipped with a Falcon 4 detector (later upgraded to Falcon 4i) in electron counting mode at 300kV at a nominal magnification of 96,000 corresponding to a calibrated pixel size of 0.824 Å. All datasets were acquired using EPU (Thermo Fisher Scientific) with total exposure time of 6.43s (Falcon 4) or 4.33s (Falcon 4i) and accumulated total dose of ~40 $e^-/Å^2$. Before processing, all images were converted to the tiff format using relion_convert_to_tiff and dose-fractionated into groups of 40 frames, corresponding to an accumulated dose of ~1 $e^-/Å^2$ per frame.

2.4.4 Cryo-EM image processing

The movies were motion and gain corrected using MotionCor2 (Zheng et al., 2017). Contrast transfer function (CTF) estimation was performed with CTFFIND-4.1.13 (Rohou and Grigorieff, 2015). Particle picking was performed using the neural networks WARP, Topaz (Tegunov and Cramer, 2019, Bepler et al., 2019) or the Laplacian-of-Gaussian auto-picking function in RELION4.0 (Kimanius et al., 2021) and extracted in RELION4.0. The picked particles were subjected to 2D classification in cryoSPARC (Punjani et al., 2017). The particles resembling intact receptor from the 2D classes were used for ab-initio model generation with 2 seeds in cryoSPARC and were subject to several rounds of heterogeneous refinement with 4 seeds to remove damaged particles or particles with preferential orientation.

For the structures presented in Chapters III and IV, the particles that were part of the best consensus reconstruction were re-extracted back in RELION4.0 and subjected to a focused-

3D classification without alignment with a TMD mask. By using this approach, I could separate resting from desensitized states as well as the asymmetric state described in Chapter IV.

For the structures presented in Chapter V the aforementioned approach did not yield satisfactory results. Therefore, all processing was performed in cryoSPARC. The consensus particles were subjected to deep 3D classification with a TMD mask and no alignment with ~30 seeds for each dataset. Each of the states classified by this approach were visually inspected and the structures which retained high-resolution features e.g. unambiguous helical pitch in the TMD region helices, were subjected to homogenous refinement followed by one round of heterogenous refinement with 3 classes using frequencies up to Nyquist. The highest-resolution class was then subjected to non-uniform refinement and anisotropic magnification, per-particle defocus and 4^{th} order aberrations corrected.

The final half-maps from both processing strategies were subjected to post-processing in RELION4.0 for resolution estimation. Local resolution plots were generated with RELION4.0. All map and model rendering were performed in ChimeraX (Meng et al., 2023). An example of the detailed processing strategy can be seen in Appendix Figure 3.

2.4.5 Model building and refinement

The models in Chapter III, IV and VI as well as the β3γ2 models in chapter V were built and refined by me. The truncated β3 and truncated α1β3 models described in Chapter V were built and refined by Tomas Malinauskas (University of Oxford). The initial models used for building were the highest resolution reported models published for both truncated and full-length $GABA_A$ receptor subunits. For the full-length α1 subunit, full-length β3 subunit and full-length γ2L subunit – PDB: 7QNE; for the truncated β3 subunit – PDB:7A5V; for the truncated α1 subunit – PDB: 7PBD. Restraints for all ligands were generated by the Grade webserver (Global Phasing Ltd; https://grade.globalphasing.org/) using Simplified Molecular Input Line Entry System (SMILES) strings from PubChem as input. Iterative rounds of refinement and model building were performed in Coot v0.9.6 (Emsley et al., 2010) and Phenix v1.19.2 (Afonine et al., 2018). The models were validated by MolProbity v4.2 (Chen et al., 2010).

Chapter III

The environment of the reconstituted $GABA_A$ receptor

3.1 Introduction

Ion channels function in the context of cellular membranes and multi-protein complexes in which they are integrated. However, the functional impact of this environment, in most cases, remains poorly understood. There has been extensive research on the functional connection between lipids and members of the pLGICs going back to the 1980s. These studies showed that the muscle-type *Torpedo* nicotinic acetylcholine receptor (nAChR) requires specific lipids to be present in the cell membrane in order to evoke a response upon agonist application. It was determined that a certain level of membrane fluidity was required to allow the transition between the low and high agonist affinity states of nAChR (Fong and McNamee, 1986, Criado et al., 1982). Furthermore, it was shown that only receptors reconstituted in a membrane containing both cholesterol and negatively charged phospholipids could undergo gating. On the other hand, receptors in membranes which lack cholesterol could bind agonist but did not undergo gating motions (Hamouda et al., 2006). This suggests that the lipids surrounding the receptor are crucial for the physiologically meaningful transitions during the gating cycle.

The functional effect of the lipid environment has also been extensively explored in the context of the $GABA_A$ receptor as well. Increasing the concentrations of phosphatidyl serine enhanced the effect elicited by benzodiazepines (Hammond and Martin, 1987), whereas depleting the cholesterol content of WSS-1 cells with MβCD diminishes the $GABA_AR$ currents in a dose-dependent manner (Nothdurfter et al., 2013). It is therefore important to establish if the structures of the $GABA_AR$ which are detergent-solubilized and then reconstituted into lipid nanodiscs retain the necessary lipids required by the receptor to undergo gating motions.

To test this, I will discuss the roles of the nanodisc scaffolding proteins, the membrane thickness as well as its rigidity. Furthermore, thus far all cryo-EM structures of $GABA_ARs$ were solved in the presence of antibody-derived fiducials (e.g Fab fragments, nanobodies or megabodies) which were thought to be necessary for particle alignment during image processing. I will therefore first explore the structural impact of nano/megabody fiducials on reconstituted receptor conformations.

3.2 The functional impact of nanobody-derived fiducials

Until recently, solving a heteromeric $GABA_AR$ structure by cryo-EM required the presence of additional binding partners that served the role of fiducials during 3D reconstruction.

Otherwise, the native differences between receptor subunits were too small to be picked up by the computational algorithms available at the time and the lack of fiducials would lead to misalignments. This problem was further complicated by the low detective quantum efficiency (DQE) of older generation direct electron detectors (DED). To overcome these issues, binders specific to subunits or to inter-subunit interfaces had to be added to the receptor samples. Such molecules, especially inter-subunit binders, could also be potent allosteric modulators of the receptors. Therefore, in order to study the gating dynamics of the receptor, it is essential to establish if the nano/megabody binders typically used in our laboratory for particle alignment during reconstruction have a structural impact on the receptor.

To test this, I focused on the synaptic full-length α1β3γ2L $GABA_A$ receptor subtype and the Mb38 megabody commonly used in our group. Mb38 was generated by grafting the Nb38 nanobody onto the HopQ scaffold (Uchański et al., 2021). At concentrations higher than 3μM, Mb38 can directly activate the receptor and desensitize it perhaps in combination with an unknown buffer component (Laverty et al., 2019).

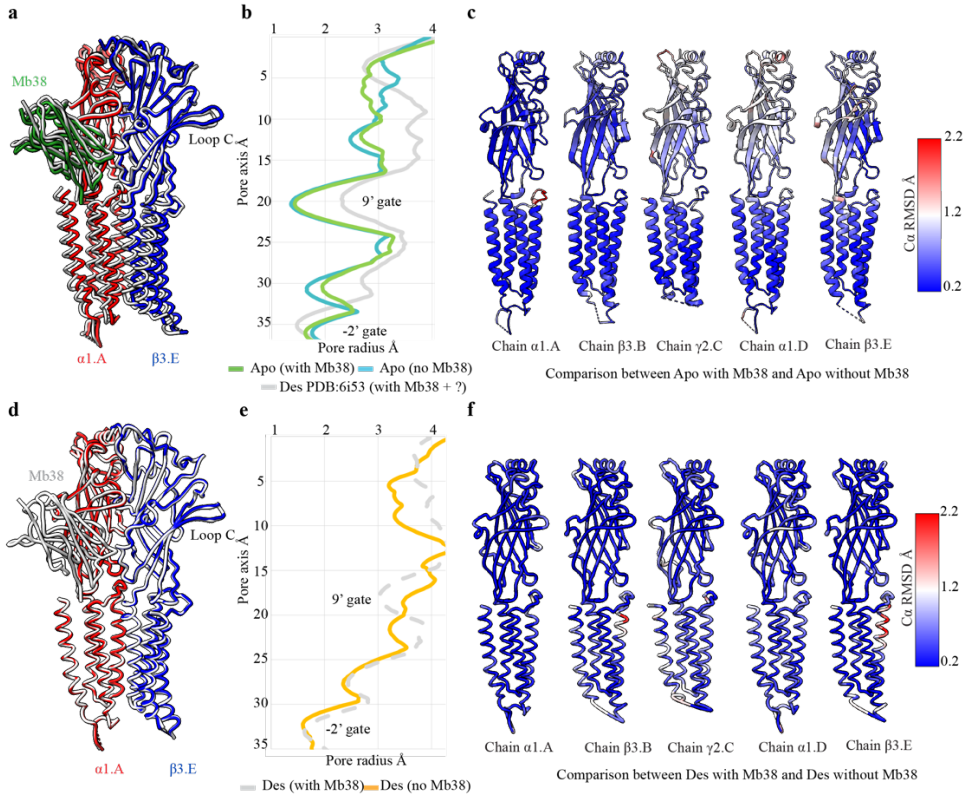


Figure 3.2 – The impact of nanobody-derived fiducials on the $GABA_A$ receptor

a) *Comparison between the Mb38-bound desensitized state (PDB: 6I53) in white and Mb38-bound resting state (coloured).* ***b)*** *Pore profiles of the Mb38-bound desensitized state, the Mb38-bound apo state and the*

Figure 3.2 continued

canonical apo state with no fiducials and ligands bound. ***c)*** *Cα RMSDs between the Mb38-bound apo and Mb38-free apo state.* ***d)*** *Comparison between the desensitized states bound to GABA and with Mb38 (white), without Mb38 (coloured).* ***e)*** *Pore profiles of the Mb38-bound, GABA-bound desensitized state and Mb38-free, GABA-bound desensitized state.* ***f)*** *Cα RMSDs between the Mb38-bound desensitized and Mb38-free desensitized state. The structures of the apo state with Mb38 and desensitized state with Mb38 were solved in collaboration with Jonas Miehling.*

I therefore tested Mb38 at 2μM, a concentration where it does not directly activate the receptor but can potentiate it. At this concentration, Mb38 predominantly binds to the $\alpha1^{+}/\beta3^{-}$ interface (Fig. 3.2a) but importantly the receptor remains in the closed/apo state with both activation and desensitization gates closed as judged by the pore profile (Fig. 3.2b). Furthermore, loop C remains open and the M4 helices of the TMD bundles have not undergone the rotation present in the desensitized state further indicating the receptor is in a resting state (Fig. 3.2a). However, in order to fully show that Mb38 had no structural impact at 2μM, an apo state structure that lacks Mb38 is required. To overcome this issue, I took advantage of the recent advances in DED and the high DQE of the F4 camera, which have recently enabled the structural characterization of the $GABA_A$ β3 homomer to 1.7Å resolution (Nakane et al., 2020). These hardware developments allowed me to solve the structure of the full-length α1β3γ2L receptor in the absence of any fiducials. Particle alignment was likely facilitated by the presence of notable differences between the subunits including the canonical β3 glycans and the structured α1 ICL regions, stabilized by PIP_2 molecules. The structure revealed that in the apo/resting state, without Mb38, both the activation (9') and the desensitization (-2') gates are shut (Fig. 3.2b).

Most importantly, the Cα RMSDs between the resting structures with and without Mb38 calculated across the five subunit chains are below 0.4 Å suggesting that the receptor adopts almost identical states (Fig. 3.2c). One notable difference, however, is that the M2-M3 loop in the structure without Mb38 is better resolved than the structure with Mb38 bound. This together with the higher resolution of the map allows its unambiguous modelling leading to slight difference in the local Cα RMSDs. The resting state without Mb38 has a resolution of 2.4 Å whereas the resting state with Mb38 has a resolution of 3 Å, allowing more accurate model building of the flexible M2-M3 loop in the higher resolution map. Despite this, the presence of Mb38 at low concentrations does not have a substantial structural impact on the apo state. I further solved the α1β3γ2L receptor structures with and without Mb38 in the

presence of 1mM GABA, in order to drive the receptor into the desensitized conformation. In this experiment Mb38 also has no structural impact based on the Cα RMSDs which are below 0.5 Å across the five subunits (Fig. 3.2d,e). I therefore conclude that Mb38, at 2μM (potentiating) concentration, does not render the receptor inactive and does not uncouple the ECD from TMD as the end states of the cycle, namely resting and desensitized, remain unaffected.

3.3 The structural impact of nanodisc scaffolds

Choosing a suitable nanodisc scaffold is a crucial consideration to ensure that reconstituted receptors can illustrate functionally-meaningful states. So far, all the structures I have presented were solved in nanodiscs formed by the MSP2N2 scaffolding protein. MSP2N2 produces nanodiscs, which have a uniform size of ~16 nm (Ritchie et al., 2009) and can theoretically accommodate two or three full-length $GABA_A$ receptors per disc. However, before nanodisc reconstitution, the receptors are solubilised from the cell membrane with detergents. It is important to note that the right choice of detergent is critical when working with $GABA_A$Rs. Previously it has been shown that solubilization of heteromeric receptors with DDM leads to the collapse of the γ2 subunit in particular and to the uncoupling of the ECD and TMD regions (Zhu et al., 2018, Phulera et al., 2018). This was overcome by using LMNG followed by MSP2N2 nanodisc reconstitution which leads to receptors with pseudo-fivefold symmetry around the pore and with intact contacts between the ECD and TMD (Laverty et al., 2019, Masiulis et al., 2019). Nevertheless, it is unclear if such receptors are indeed functionally active. To test this, I turned my attention to two other reconstitution approaches. Firstly, I tested the role of the scaffolding protein by replacing MSP2N2 with the Saposin A scaffold (Flayhan et al., 2018). Secondly, to avoid detergent solubilization, I used styrene-maleic acid (SMA) copolymers which disrupt membranes and extract receptors surrounded by a layer of native cellular lipids (Postis et al., 2015).

3.3.1 The Saposin A scaffold

The MSP2N2 scaffold generates nanodiscs which are uniform in size. Although, as mentioned above, these are wide enough to accommodate multiple full-length $GABA_A$ receptors, one cannot exclude the possibility that they might somehow restrict the range of possible conformational changes. No structure of an open state $GABA_A$ receptor has been reported so far, therefore one might argue that receptors cannot sample such conformations in nanodiscs. Instead, they appear to undergo direct transitions between the resting and

desensitized states. I therefore turned my attention to Saposin A which is a scaffold that can adapt to the size of the incorporated membrane (Flayhan et al., 2018).

Previously, truncated α1β2γ2 $GABA_A$ receptor structures were successfully resolved within saposin A discs (Kim et al., 2020). Prompted by this study, I reconstituted the α1β3γ2L receptor in the same disc type. The structures I could solve in saposin A illustrate resting and desensitized states with pseudo-symmetrical pores (Fig. 3.3.1a-b), and only minor variations when compared to the MSP2N2 structures with RMSDs between the five subunits below 0.6 Å for the resting state and 0.45 Å for the desensitized state. However, approximately one-third of the desensitized receptors exhibit a collapsed γ2L subunit, with uncoupled ECD and TMD (Fig. 3.3.1c). Such states have not been observed for MSP2N2 disc structures.

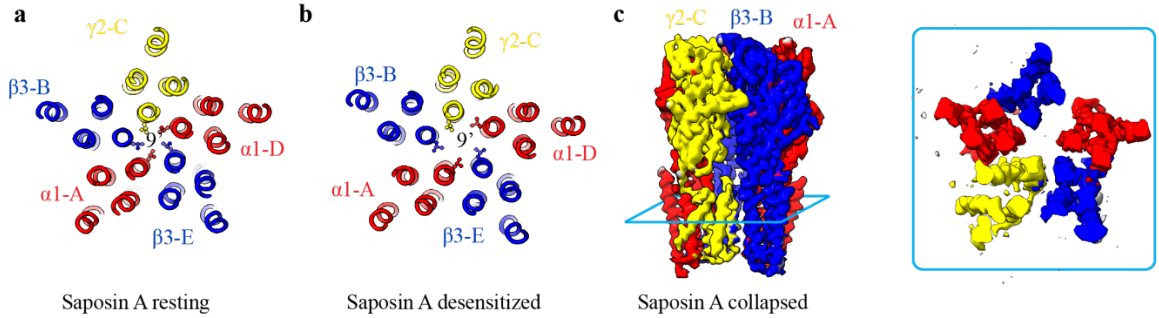


Figure 3.3.1 - α1β2γ2L $GABA_A$ receptor reconstituted in Saposin A nanodisc

a) *The activation gate of the apo/resting state in Saposin A.* ***b)*** *The activation gate of the desensitized state in Saposin A.* ***c)*** *The collapsed γ2L subunit in Saposin A discs and a cross-section at the level of the activation gate.*

It is important to mention that although Kim et al. did not specifically address these collapses, they did observe fragmented γ2 subunit density and applied local 3D classification techniques to remove particles with uncoupled γ2 subunit. Moreover, further studies have revealed that saposin A effectively maintains a membrane thickness of approximately 3nm in the case of the α7 nicotinic acetylcholine receptor (Noviello et al., 2021). This finding presents a contradiction to the previously established range for the membrane thickness of neurons (Ingólfsson et al., 2017, Gentet et al., 2000, Caspar and Kirschner, 1971, Unwin, 2022). Taken together, saposin A nanodiscs therefore may not be representative of the actual membrane environment and could result in the emergence of non-physiological states.

3.3.2 The $GABA_A$ receptor in SMA lipid nanodiscs

SMA copolymers allow the direct isolation of membrane-embedded receptors in complex with endogenous lipids, in disc-like particles called SMALPs. These might therefore be more representative of a physiologically relevant environment in terms of the lipid composition (Dörr et al., 2016). However, it is unknown whether receptors isolated in this way can undergoes motions in a meaningful timescale and whether such motions are functionally accurate. Recently, the structure of the glycine receptor (GlyR) was solved in SMALPs (Yu et al., 2021). The authors of this study reported several distinct states of the receptor bound to the full agonist glycine as well as the partial agonists taurine and GABA. Along the canonical apo and desensitized states, the authors also present a putative open and 'expanded-open' state. The authors use the term 'expanded-open' to describe a state where the pore has a minimum diameter of ~7 Å. This radius, however, is bigger than the reported maximum size of the pore by electrophysiological sizing experiments (Lynch, 2004). Interestingly, the open state reported in this study is perfectly symmetrical along the pore and the RMSDs between the open and desensitized state in the TMD region is 0.6 Å. This also contrasts to studies where ligand application in the millisecond timescale on a heteromeric nAChR embedded in its native lipid environment report an asymmetric gating cycle for an otherwise pseudo-symmetric receptor in the apo and desensitized states (Unwin and Fujiyoshi, 2012).

It is important to note that the experiments reported by Yu et al. were performed under time constraints, namely the sample was frozen within 10s. The authors therefore propose that by using their 'time-resolved' approach one could capture the gating cycle of the channels. The states observed indeed have a pore radius large enough to allow a fully dehydrated chloride ion to go through. However, it is crucial to discuss if such states are physiologically meaningful. Yu et al. report that in the presence of 10mM glycine, the GlyR adopts an open state in 55% of all particles, 15% of the particles are desensitized and 35% are 'expanded-open'. The percentage of particles in the three states, however, is not consistent with the electrophysiological experiments performed in the very same study which reports that the receptors in a patch desensitize and reach steady-state currents in around 500ms meaning that most if not all receptors will be already desensitized under the 10s experimental condition. This, together with the fact that the authors report an 'expanded-open' state brings up the question whether any of these structures resemble the actual open states of the GlyRs in native membranes. Moreover, the authors of the study also report that in the same

timescale, all receptors are desensitized when reconstituted into MSP2N2 nanodiscs which is what is expected based on the electrophysiology data.

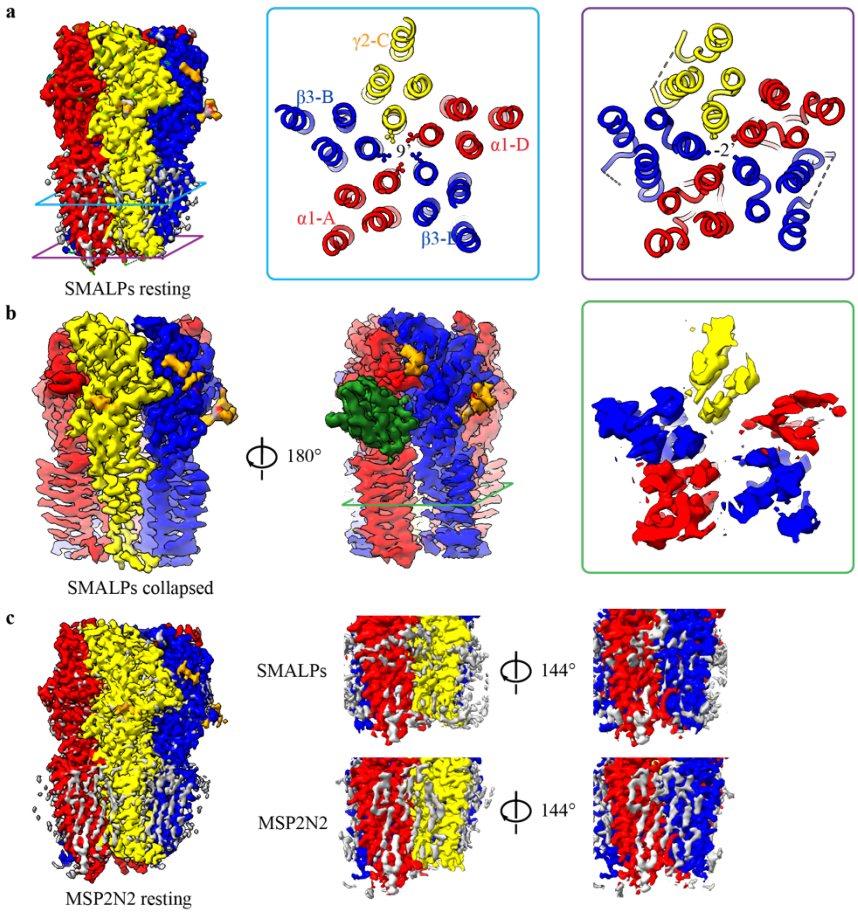


Figure 3.3.2 - $GABA_A$ receptor reconstituted in SMALPs.

a) *The activation (middle) and desensitization (right) gates of the apo/resting state in SMALPs.* ***b)*** *The collapsed γ2 (left) and broken α1/β3 interface (middle) upon GABA binding in SMALPs. Cross-section of the TMD at the 9' level (right).* ***c)*** *Comparison between the lipid composition in SMALPs (top) and MSP2N2 nanodisc (bottom).*

To explore whether SMALP nanodiscs may allow a structural analysis of the $GABA_A$ receptor gating motions, I solubilized the α1β3γ2L assembly using the GlyR protocol used by Yu et al. The $GABA_A$ receptor was supplemented with 1mM GABA by applying the ligand directly to the sample on the grid followed by immediate blotting and plunging into liquid ethane resulting in a 10s exposure to GABA. The dataset was cleaned-up by 2D classification and heterogenous refinements in cryoSPARC leaving 400k 'good' particles that were used to generate a consensus map. The particles were then classified into distinct classes by focused 3D classification on the TMD region. In total, 20% of all particles were in the resting states (Fig. 3.3.2a). Crucially, 80% of the particles had densities for GABA

bound below loop C at the $\beta3^{+}/\alpha1^{-}$ interfaces, however, upon the activation of the receptor, the TMD region was dramatically distorted. Unlike the uncoupled state in Saposin A, in the SMALPs dataset the density for the γ2 subunit's TMD is entirely fragmented and is no longer contacting the neighbouring subunits. Moreover, the interface between the α1-A and β3-B subunits is also broken (Fig. 3.3.2b).

What is the cause for this dramatic collapse remains unclear, however, one explanation could be that the SMA co-polymers cannot provide enough lateral support to the disc leading to less rigidity relative to native membranes and MSP2N2 nanodiscs. It is therefore evident that the receptor cannot undergo physiological gating in SMALPs because it cannot reach the 'canonical' desensitized state. Therefore, pLGICs conformations in SMALPs should be considered with caution.

Nevertheless, the resting/apo state in SMALPs is intact with coupled ECD to TMD in all subunits, which suggests that the collapse may only happen in the presence of an agonist. Despite the collapse of the desensitized state, the resting state in SMALPs sheds light on the native lipid environment of the receptor. By comparing it to the resting state in MSP2N2 discs, no significant differences regarding lipid densities can be observed (Fig. 3.3.2c). The lipids are indeed even better resolve in the MSP2N2 nanodisc due to the higher resolution of the reconstruction. Since MSP-reconstituted receptors show a similar lipid profile (Fig. 3.3.2c), it appears that essential lipids remain associated with the receptors during detergent solubilization.

3.4 The impact of nanodisc thickness

Neuronal cells must transmit signals between each other effectively and fast which is critical for information processing in the networks they form (Markram et al., 2015). This property of the neuron is driven by its capacitance which is determined by the membrane thickness and the lipid composition of the cell. In the case of the cultured neuronal cells, the membrane thickness has been estimated to be ~3.5nm (Liu et al., 2020), which is consistent with the disc thickness i.e. the distance between the lipid headgroups, I observe in MSP2N2 nanodiscs. However, the native lipid composition required for $GABA_A$ receptor gating may be different. When forming nanodiscs we use lipids in ratio 70:30=POPC:BBE (bovine brain extract) (w/w) but it is possible that the lipids present in this mixture cannot mimic the neuronal cell membrane entirely. To test if this is the case, I reconstituted the receptor in the nanodisc scaffolding protein MSP2N2 and varied the acyl chain length of the 16:0-18:1

POPC lipids used. POPC has two acyl chains with 16 and 18 carbons respectively which may not be long enough to support a functional receptor. I therefore replaced POPC keeping the same proportion to BBE with di20:1 POPC for the FL β3 homomer (Fig. 3.4a), di22:1 POPC for the FL β3 homomer (Fig.3.4b), di24:1 POPC for the FL α1β3γ2L (Fig. 3.4c) and Sphingomyelin (d18:1/24:0) for the FL α1β3γ2L (Fig. 3.4d) to form the nanodisc. Furthermore, these lipids are more unsaturated which allows a higher mobility of the acyl chains. For the FL β3 homomer I used 100μM of the general anaesthetic etomidate (ETM) that directly activates this receptor subtype (Miller and Aricescu, 2014, McMullan et al., 2023) and incubated it with the sample for 10s with the aim of visuailizing an open state of the receptor (using the same approach as described in chapter 3.3.2). Virtually all particles in this dataset however have ETM bound and are driven into the desensitized state indicating that changing the acyl chain length does not affect the structure of the receptor (the RMSDs between the structures were around 0.3 Å) and it does not interfere with the equilibrium between open and desensitized states at this timescale (Fig. 3.4a-b).

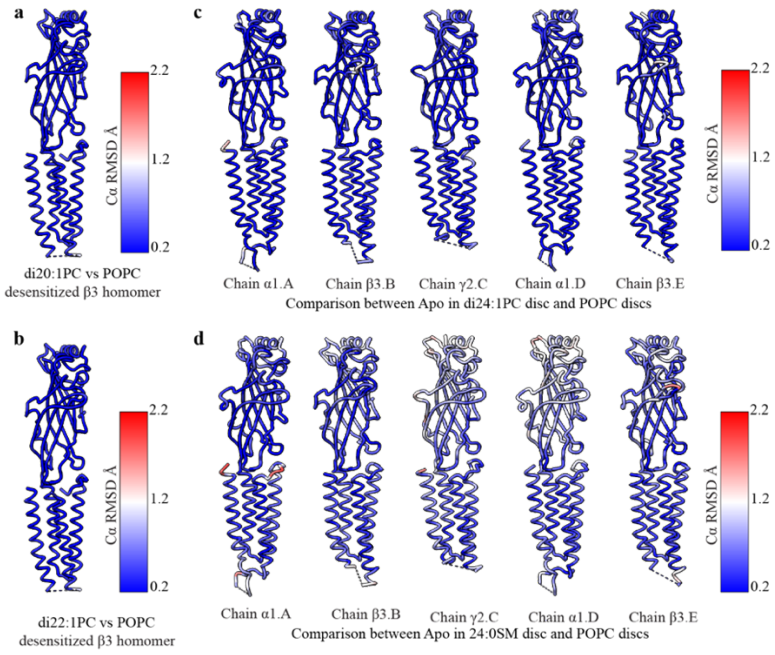


Figure 3.4 - $GABA_A$ receptors reconstituted in discs with different acyl chain lengths.

a) *Comparison between the FL β3 homomer in the desensitized state bound to ETM in di20:1PC versus POPC nanodiscs.* ***b)*** *Comparison between the FL β3 homomer in the desensitized state bound to ETM in di22:1PC versus POPC nanodiscs.* ***c)*** *Comparison between the FL α1β3γ2L in the resting state in di24:1PC versus POPC nanodiscs.* ***d)*** *Comparison between the FL α1β3γ2L in the resting state in Sphingomyelin (d18:1/24:0) versus POPC nanodiscs.*

I then turned my attention FL α1β3γ2L in nanodiscs loaded with di24:1 POPC and Sphingomyelin (d18:1/24:0) and compared the resting state in these environments to the canonical nanodisc with POPC and BBE. Once again there is little deviations in the Cα RMSDs when comparing the structures. In both cases the overall RMSDs between the five subunits were below 0.5 Å (Fig. 3.4c-d). It therefore seems that variations in the lipid composition and acyl chain length have limited or no structural impact, likely because our purification strategies ensure the preservation of an inner layer of lipids that surrounds the receptors and originates directly from the cell as evident from the SMALPs reconstitution where the resolved lipids between SMALPs and MSP2N2 discs are similar (Fig. 3.3.2c).

3.5 The influence of cholesterol on the nanodisc

The $GABA_A$ receptor functions in a complex environment situated at the synaptic cleft. There are many auxiliary proteins which associate with the receptor such as gephyrin, LH4, Neuroligin-2 and Neurexinβ (Choii and Ko, 2015, Yamasaki et al., 2017, Zhang et al., 2010). These proteins are necessary to tether the receptor in the synaptic cleft in close proximity to the neurotransmitter release site thus forming trans-synaptic nanocolumns (Südhof, 2018, Tang et al., 2016). This, however, is only one among a myriad of mechanisms by which location, trafficking and signalling of neurotransmitter receptors can be modulated (Allen et al., 2007). It has been established that the composition of the inhibitory synaptic membrane is mainly composed of cholesterol and sphingomyelin which form membrane microdomains with high rigidity termed lipid rafts (Cotman et al., 1969). These are likely to further restrict the distribution of the receptors at the cell surface (Simons and Toomre, 2000). Interestingly, it has been shown that depleting cholesterol from cell membranes can negatively affect the modulation of $GABA_A$ receptors by diazepam (Nothdurfter et al., 2013). Furthermore, cholesterol has been shown to play a key role in signalling and localization of the *Torpedo* nAChR (Unwin, 2022). I therefore tested the effect of cholesterol and membrane rigidity on the $GABA_A$ receptor by artificially adding extra cholesterol to the disc. This was done by the addition of the soluble MβCD-cholesterol complexes, a strategy that has been extensively used to enrich the level of cholesterol in cellular membranes (Zidovetzki and Levitan, 2007).

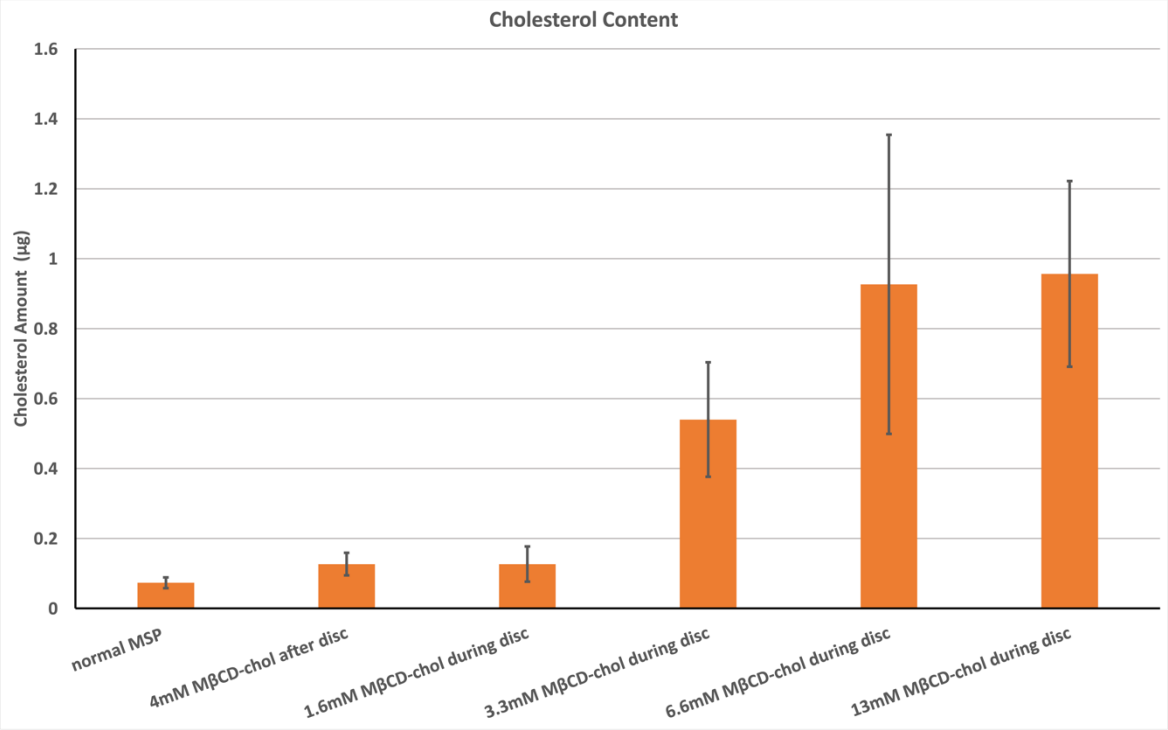


Figure 3.5.1 – Cholesterol content of the MSP2N2 disc upon MβCD-cholesterol application

A plot showing the cholesterol content of MSP2N2 discs under different conditions. Cholesterol enrichment after the disc is already formed is not possible, however, cholesterol levels can be increased linearly with increasing MβCD-cholesterol concentration when enrichment is performed during disc formation. Saturation is achieved roughly at 7mM MβCD-cholesterol.

As shown in Fig3.5.1, the 'standard' MSP discs contain only small amounts of cholesterol (~0.1 µg in 20µL sample), which translates to ~5 molecules of cholesterol per disc. In comparison, nAChR receptors in membranes with low cholesterol content could bind agonist but did not undergo gating motions (Hamouda et al., 2006). Therefore, the amount of cholesterol in our disc may not be sufficient to allow the gating of the receptor. To overcome this problem, I added MβCD-cholesterol after the formation of the disc. However, no substantial increase in cholesterol levels could be observed (Fig. 3.5.1). This implies that MβCD-cholesterol loading could only happen during disc formation. Evidently, the cholesterol levels could be increased substantially when MβCD-cholesterol was added during the disc formation. In the case where 6.6mM MβCD-cholesterol was added, 1µg of cholesterol could be detected in the sample which is a 10-fold increase when compared to the normal prep and translates to ~80 cholesterol molecules in the disc. Importantly, the cholesterol content becomes saturated as adding 13mM MβCD-cholesterol cannot incorporate more cholesterol in the nanodisc (Fig. 3.5.1). It has been estimated that the

number of Dipalmitoylphosphatidylcholine (DPPC) lipid molecules in an empty MSP2N2 disc is ~300 (Grinkova et al., 2010). In the case where a membrane protein is inserted the amount of lipid will dramatically decrease. The $GABA_AR$ can be estimated to take up roughly 1/3 of the nanodisc volume therefore leaving space for ~200 lipids. Since cholesterol has a molecular weight of 386.7g/mol and an 'average' lipid has a molecular weight of ~600g/mol, we can approximate that when 13mM MβCD-cholesterol is added, the concentration of cholesterol is roughly 40-50 mol % of the total lipids which is similar to the amount seen in acetylcholine receptor *Torpedo* membranes (Rotstein et al., 1987).

Having the disc loaded with cholesterol, I proceeded to study the gating motions of the FL α1β3γ2L receptor in such environments. When FL α1β3γ2L are gated by GABA, they desensitize very rapidly. Therefore, I used the general anaesthetics etomidate (ETM) and propofol (PPF) and a 10s ligand application approach described in section 3.3.2 above. ETM and PPF can directly activate the receptor with a slower desensitization rate when compared to 1mM GABA.

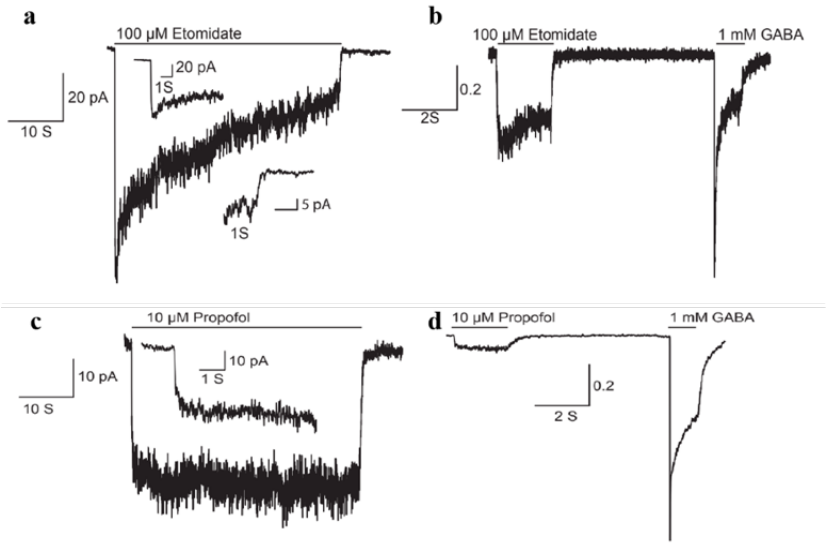


Figure 3.5.2 – Etomidate and propofol directly activate α1β3γ2L $GABA_A$ receptors

a) *A representative current trace evoked by a 40s application of etomidate (100 µM) to outside-out patches. The insets show the activation and closing phases of the current at an expanded scale.* ***b)*** *A representative current trace obtained from outside-out patches with the standard two-pulse protocol. The current trace is normalized to the peak current amplitude obtained with 1mM GABA in the second pulse.* ***c)*** *A representative current trace obtained from a 40s application of 10µM propofol to outside-out patches. The inset shows the activation phase with an expanded time scale.* ***d)*** *Using the standard two pulse protocol with 10µM propofol. The electrophysiology experiments were performed by Rooma Desai, Harvard Medical School.*

Nevertheless, after 10s of ligand application, most of the receptors have already reached steady state so one would expect only a small population of all receptors to be open (Fig. 3.5.2). For each dataset I could separate 2 states – resting and anaesthetic-bound desensitized. Despite extensive 3D classifications and efforts to separate a class in the open state, no such class could be observed (Fig. 3.5.3a,c,e). Surprisingly, I also could not observe density for a cholesterol binding site in the end states of the gating cycle, despite the fact that binding sites have been postulated to exist based on molecular dynamics simulations (Dämgen and Biggin, 2021). Moreover, when I compare the receptor in discs without additional cholesterol and discs where 13mM MβCD-cholesterol is added during disc formation, no major difference can be seen and the Cα RMSDs between the structures were below 0.6 Å (Fig. 3.5.3b,d,f).

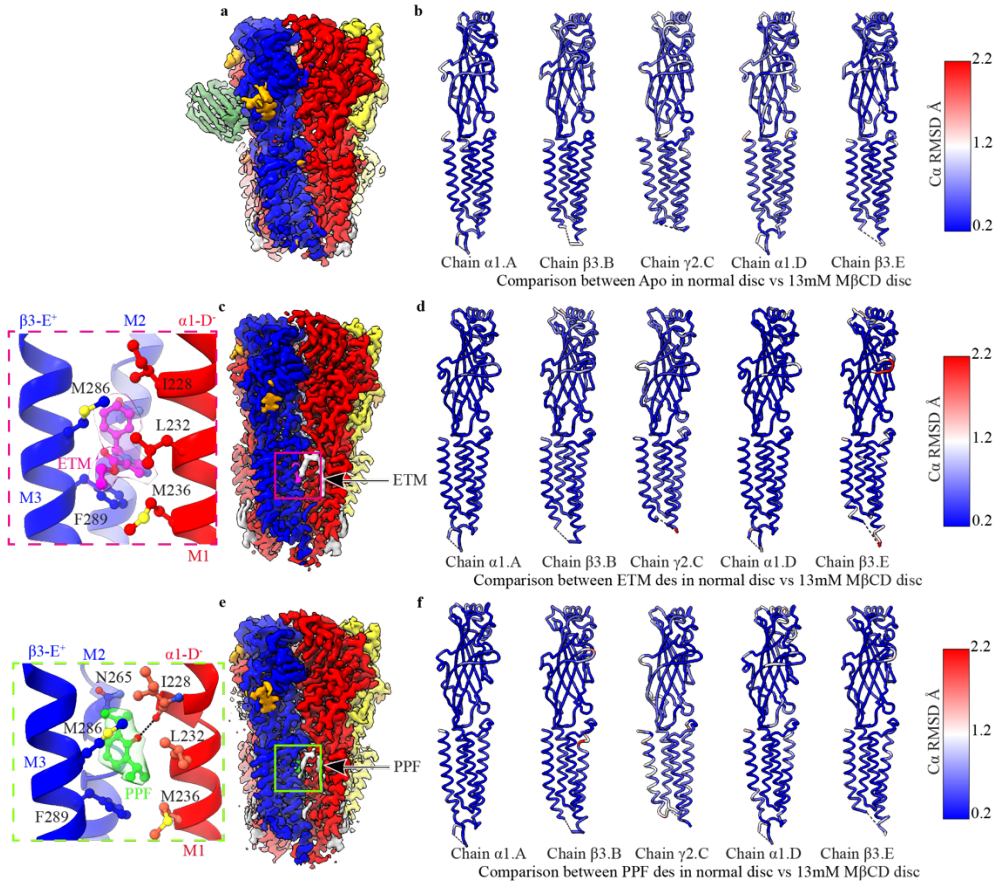


Figure 3.5.3 – The $GABA_A$ receptor in cholesterol-rich nanodiscs

a) *The apo state in cholesterol-enriched disc.* ***b)*** *Cα RMSDs between the apo state in normal MSP disc versus the apo state in cholesterol-enriched MSP discs.* ***c)*** *The desensitized state with ETM bound in cholesterol-enriched disc.* ***d)*** *Cα RMSDs between the desensitized state with ETM in normal MSP disc versus cholesterol-enriched MSP discs.* ***e)*** *The desensitized state with PPF bound in cholesterol-enriched disc.* ***f)*** *Cα RMSDs between the desensitized state with PPF in normal MSP disc versus in cholesterol-enriched MSP discs*

Taken together, this suggests that cholesterol does not directly bind the α1β3γ2L $GABA_A$ receptor and perhaps modulates its function solely through the rigidity of the membrane. Alternatively, cholesterol may be needed for the transition into the open state where it could stabilize newly formed interfaces which are not present in the resting and desensitized states. Such transitions, however, happen on the millisecond timescale, and hence are not sampled with the 10s approach used here and for the GlyR (Mortensen et al., 2004, Yu et al., 2021).

To further determine the physiological significance of the cholesterol enriched disc, I performed mass spectrometry analysis of the lipid contents from nanodisc extracts. As shown in Fig 3.5.4, a large number of lipids with variable acyl-chain length can be detected in our discs. Furthermore, sphingomyelin (SM) seems to be the most predominant lipid present. Since SM is a major component of lipid rafts and it is present in high quantities, together with the physiological cholesterol content upon enrichment, the lipid composition of the nanodiscs appears to be as close to physiological as possible. This further supports the hypothesis that during detergent-solubilization with LMNG, the $GABA_A$ receptors retains an inner layer of lipids emerging directly from the cell membrane (Chapter 3.4).

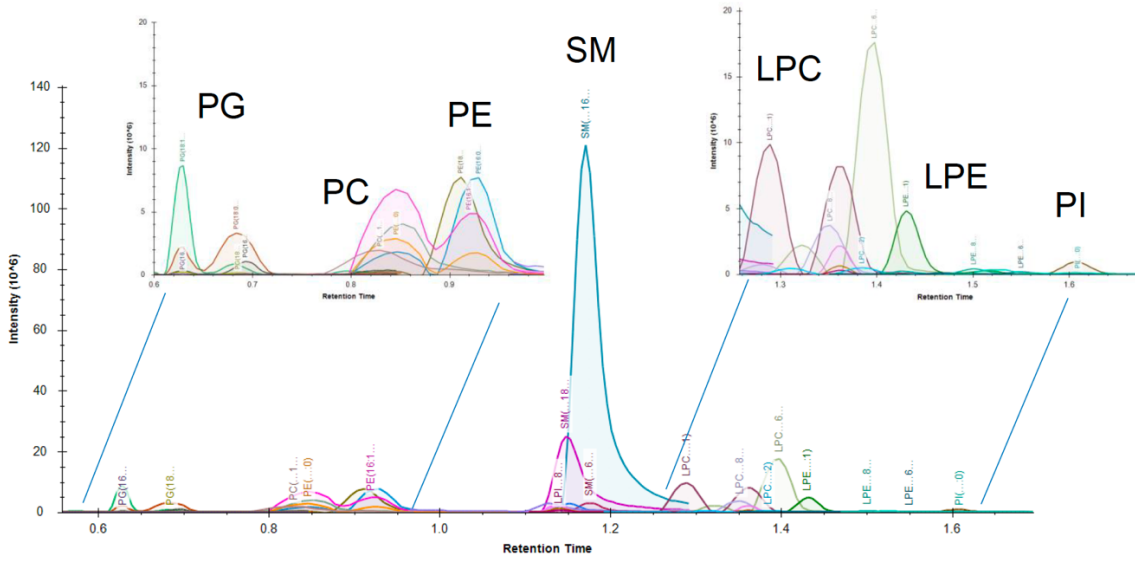


Figure 3.5.4 – Mass spectrometric analysis of nanodisc lipid extracts

Mass spec results of the lipids present in the MSP2N2 nanodiscs. The discs are particularly enriched in sphingomyelin (SM) as well as phosphatidylglycerol (PG), phosphatidylcholine (PC), phosphatidylethanolamine (PE), lysophosphatidylcholine (LPC) and lysophosphatidyethanolamine (LPE) with variable acyl-chain lengths. The experiments were performed by Samantha Ferries and Nyasha Munjoma, (Waters Corp).

3.6 Discussion

All integral membrane proteins carry out their functions within the context of a lipid bilayer. Hence, it is crucial to comprehensively understand the impact of lipids when studying such proteins. For instance, having an incorrect lipid composition for the *Torpedo* nAChR can result in the receptor becoming uncoupled and non-functional. However, in contrast to the nAChR, investigating the signalling mechanism of the $GABA_A$ receptor in its native environment is challenging. This challenge is partly attributed to the absence of a tissue source that expresses large quantities of the receptor, as is the case with the *Torpedo* electric organ. Currently, high-resolution structural analysis in entirely physiological environments would only be feasible through *in situ* cryogenic electron tomography (cryo-ET). However, it is worth noting that this approach is currently limited to large and abundant targets such as the ribosome and viruses (Gemmer et al., 2023, Bharat et al., 2011). While cryo-ET structural studies on $GABA_A$ receptors have been attempted, the achievable resolution thus far is not sufficient to gain insights into the signalling mechanism (Liu et al., 2020). It is therefore important to establish what artificial environment would work best to study the detailed gating motions of $GABA_A$ receptors by high-resolution reconstruction.

In this chapter, I conducted a systematic investigation to assess the impact of different scaffolding proteins within the nanodisc environment. The results clearly demonstrate that when reconstituted in Saposin A or SMALPs discs, $GABA_A$ receptors assumes non-physiological conformations. In both cases, the receptor fails to undergo desensitization in the canonical pseudo-symmetric conformation. The γ2 subunit, in particular, becomes uncoupled, resulting in disrupted contacts between its extracellular and transmembrane domains. Conversely, this uncoupling phenomenon is not observed in MSP2N2 nanodiscs. Consequently, it can be inferred that MSP2N2 represents the optimal scaffolding protein for studying the receptor dynamics within an artificial environment. I further expanded my investigations to explore the impact of disc thickness by altering the acyl-chain length of the lipids incorporated during nanodisc reconstitution. To my surprise, no discernible changes were observed in the receptor's structure, even when the predominant lipid component in the disc was di24:1PC. This finding strongly implies that a significant portion of the lipids present in the discs likely originates directly from the cell, a conclusion supported by mass spectrometry analysis of the nanodisc contents. Furthermore, this is also reinforced by the consistent lipid profile observed in the SMALPs resting state structure (Fig. 3.3.2). Finally, I explored the influence of cholesterol on the $GABA_A$ receptor by enriching the nanodisc

with approximately 50 mol% cholesterol, aiming to closely mimic the actual membrane environment. Intriguingly, no significant structural disparities were detected between the receptor structures within discs with little cholesterol and those within discs with around 50 mol% cholesterol content. Additionally, I could not identify a specific cholesterol binding site within either the resting or desensitized states, suggesting that cholesterol might exert its influence on the receptor indirectly. An alternative possibility is that cholesterol is a requisite component for transitions to the short-lived intermediate states. However, it is important to note that such states could not be observed within the limitations of classical plunge-freezing on a 10-second timescale.

To overcome these limitations, I decided to test open-channel blockers that could stabilize the receptor in an active conformation by using the most physiologically relevant environment for the $GABA_A$ receptor, namely reconstituted in cholesterol-enriched MSP2N2 nanodiscs and supplemented with POPC and bovine brain extract lipid mix.

Chapter IV

Inhibition of synaptic $GABA_A$ receptors by β-lactam antibiotics

4.1 Introduction

$GABA_A$ receptors are crucial for many aspects of animal physiology. Therefore, they are targets for a diverse set of drugs (Sieghart and Savić, 2018). Positive allosteric modulators such as diazepam and alprazolam effectively treat anxiety, epilepsy, and sleep disorders. On the other hand, general anaesthetics, widely used during surgery, can function as both potent allosteric modulators and agonists (Martin and Lowery, 2018, Thompson et al., 1996, Bai et al., 1999a).

The vast allosteric landscape of the $GABA_A$ receptor family, however, also makes it a potent target for noncompetitive antagonists that could lead to unwanted and unpredictable side effects (Olsen, 2018, Cascio, 2006). One such class of molecules are the β-lactam antibiotics, which have been associated with myoclonic jerks and seizures in clinical studies (Meyer, 2014, Sugimoto et al., 2003, Man and Fu, 2015). The first recorded report of neurotoxicity linked to β-lactam antibiotics, which are widely used for the treatment of bacterial infections, dates back to 1945 (Walker et al., 1945). However, mechanistic understanding for these adverse side effects is currently lacking. Nevertheless, electrophysiology experiments have shown that the prototypical β-lactam penicillin G (PenG) can cause severe side effects in the CNS by acting as a channel blocker for the $GABA_A$ receptor (Twyman et al., 1992). This is further supported by evidence for a competitive interaction between PenG and the prototypical channel blocker picrotoxin (PTX) (Bali and Akabas, 2007, Fujimoto et al., 1995, Krishek et al., 1996). At the same time, the mechanisms of PenG and PTX action are different because agonists can dissociate in the presence of PTX but cannot when PenG is bound (Rossokhin et al., 2014, Bali and Akabas, 2007). This is also in line with recent structural data that reports the structure of the α1β3γ2L $GABA_A$ receptor bound to GABA and PTX, where the receptor is reported in a closed state despite the fact that GABA is bound, likely representing an intermediate step before agonist dissociation or alternatively the receptor could be trapped in a pre-active state with agonist bound but the TMD still in the resting state (Masiulis et al., 2019). PenG on the other hand has been proposed to act as an open channel blocker, based on the presence of tail currents upon the termination of co-application of GABA and PenG (Rossokhin et al., 2014).

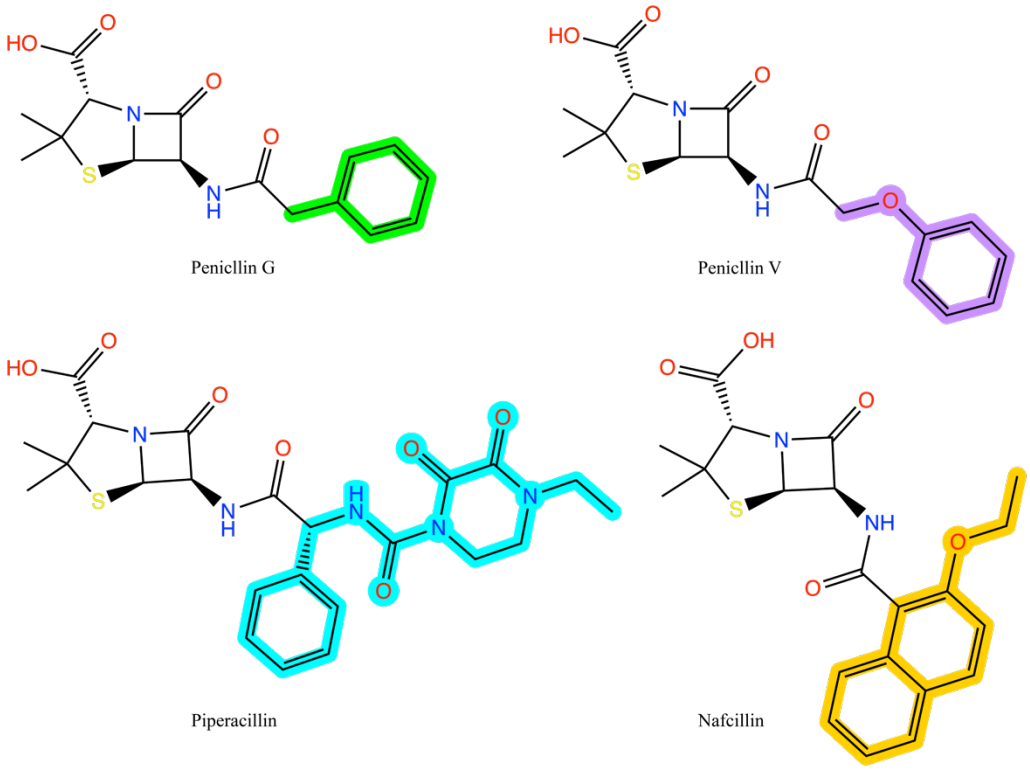


Figure 4.1 – The chemical structures of the different β-lactams associated with neurotoxic effects

The chemical structure of the β-lactams used in this chapter. The variable groups are highlighted in green for penicillin G, purple for penicillin V, cyan for piperacillin and orange for nafcillin

To elucidate the inhibitory effects of β-lactams on GABAergic signalling and their role in the receptor's gating cycle, I conducted structural studies on the synaptic α1β3γ2L $GABA_A$ receptor subtype in complex with four different antibiotics: penicillin G (PenG), penicillin V (PenV), piperacillin and nafcillin along with GABA (Fig. 4.1).

My findings reveal a shared mechanism of channel blocking through binding within the TMD. However, despite their similar chemical structures, the β-lactams exhibit distinct binding modes. Additionally, I demonstrate that nafcillin can both potentiate and inhibit the receptor by binding to the benzodiazepine and general anaesthetic pockets while also blocking the pore. Furthermore, I report a novel receptor state with one β3/α1subunit pair in a rotated conformation, breaking the pseudo-symmetry of the pore. This suggests that the gating motions of $GABA_A$ receptors might include asymmetric intermediate states. However, this state was only observed in the presence of nafcillin and GABA, and not for the other β-lactams tested, indicating that nafcillin has different properties compared to PenG, PenV and piperacillin.

Taken together, the results in this chapter shed light on the mechanisms of $GABA_A$ receptor modulation by β-lactam antibiotics and propose that co-administration of a $GABA_A$ receptor positive allosteric modulator might prevent potential neurotoxic side effects when high-dose β-lactam treatments are required.

4.2 Mechanism of $GABA_A$ receptor inhibition by PenG and PenV co-applied with GABA

I first determined the structure of the benzodiazepine-sensitive α1β3γ2L $GABA_A$ receptor bound to 10mM PenG and 50μM GABA (Fig.4.2). PenG binds lower in the channel pore compared to PTX, obstructing the channel between the -2' and 6' positions of the M2 helices (Fig. 4.2a). This disagrees with previous molecular modelling results, which have predicted that PenG, like PTX, binds between the 2' and 9' M2 levels (Rossokhin et al., 2014). Nonetheless, there is an overlap between the binding sites of PenG and PTX which explains their competitive interaction (Bali and Akabas, 2007). PenG is stabilized in the pore by the formation of putative hydrogen bond interactions with the 6' residues β3Thr256 and γ2Thr271 (Fig. 4.2a). The critical role of β3Thr256 has been previously identified for the mouse β2 gene where the mutation of Tyr256 to Phe greatly reduces the efficacy of PenG channel blocking (Sugimoto et al., 2002). Although the mutational analysis was performed on the mouse β2 gene, it has been previously demonstrated that mouse β subunits can functionally replace human β subunits (Darlison, 1992, Harvey et al., 1991). The PenG benzyl tail is buried in a hydrophobic pocket formed by the 2' and -2' residues and blocks the -2' desensitization gate (Fig. 4.2a). Notably, it has been shown that in the presence of GABA and PTX, the 9' and -2' gates can close, leading to a 'trapped' PTX molecule. However, this cannot happen in the presence of PenG (Fig. 4.2a,c).

Previous reports have suggested that PenG binds to the open state of the channel and stabilizes it, owing to the emergence of tail currents after the co-application of GABA and PenG is terminated (Rossokhin et al., 2014). The conformations I observe, however, are desensitized with an open 9' gate and closed -2' gate with a radius of ~1.5 Å that is too small to permit the passage of a fully dehydrated chloride ion (Fig. 4.2c) (Laverty et al., 2019) and have little deviation to the canonical desensitized state in the presence of GABA alone as judged by the 0.45 Å Cα RMSDs between the five subunits (Fig. 4.5a).

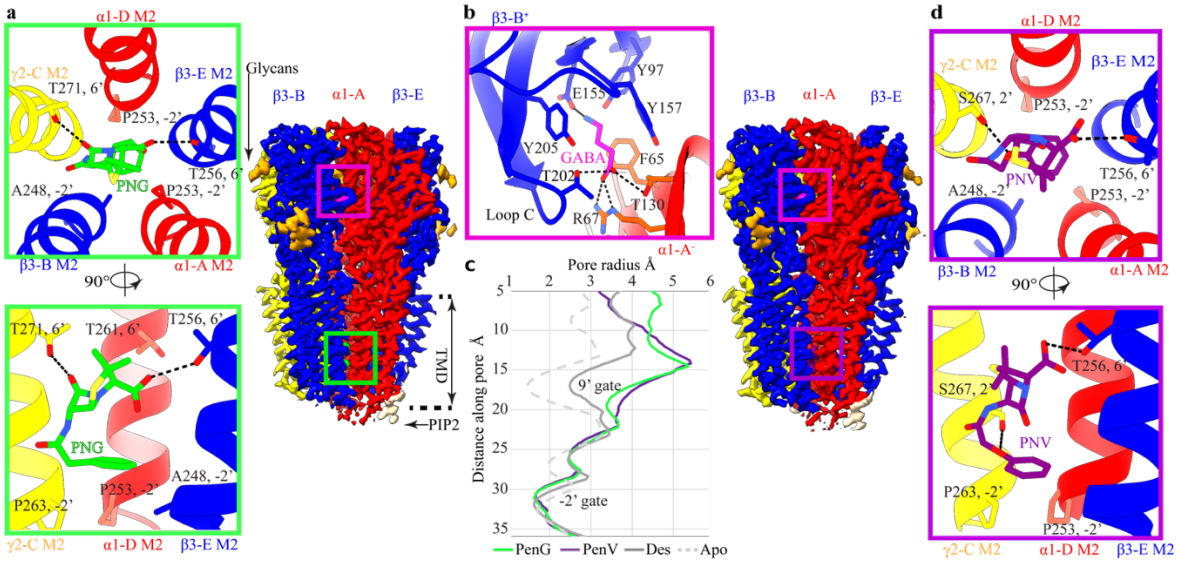


Figure 4.2 – Binding modes of PenG and PenV to the α1β3γ2L GABA$_A$ receptor

a) *The binding mode of PenG (green) in the pore.* ***b)*** *GABA (magenta) bound to the β3$^+$/α1$^-$ agonist binding pockets.* ***c)*** *Pore profiles of the PenG and PenV blocked states generated with HOLE.* ***d)*** *The binding mode of PenV (purple) in the pore.*

Since Penicillin G could not stabilize an open state, I decided to test β-lactams with longer variable groups (Fig 4.1) with the rational that the longer group may protrude past the -2' desensitization state and trap the GABA$_A$ receptor in intermediate, open-like conformations.

I therefore further solved the structure of 10mM PenV in complex with 50μM GABA and surprisingly observed an almost identical binding mode to that of PenG (Fig. 4.2d). The similar binding modes of these molecules perhaps arises through the flexibility of the phenoxymethyl group in PenV, which allows the benzyl ring to occupy the same hydrophobic pocket (Fig. 4.2a,d). PenV is stabilized in the pore through the formation of putative hydrogen bonds with β3Thr256 and γ2Ser267 and just like PenG binds in the region between the -2' and 6' M2 levels. The receptor, however, again adopts a desensitized conformation as determined by the pore radius and the Cα RMSDs which deviated by 0.5 Å when compared to the canonical desensitized state (Fig. 4.2c, Fig. 4.5b).

4.3 Differential blocking properties of piperacillin

To further understand the mechanism of action of β-lactam antibiotics on GABA$_A$ receptors I sought to solve the structure of a penicillin with a longer and bulkier variable group – namely piperacillin (Fig. 4.1). It has been reported that the administration of piperacillin could lead to neurotoxicity manifested by slurred speech, mental confusion and seizures with neurotoxic side effects present in 50% of patients where high dose of piperacillin is

required (Roger and Louart, 2021, Malanga et al., 1997, Lin et al., 2007, Meyer, 2014). These high doses be as high as 10g of piperacillin (Lin et al., 2007). Despite these adverse side effects, little is known regarding its mode of action. To address this issue, I solved the structure of the α1β3γ2L $GABA_A$ receptor bound to 10mM piperacillin and 50μM GABA (Fig. 4.3).

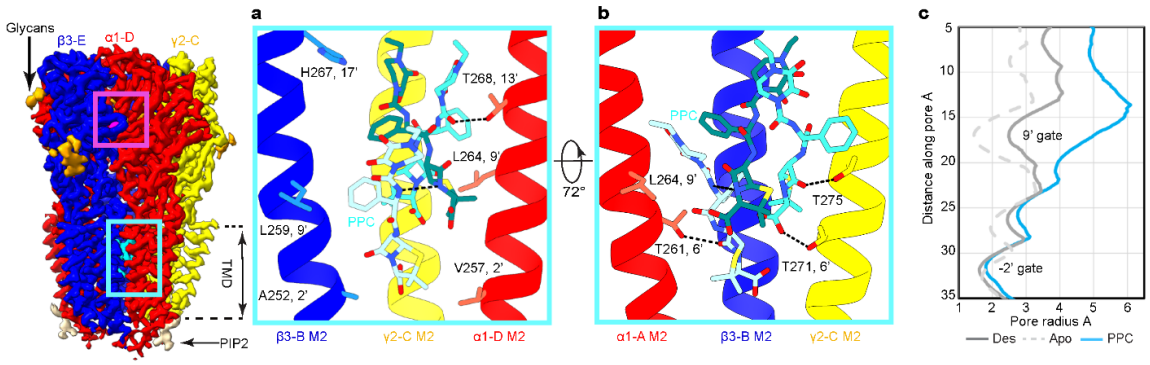


Figure 4.3 – Mechanism of channel block by piperacillin.

a,b) *The binding mode of piperacillin in the pore (cyan; the three molecules are coloured in different shades of cyan for representation purposes);* ***c)*** *Pore profiles of the Piperacillin blocked state*

Strikingly, the piperacillin binding mode is completely different to that of PenG and PenV. Specifically, I could identify three prominent piperacillin densities inside the channel pore stretching from the 2' ring all the way to the 17' level. The molecules are stabilized by a putative hydrogen bond network between α1Thr268-D, α1Thr261-A, γ2Thr275, γ2Thr271 and the oxygen atoms of the penicillin and dioxopiperazine groups. The hydrophobic benzyl rings of piperacillin form π-stacking interactions between themselves or are buried at the hydrophobic interface between the γ2L and α1 subunits (Fig. 4.3a,b). Notably, the presence of the 4-ethyl-2,3-dioxopiperazin group in piperacillin leads to the adoption of a different binding mode but not to a change in function. Piperacillin is a channel blocker despite the chemical difference to PenG and PenV thus illustrating yet again the vast allosteric landscape of the $GABA_A$ receptor. Furthermore, analogous to the PenG and PenV bound structures, the piperacillin bound receptor also adapts a desensitized state with the narrowest point of the pore at the -2' desensitization gate and 0.7 Å difference in the Cα RMSDs compared the desensitized state with GABA alone (Fig. 4.3c, Fig. 4.5c).

4.4 Nafcillin is a multi-site allosteric modulator of the α1β3γ2L $GABA_A$ receptor

To further test the role of the variable group of the β-lactam antibiotics I next explored the binding mode of nafcillin at 3mM concentration. Nafcillin crucially is also a potent

neurotoxic agent (Meyer, 2014). In contrast to PenG, nafcillin harbors an ethoxy-naphthoyl group instead of a benzyl group but keeps its hydrophobic properties thus perhaps allowing it to protrude past the -2' gate and into the cytoplasmic space (Fig. 4.1).

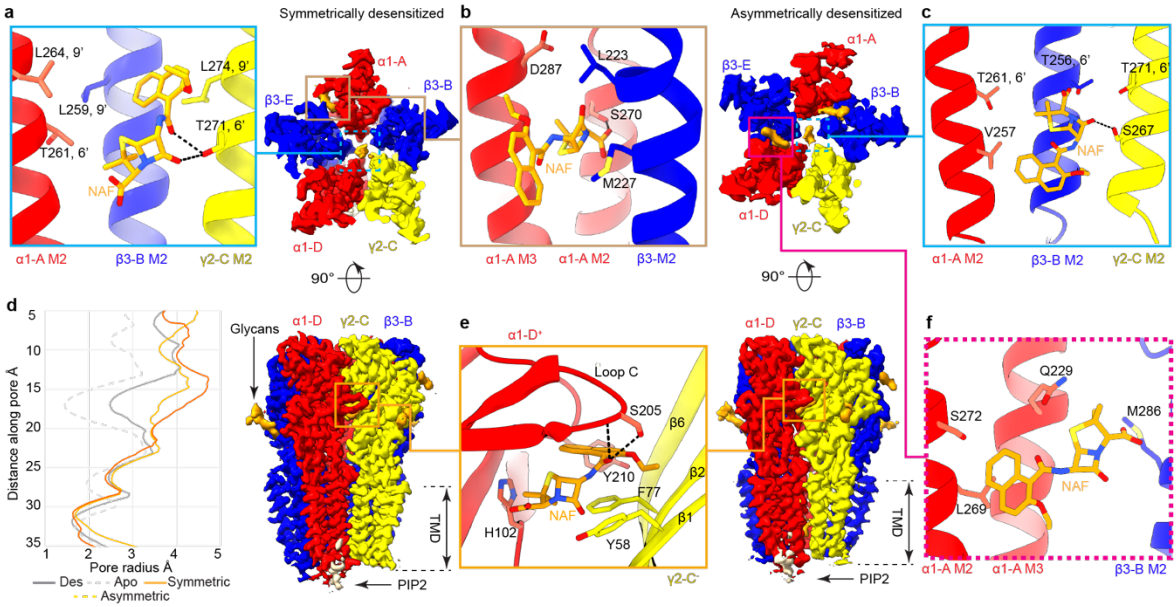


Figure 4.4.1 - Nafcillin binding sites in the symmetrically and asymmetrically desensitized states

a) *The binding mode of Nafcillin in the pore of the symmetrically desensitized state.* ***b)*** *Binding pocket at the $\alpha1^{+}/\beta3^{-}$ TMD interface in the symmetric state.* ***c)*** *Pore binding mode in the desensitized asymmetric state.* ***d)*** *Pore profiles of the symmetric and asymmetric states.* ***e)*** *Nafcillin binding the benzodiazepine pocket of both states.* ***f)*** *The $\beta3^{-}/\alpha1^{+}$ TMD binding site in the asymmetric state.*

Following an exhaustive 3D classification of the cryo-EM dataset, I detected the manifestation of two discrete states – symmetrically desensitized and asymmetrically desensitized. Importantly, the emergence of these states synchronizes with the interaction of nafcillin at distinct binding sites within the channel pore, as well as discrete pockets within the $\beta3^{+}/\alpha1^{-}$ TMD interfaces that are known binding sites for a diverse set of general anaesthetics (Kim et al., 2020) (Fig. 4.4.1).

In the symmetrically desensitized state, nafcillin binds inside the channel pore, situated between the 6' and 13' M2 levels. This engagement is stabilised by putative hydrogen bond interactions with γ2Thr271. Notably, the orientation of the penicillin ring is directed toward the intracellular side, while the hydrophobic ethoxy-naphthoyl group assumes a position facing the extracellular environment, surrounded by the 9' Leu residues (Fig. 4.4.1a). Within this state, nafcillin additionally binds at the interface of the $\alpha1^{+}/\beta3^{-}$ TMD, in the same pocket as the general anaesthetic 4-benzoyl-propofol (Jayakar et al., 2019). In this context, the

ethoxy-naphthoyl moiety of nafcillin projects into the hydrophobic lipid surroundings, achieving stability within the pocket through multiple hydrophobic interactions and a putative hydrogen bond with α1Ser270 (Fig. 4.4.1b).

Surprisingly, in the asymmetrically desensitized state, the pore binding mode of nafcillin is completely different to that of the symmetrically desensitized. In this state, the ethoxy-naphthoyl group faces the intracellular side, protrudes past the -2' gate and forms a putative hydrogen bond with γ2Ser267 (Fig. 4.4.1c). Even though I could separate two distinct states, the pore radius at the -2' gate in both remains too narrow to allow the passage of chloride ions suggesting they are both desensitized (Fig. 4.4.1d). Furthermore, the subunits in the symmetric desensitized state reported do not deviate from the conformation observed in the 'canonical' desensitized state (Masiulis et al., 2019). However, the α1-A and β3-B subunits of the asymmetric state adopt novel conformations (Fig. 4.4.2a-b, Fig. 4.5d-e). Nafcillin is also present in the benzodiazepine pocket at the $\alpha1^{+}/\gamma2^{-}$ ECD interface in both states, stabilized by hydrogen bonds with α1Thr207 and γ2Tyr58. The ethoxy-naphthoyl on the other hand lies in a hydrophobic pocket formed by α1Tyr160 and γ2Phe77 (Fig. 4.4.1e). Intriguingly, nafcillin does not bind $\alpha1^{+}/\beta3^{-}$ TMD interface in the asymmetrically desensitized state. However, I observe two unambiguous densities corresponding to the β-lactam at the $\beta3^{+}/\alpha1^{-}$ TMD interfaces, in pockets where the general anaesthetics etomidate and propofol have been shown to bind (Forman and Miller, 2011, Kim et al., 2020).

In contrast to etomidate and propofol, however, nafcillin binds further inside the anaesthetics pocket with the ethoxy-naphthoyl sandwiched between the $\beta3^{+}/\alpha1^{-}$ M2 helices and is held in place mainly by hydrophobic interactions (Fig. 4.4.1f). Taken together this suggests that nafcillin could both potentiate the receptor through binding pockets usually occupied by positive allosteric modulators and inhibit it by blocking the pore. The occupancy of these pockets is importantly state dependent.

The nafcillin-bound asymmetrically desensitized state provides a hint that the gating cycle of the $GABA_A$ receptors may include asymmetric steps, such as the partial rotation of a β3/α1 pair reported here (Fig. 4.4.2a,b). The state arises from an overall translation and rotation of the β3-B/α1-A module, consisting of two subunits.

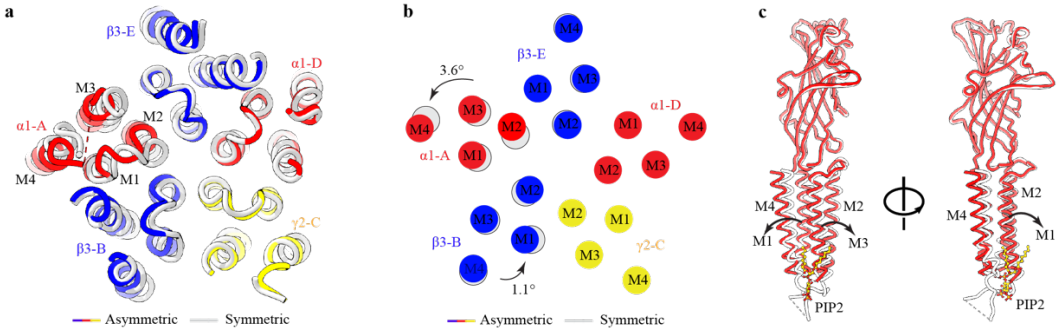


Figure 4.4.2 – Comparison between the symmetric and asymmetric states.

a) *Comparison between the asymmetric state (coloured) and the symmetric state (grey) as view from the intracellular region.* ***b)*** *Representation of the helices and their overall rotation in asymmetric state compared to the symmetric state at the level of the 9' activation gate as seen from the intracellular region.* ***c)*** *Comparison between the overall differences between α1.D in the symmetric and asymmetric states, showcasing the more discorded ICD and lack of PIP_2 in the asymmetric state.*

By comparing the Cα R.M.S.D of the α1-A in the asymmetrically desensitized receptor to the 'canonical' desensitized state, it is evident that the α1-A subunit undergoes the most significant changes (Fig. 4.5e), displaying clear 3.6° rotation and translation of the four-helical bundle. The β3-B subunit also experiences a 1.1° rotation (Fig. 4.4.2b). The rest of the subunits are already desensitized and arranged symmetrically around the central pore (Fig. 4.4.2b, Fig. 4.5e). Moreover, the ICD of α1-A is more disordered than in the 'canonical' apo and desensitized states which coincides with the binding site of PIP_2. In the asymmetric state conformation, importantly, PIP_2 is no longer resolved which implies that the lipid may play a role in controlling the rate of opening and overall receptor motion by structuring the α1 M3-M4 intracellular loop and enabling its interaction with the β3 ICD (Fig. 4.4.2c). Notably, the resolved part of the ICD region of the asymmetric α1-A is shorter since it is only structured when PIP_2 is present further implying that PIP_2 is not bound in the asymmetric state.

4.5 Discussion

In this chapter I present cryo-EM structures of the synaptic α1β3γ2L $GABA_A$ receptor bound to four different β-lactams in the presence of GABA. I show that the β-lactams share the same mechanism of inhibition of $GABA_A$ receptor currents by binding to the pore and blocking the influx of chloride ions. Surprisingly, despite the shared mechanism between these molecules, they have different binding modes. This change is dictated by the presence of variable groups attached to the penicillin ring that have an impact on the binding site but not on their function as channel blockers. For PenG and PenV I identify one unambiguous

density deep in the channel's pore between the -2' and 6' levels. In contrast to PenG and PenV, piperacillin has three binding sites in the pore stretching all the way between the 2' and 17' level and completely blocking the pore. These structures, however, are desensitized as judged from the pore profiles and Cα RMSDs values relative to the 'canonical' desensitized state (Fig. 4.5a-d).

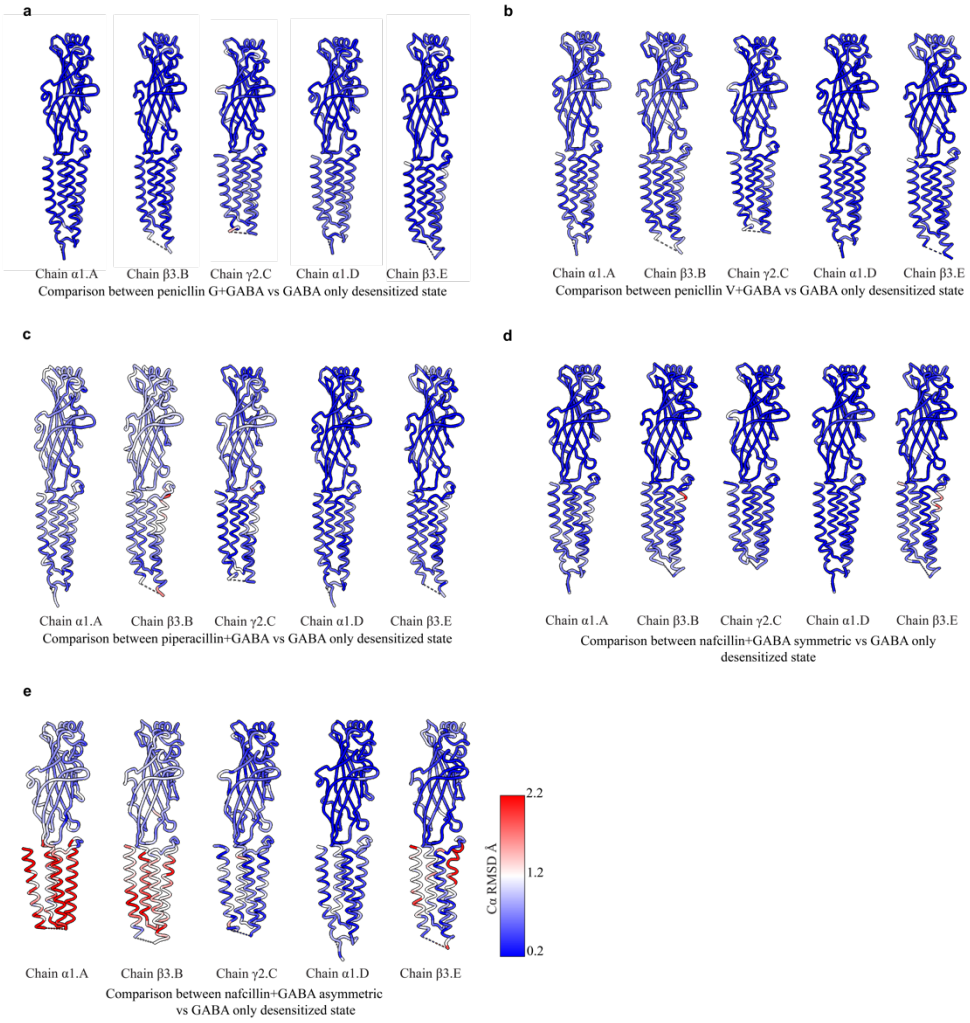


Figure 4.5 - Cα RMSDs between β-lactams plus GABA bound and GABA only bound receptors

a) *Cα RMSDs between PenG+GABA and GABA only states.* ***b)*** *Cα RMSDs between PenV+GABA and GABA only states.* ***c)*** *Cα RMSDs between piperacillin+GABA and GABA only states.* ***d)*** *Cα RMSDs between nafcillin+GABA symmetric and GABA only states.* ***e)*** *Cα RMSDs between nafcillin+GABA asymmetric and GABA only states*

These results appear to contradict the electrophysiology experiments which propose that PenG binds and stabilizes the receptor in the open state (Rossokhin et al., 2014). This discrepancy could be explained by the fact that when PenG is bound, agonist dissociation is precluded. Thus, during the wash out of both GABA and PenG, PenG dissociates first due

to its high on and off rates while GABA may remain bound allowing the receptor to open (Chow and Mathers, 1986, Twyman et al., 1992). Another possibility is that PenG binds both the desensitized and open states without interfering with the conformational dynamics of the receptor during the gating cycle. The observed tail currents therefore may arise from receptors that have reached steady-state and become unblocked after the PenG wash out.

I further determined the structure of α1β3γ2L $GABA_A$ receptor bound to nafcillin and GABA. Unexpectedly, I could separate two distinct conformational states from this dataset – asymmetrically and symmetrically desensitized. The fact that nafcillin binds to the benzodiazepine pocket as well as pockets usually occupied by general anaesthetics, in addition to blocking the channel pore, suggests that it can play a dual allosteric role i.e. simultaneously potentiating and inhibiting the receptor. The major motion in the asymmetric state occurs for α1-A subunit, which moves away from the β3-E subunit. This is triggered by the overall rotation of the β3-B^+/α1-A^- pair which harbours the GABA binding site. This suggests that GABA binding to the ECD can lead to the overall movement of the β3-B^+/α1-A^- pair as a cohesive unit. The remaining subunits have already transitioned into a 'canonical' desensitized conformation, as indicated by their Cα RMSD compared to the desensitized receptor (Fig. 4a, b, Fig. 4.5). Intriguingly, PIP_2 is not resolved in the asymmetric α1-A subunit (Fig. 4c). This implies that PIP2 may indeed play a role in the gating the $GABA_A$ receptors, as previously proposed (Laverty et al., 2019, Masiulis et al., 2019).

The emergence of the asymmetric state can occur through one of two mechanisms - either the binding of nafcillin disrupts the receptor and induces the conformation, or nafcillin binds to the receptor when it is already in this conformation. I propose that this conformation represents an open-like state of the β3-B^+/α1-A^- pair, while the remaining subunits adopt a desensitized state. The observed state represents a two-subunit asymmetric intermediate, suggesting that gating may propagate through pairwise movements of β3-B^+/α1-A^- pair, consistent with the number of agonist pockets. This further implies that the fifth subunit in the ensemble may move independently of the two β3/α1 pairs. Moreover, single channel recordings indicate that the channel can assume at least two open and four desensitized states at saturating GABA concentration (Mortensen et al., 2004). This finding provides additional evidence supporting the hypothesis of such gating intermediates. Hence, it is likely that nafcillin binds to the receptor when it is in the open state; however, it prevents the desensitization of the β3-B^+/α1-A^- module. Interestingly, in the asymmetrically desensitized

state, the -2' gate remains too narrow for chloride ion permeation, indicating that one two-subunit pair in an open-like conformation is not sufficient to activate the receptor.

It is worth noting that this particular conformation has not been observed in other open state structures proposed for other pLGICs. For the 5-HT_{3A} serotonin receptor, α7 nicotinic acetylcholine receptor and glycine receptors no such pronounced rotation of the subunits is evident, which suggests that these conformational changes may be unique to the $GABA_A$ receptors (Zhang et al., 2021b, Yu et al., 2021, Noviello et al., 2021). In the case of the 5-HT_{3A} serotonin receptor, the authors report an asymmetric gating cycle with conformation that appears different to the one I observe. However, structures obtained in the nanodisc scaffolding protein Saposin A should be considered with caution because they are likely non-physiological, as discussed in Chapter III.

Nonetheless, I cannot disregard the possibility that the nafcillin asymmetric state may arise from the binding pocket occupied by the β-lactam, which could potentially interfere with the structural integrity of the β3-B/α1-A pair and induce the conformational change observed. Therefore, in order to fully interpret the results I have presented, it is crucial to obtain structures of a $GABA_A$ receptor in open states. Electrophysiological experiments suggest that the transitions between these states are of very short durations and several distinct open states may exist (Macdonald et al., 1989, Chakrapani and Auerbach, 2005). Capturing the open states using the currently available structural techniques poses a challenge due to their transient nature. To overcome this, time-resolved cryo-electron microscopy is required. I will discuss this approach in detail in Chapter V.

The structures I report are complexes with four β-lactams heavily used in the clinic which have been shown to cause myoclonic jerks, convulsions and seizures in patients by various clinical studies. Therefore, these structures may provide useful information for the generation of anti-microbials that will not have a negative impact on the inhibitory neurotransmission mediated by the $GABA_A$ receptors. Furthermore, I propose that when a high dose β-lactam therapy is required, a $GABA_A$ receptor positive allosteric modulator such as benzodiazepines could be co-administered to reduce neurotoxic side effects.

Chapter V

Structural dynamics of $GABA_A$ receptor gating on the millisecond timescale

5.1 Introduction

All pLGICs have evolved to transmit signals in a quick and timely manner (Salari et al., 2014). Upon agonist binding, the channel opens briefly and desensitizes quickly on the millisecond timescale as shown by single-channel recordings (Mortensen et al., 2004). Generally, the activation mechanism of the Cys-loop receptor family is described through the Monod–Wyman–Changeux (MWC) model for allostery (Monod et al., 1965). The model is widely accepted due to the fact that there are two or more orthosteric ligand binding sites, which have been proposed to work cooperatively based on electrophysiological analyses (Mozrzymas et al., 2003a).

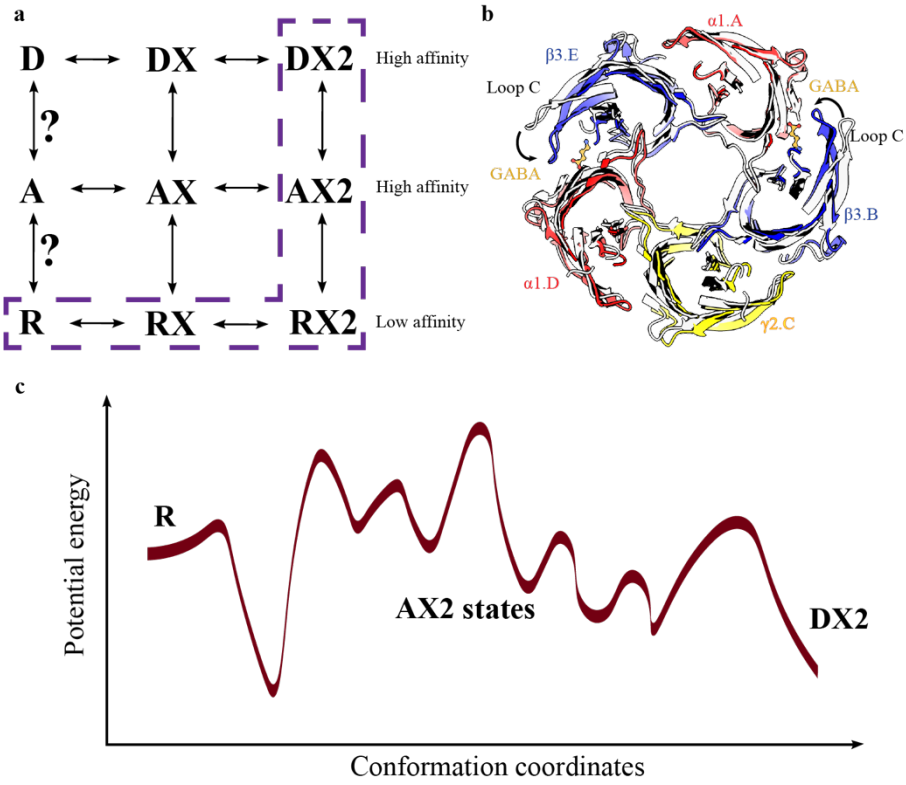


Figure 5.1 – The MWC model and energy landscape of $GABA_A$ receptor gating

a) *The MWC model for channel activation where X is ligand, R is resting state, A is active state and D is desensitized state, upon exposure to non-saturating ligand concentrations, the receptor can go through RX to AX and finally DX. When saturating concentrations of ligand are present the receptor will follow the encircled in purple dashed line pathway. Some receptors have also been observed to gate spontaneously in the absence of ligand depicted with question marks on the scheme.* ***b)*** *The conformational changes of the ECD of the full-length α1β3γ2L upon GABA binding. The ECD undergoes an iris-like motion with the closure of loop C contracting the ECD and an overall anti-clockwise rotation takes place.* ***c)*** *A schematic energy diagram of the $GABA_A$ receptor gating cycle. The presence of agonist would lower the activation energy required for entry into the active states.*

The general scheme for Cys-loop channel gating starts with the resting state (R) where no ligand is bound. The affinity for ligand in this state is low and the state is considered to be generally stable (Fig. 5.1 a,c) (Gonzalez-Gutierrez et al., 2017). Upon ligand binding, the receptor enters the high-affinity state which is associated with the closure of loop C and the unblooming of the ECD. As viewed from the extracellular side, the receptor's ECD works analogous to an iris. In the resting state the ECD is dilated, however, upon agonist binding the ECD constricts, and the receptor enters the high-affinity state (Fig 5.1b). This is associated with the activation of the channel which now enters the active i.e. open state (A), where several local minima and distinct active states could be present (Fig. 5.1c). It is important to note that a further state between the resting and active is postulated to exist, termed pre-active or 'flipped' with the ECD bound to agonist but the TMD still in the resting state, depicted as RX_2 in the MWC scheme described in Fig 5.1c (Gielen and Corringer, 2018). Soon after the receptor activates, it quickly enters the high affinity desensitized (D) state with the -2' gate closed and the channel non-conducting, which is the most thermodynamically stable state. Importantly, at high GABA concentrations, the receptor would only undergo the transitions highlighted in the dashed area in Fig 5.1c with both GABA pockets fully occupied. Nevertheless, single-channel experiments have shown that several active and desensitized states are associated with the gating of the channel (Mortensen et al., 2004). The conformational changes between these states, however, are extremely rapid and as of yet not structurally characterized.

Due to the transient nature of the transitions during the activation of pLGICs, it is impossible to obtain structural insights into their gating cycle in timescales several orders of magnitudes longer than a few milliseconds. There have been many structural studies which propose to have solved an open channel state for a range of pLGICs as well as different timescales ranging from days (Hilf and Dutzler, 2009), hours (Zhang et al., 2021b, Noviello et al., 2021) to several seconds (Yu et al., 2021). Nevertheless, such states make little to no physiological sense as the channels would have entered the last desensitization state in a fraction of the time for all of the above examples. The emergence of such states is therefore likely stemming from the fact that the channels are reconstituted in non-physiological conditions therefore implying that the open states observed are also different to what actually happens *in vivo* (discussed in more detail in Chapter III). It is therefore important to determine the gating cycle of such channels in a physiologically meaningful timescale and environment. Such studies have been performed previously for the *Torpedo* nAChR in a native membrane by

Nigel Unwin and colleagues (Berriman and Unwin, 1994, Unwin, 1995, Unwin and Fujiyoshi, 2012), where an asymmetric gating cycle for the nAChR when imaged after ~5ms ligand exposure was reported. I therefore sought to determine the gating motions of the $GABA_AR$ using this approach.

5.2 Experimental setup and considerations

The experimental setup was similar to that described previously (Berriman and Unwin, 1994), with the grid placed 3.5cm above the liquid ethane level and an atomizer spray adjusted to ~0.5cm above the surface of the ethane (Fig. 5.2.1). The atomizer sprayer generates a jet of small droplets containing the ligand which is controlled by an optical switch at the top of the plunger. Using Newton's law of gravity one can calculate how long it takes for the grid to plunge: $d = \frac{1}{2}gt^2$, where d is the distance the object has to travel, g is the gravitational constant of 9.8m/s^2 and t is the time it takes to travel the distance.

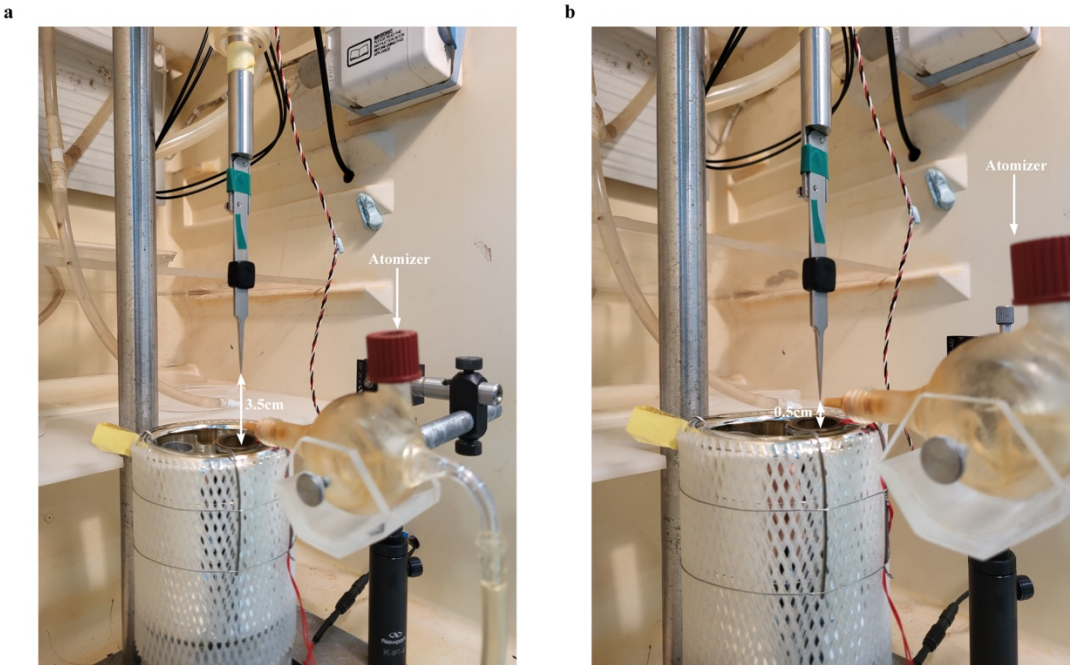


Figure 5.2.1 – Experimental setup

a) *The grid is placed 3.5cm above the surface of the ethane and the atomizer aligned in such a way that the grid passes through the middle of the ligand droplets.* ***b)*** *The atomizer is placed ~0.5cm above the ethane's level ensuring 10ms ligand exposure.*

Therefore, at free fall from 3.5cm the grid will be plunged in 84ms. Since the sprayer is located 0.5cm above the ethane's surface, the grid will reach the spray droplets in 76ms. This therefore limits the exposure to the ligand to ~10ms. The resulting droplets on the grid varied in size but generally had a radius of around 2-5 μm (Fig. 5.2.2a-b). When 2mg/mL

ferritin, chosen for the fact that it has an iron core readily detectable via electron microscopy, was added to the ligand, one could observe it diffusing to the edge of the droplet where the ice is still substantially thick (Fig. 5.2.2a-b). This limits the achievable resolution by cryo-EM due to fact that more inelastic scattering takes place (Dickerson et al., 2022). To overcome this, one has to collect data just next to the ligand droplet. Nevertheless, since GABA is smaller, it will diffuse further due to its larger diffusion coefficient, $D_{GABA} = 0.8$ $\mu m^2/ms$ (Rusakov et al., 2011, Longsworth, 1953), whereas $D_{ferritin} = 0.01$ $\mu m^2/ms$ (Berriman and Unwin, 1994, Clough and Michel, 1981). To determine the concentration of the diffusible molecule, one can use the equation for diffusion from a cylindrical source such as the sprayed ligand droplet (Crank, 1979).

$$C = \frac{C_0}{2Dt} e^{(-r^2/4Dt)} \int_0^a e^{(-r'^2/4Dt)} I_0\left(\frac{rr'}{2Dt}\right) r' dr'$$

In this equation C is the final concentration of the ligand, C_0 is the initial concentration of the ligand, t is the time for diffusion, in this case 10ms, D is the diffusion constant of the molecule, r is the total diffusible distance from the center of the droplet and a is the initial radius of the droplet. This equation was fitted to the available experimental data for ferritin and falls well in line with it (Berriman and Unwin, 1994). Since the ice is only thin immediately next to the droplet and the droplets differ in size, the concentration of GABA will also differ. The ice thickness where one can perform high resolution imaging is optimal at a range between 1μm to 3μm away from the edge of the droplet (Fig. 5.2.2b). Therefore, in the case of a small droplet with radius a = 2μm, the concentration of GABA at 1μm to 3μm away will range from $0.06 \times C_0$ to $0.02 \times C_0$. Moreover, the further one collects from the center of the droplet, the lower is the exposure time to the ligand allowing a temporal resolution of 2ms or less. As the droplet becomes larger, the concentration of GABA near the droplet also increases and a droplet with a radius of 5μm will therefore have $0.3 \times C_0$ to $0.1 \times C_0$ of GABA immediately next to it (Fig. 5.2.2c). Moreover, this also assumes diffusion in 3D space which is not the case for a grid. On a grid, the ligand also has to diffuse over the carbon support which is covered by a thin layer of liquid. What is more, this also assumes the source to be cylindrical which is not the case. Lastly, the droplet is flying at high speeds, therefore upon impact the liquid can first expand and then retract which may further limit the diffusion of GABA. Importantly, when 1M NaCl was used in the spraying mix with erythrocyte bodies as osmotic detectors, NaCl diffused only 3μm further than ferritin for a

droplet with a 2µm radius (Berriman and Unwin, 1994). Na^{2+}, however, has a larger diffusion coefficient than GABA hence GABA will diffuse slower. Therefore, to ensure an optimal concentration of agonist regardless of the size of the droplet that would lead to a maximal P_{open} of the channel, I used between 100mM and 300mM of the ligand of choice for spraying.

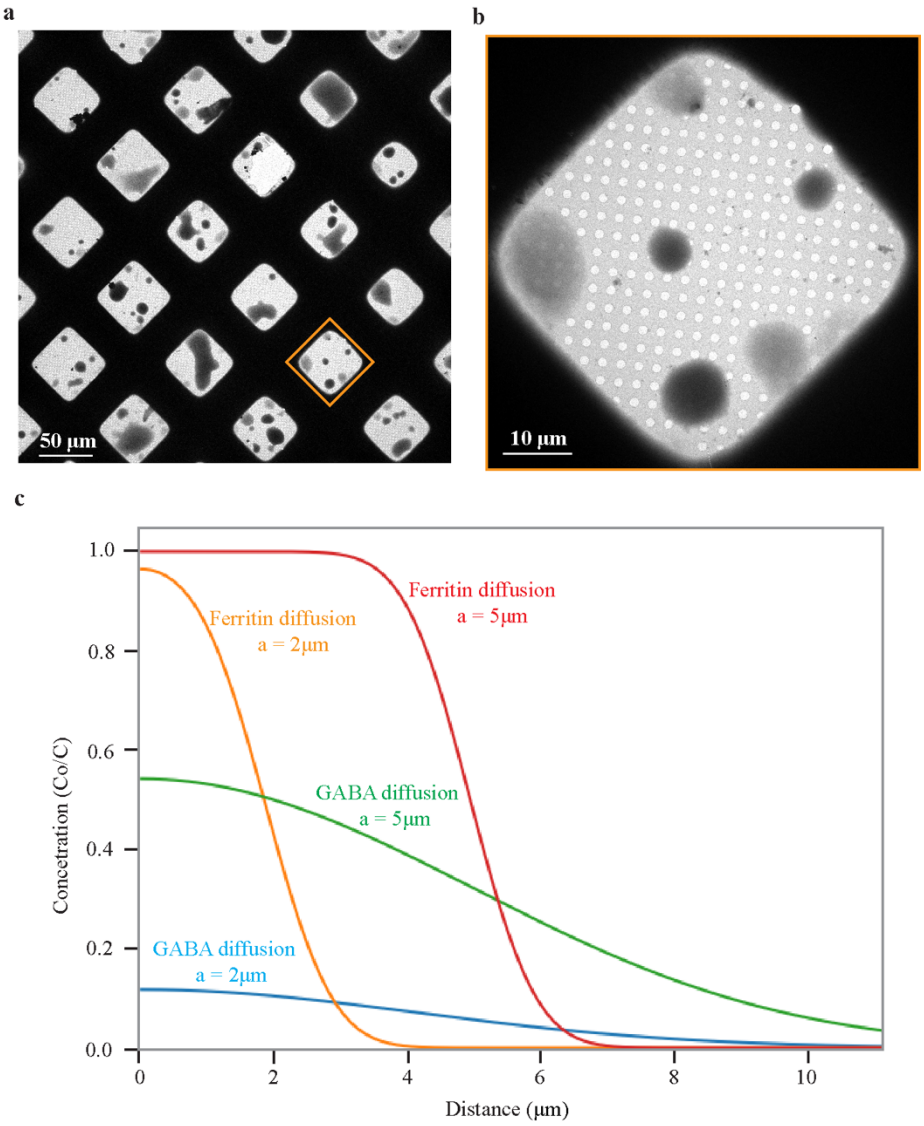


Figure 5.2.2 – Spray distribution and ligand diffusion

a) *A representative image at atlas magnification showing the spray distribution across the whole grid. All dark spots on the gridsquares are ligand droplets.* ***b)*** *A zoom-in image of a gridsquare with 6 distinct ligand droplets ranging in radius from 2 to 5 µm.* ***c)*** *Plot using the equation for diffusion from a cylindrical source of radius 2 µm and 5 µm for both ferritin and GABA and diffusion time of 10ms. The concentration of ferritin drops sharply with distance whereas the concentration for GABA decreases more gradually. The calculations and plots discussed here were done in collaboration with Dr. Katerina Naydenova, MRC LMB.*

5.3 The β3 homomeric $GABA_A$ receptor gates through asymmetric short-lived intermediate states

The $GABA_A$ receptor forms pentameric channels consisting of five subunits, and the complexity of these pentamers, as well as the pharmacological modulation they undergo, can be finely tuned by variable subunit composition (Sente et al., 2022). This versatility allows $GABA_A$ receptors to take on different configurations, such as homomers (Miller and Aricescu, 2014), diheteromers (Kasaragod et al., 2022), triheteromers (Sente et al., 2022, Masiulis et al., 2019, Laverty et al., 2019) and even tetraheteromers (Sun et al., 2023). By assembling from different subunits, these receptors alter their signalling landscapes, introducing an added layer of complexity to their gating mechanisms.

For instance, in the case of the α1β3 diheteromer, single-channel electrophysiology studies have revealed the presence of at least two open state and three desensitized states (Kasaragod et al., 2022). In contrast, the α1β3γ2 triheteromer demands at least two open and four desensitized states to accurately fit the exponential curves in single-channel recordings (Mortensen et al., 2004). Therefore, as the number of different subunits in the assembly increases, so does the intricacy of the receptor's gating cycle. To investigate the disparities in gating behaviors among these diverse ensembles, I initially focused on the simplest receptor type: the truncated β3 homomer, which is activated by the neurotransmitter histamine (HSM) (Miller and Aricescu, 2014, Nakane et al., 2020). The reason for choosing the truncated subunit is that the full-length β3 homomer tends to aggregate on the EM grid and requires substantially longer data collection. Notably, since the receptor is a homomer it has a five-fold symmetry in respect to the center of the pore. Upon spraying the β3 homomer with the agonist HSM, I determined six distinct states with spatial resolution ranging from 3.5 Å to 2.5 Å and temporal resolution better than 10 ms. These included the canonical apo state and the desensitized state, both of which displayed perfect five-fold symmetry. Additionally, a state emerged where the ECD was in the activated state, with loop C closed and HSM bound, while the TMD remained in the resting state, and this structure too exhibited five-fold symmetry. This likely represents the pre-active state of the receptor, denoted as RX_2 in Figure 5.1a, and its determination was facilitated by the high temporal resolution of the millisecond-scale experimental setup. Importantly, in contrast to α1β3γ2 heteromer, which has a single activation gate at the 9' level, the β3 homomer introduces an additional gate at the 17' position, formed by His 267 (Fig. 5.3.1b).

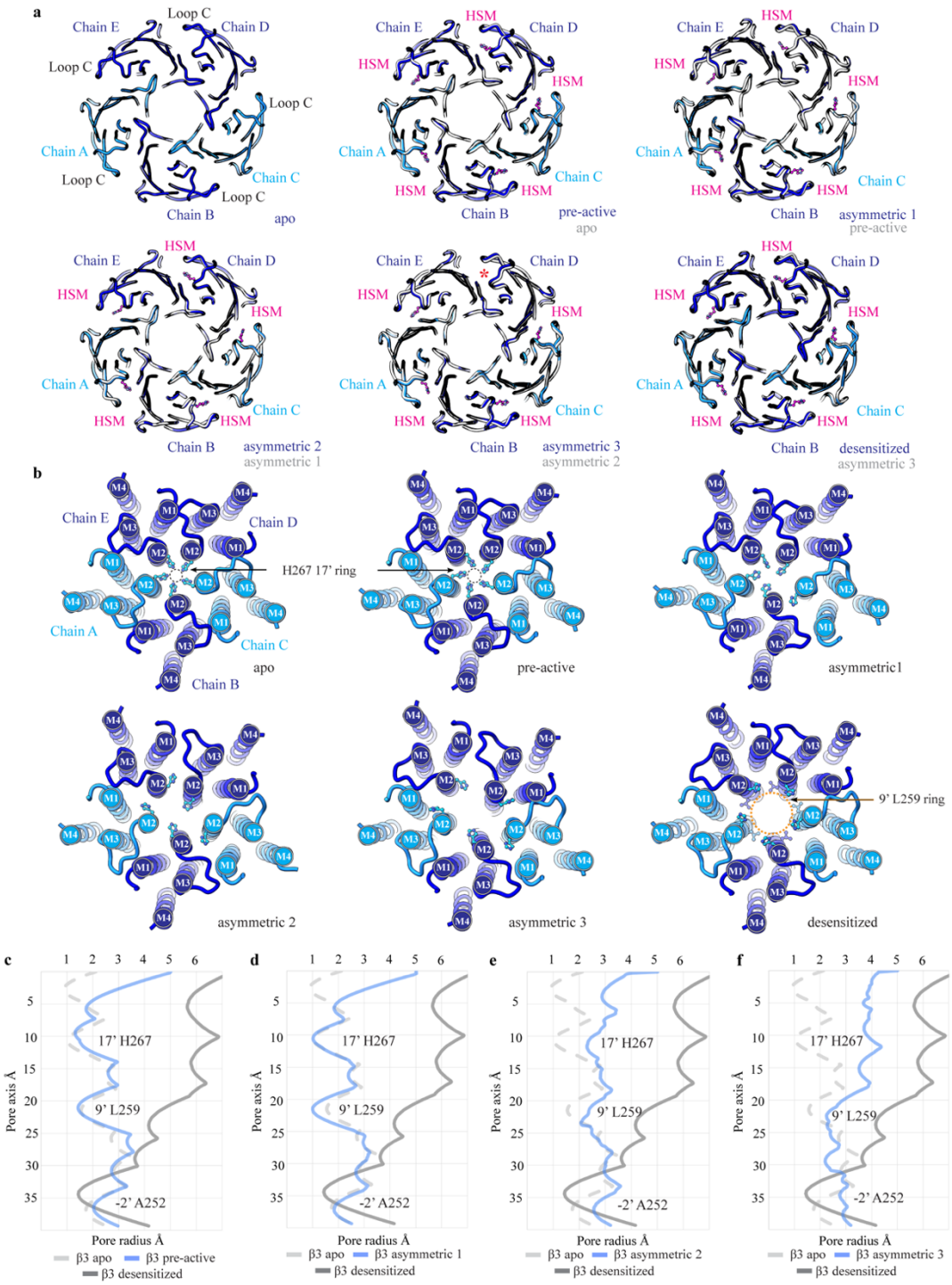


Figure 5.3.1 – The asymmetric gating cycle of the β3 homomer

a) *The extracellular domain and the agonist binding site for all 6 states classified from the dataset. Binding of HSM to the orthosteric site leads to the closure of loop C. Interestingly, only 4 HSM molecules were identified bound to asymmetric 3. Asterisk (*) denotes HSM is not bound to this interface.* ***b)*** *Cross section of the TMDs for the 6 states highlighting the rotations and symmetry break facilitated in part by the His 267 17' activation gate.* ***c)*** *Pore profiles of the pre-active state compared to the apo and desensitized states. Pore profiles of* ***d)*** *the asymmetric 1 state compared to the apo and desensitized states,* ***e)*** *the asymmetric 2 state compared to the apo and desensitized states,* ***f)*** *the asymmetric 3 state compared to the apo and desensitized states.*

This gate occludes the pore in the apo and pre-active states but opens in the desensitized state together with the 9' activation gate, as previously established (Miller and Aricescu, 2014, Nakane et al., 2020). In the case of the desensitized state, the pore closure is driven by the -2' gate (Fig 5.3.1c).

Surprisingly, during this study, I was able to determine three additional states from the dataset. These structures, labeled as asymmetric 1, asymmetric 2, and asymmetric 3, deviated from the previously observed symmetrical configurations. Importantly, these asymmetric states had not been identified when the ligand was incubated with the receptor for prolonged periods e.g overnight (Nakane et al., 2020) or two hours (McMullan et al., 2023), suggesting that they represent transient transitions in the gating cycle occurring on the millisecond timescale. The order of events in these transitions could be readily determined by assessing the extent of the 17' gate opening. In the asymmetric 1 state, chain C undergoes a notable movement away from the receptor bundle, and His267 flips away from the central pore. it is important to note that the initial subunit to move is labeled chain C for descriptive purposes, but this sequence of events could occur with any subunit in the homomeric receptor. Subsequently, this state transitions into asymmetric 2, characterized by the rotation and translation of both chain A and chain E, intensifying the level of asymmetry. In the final state, asymmetric 3, chain C moves entirely out of the bundle, resulting in the formation of the pore primarily by the M2 helices of the remaining four subunits (Fig. 5.3.1b). To verify whether these states indeed represent open conformations of the receptor, I conducted an analysis of their pore profiles using HOLE (Smart et al., 1996). To classify a pore as open, it should exceed the diameter of a fully dehydrated chloride ion, which has a Pauling radius of approximately 1.8 Å (Laverty et al., 2019). Consequently, the analysis revealed that asymmetric 1 maintains a closed pore with constrictions at the levels of all three gates (Fig. 5.3.1d). In contrast, asymmetric 2 and asymmetric 3 both exhibit minimum pore radii of 2 Å and 2.2 Å, respectively, meeting the criteria for an open state (Fig. 5.3.1e-f).

The sequencing of events within the gating cycle of the β3 homomer is intricate, characterized by subunits moving in a coordinated manner rather than independently. To illustrate these concerted motions, I conducted an analysis of the inter-subunit movements by plotting the distances between the Cα atoms of specific residues, including Leu259 (part of the 9' gate in M2), Thr233 (M1), Phe435 (M4), and Val290 (M3), which are situated roughly on the same plane (Fig. 5.3.2a).

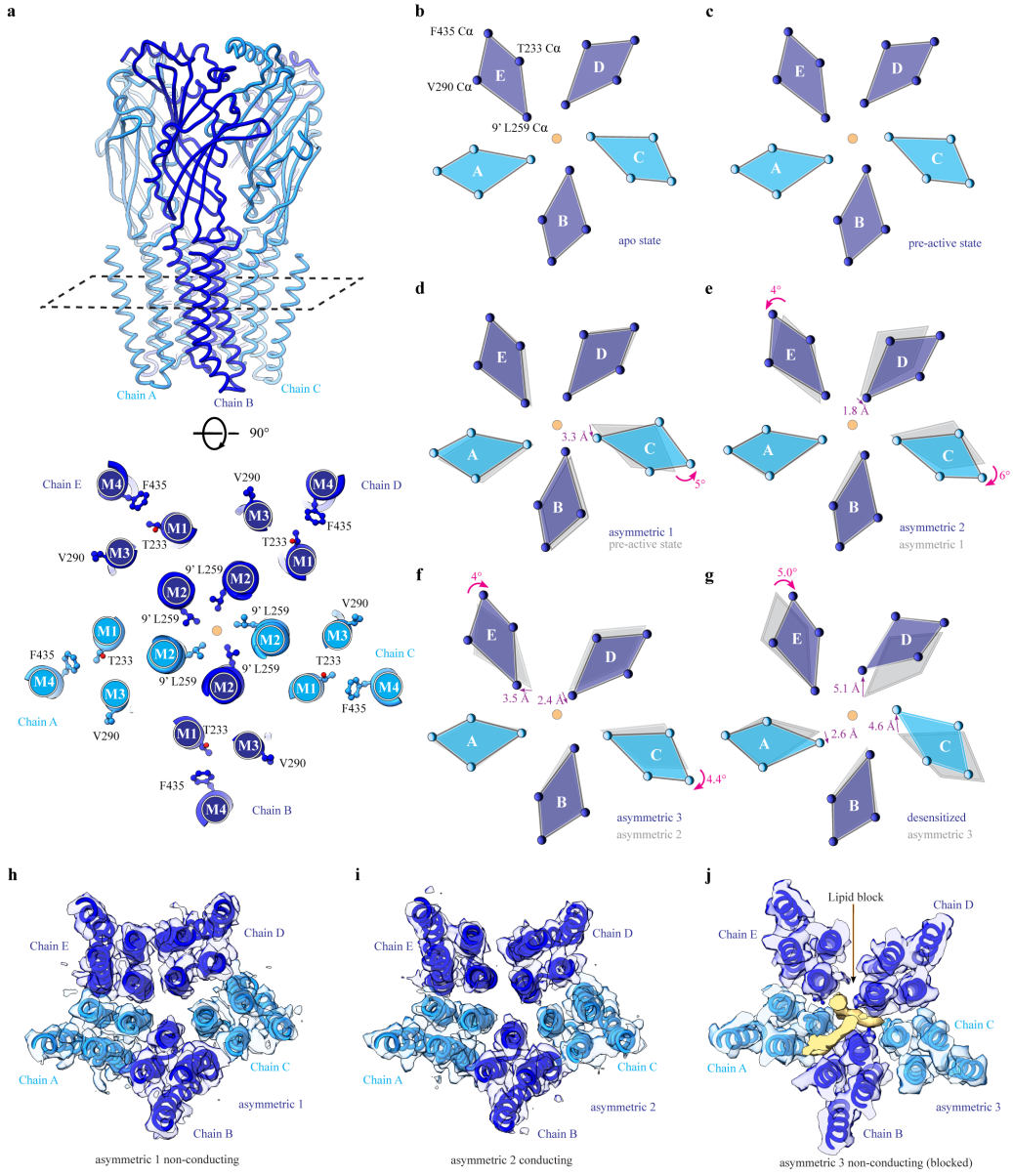


Figure 5.3.2 – Gating of the β3 receptor is orchestrated by concerted motions

a) *A cross section at the level of the TMD of the apo state highlighting the residues (M2's 9' gate Leu 259, M1's Thr 233, M3's Val 290 and M4's Phe 435) used to generate the tetragons used thereafter. The orange circle depicts the center of the pore of the apo state.* ***b)*** *The tetragons of the apo state highlighting its perfect symmetry generated from the Cα atoms of the residues in panel a).* ***c)*** *The tetragons of the pre-active state whose TMD does not deviate substantially from the apo state. For all panels d-g, rotations were measured by calculating the angle between the M4's Cα atoms and the center of the pore of the apo state whereas translation were measured by determining the distance between the M2's Cα atoms. Comparison between the tetragons in* ***d)*** *the pre-active and asymmetric 1,* ***e)*** *asymmetric 1 and asymmetric 2,* ***f)*** *asymmetric 2 and asymmetric 3,* ***g)*** *asymmetric 3 and the desensitized state. Cryo-EM map density of* ***h)*** *asymmetric 1 at the level of the 9' gate,* ***i)*** *asymmetric 2 at the level of the 9' gate,* ***j)*** *asymmetric 3 at the level of the 9' gate also highlighting the lipid block.*

Upon binding of the agonist HSM, the receptor transitions from the apo state to the pre-active state with almost no structural rearrangements in the transmembrane domain (TMD) (Fig. 5.3.2b-c). However, in the case of asymmetric 1, chain C undergoes a counter-clockwise rotation and translation, consequently breaking the receptor's symmetry, particularly disrupting the 17' ring (Fig. 5.3.1b, 5.3.2d). Subsequently, during the transition from asymmetric 1 to asymmetric 2, chain E experiences further clockwise rotation, chain D translates, and chain C undergoes a clockwise rotation, creating a contrast between these two states (Fig. 5.3.2e).

As the receptor moves from asymmetric 2 to asymmetric 3, both chain C and chain E continue to rotate clockwise, eventually leading to the exclusion of chain C from the pore and the opening of the interface between chains D and E (Fig. 5.3.2f). Throughout the desensitization process, chain C and chain D undergo substantial translation, while chain E experiences a pronounced clockwise rotation. Interestingly, chain B does not display such pronounced conformational changes. it is noteworthy that I have previously established that asymmetric 1 is a non-conducting state and is closed, as confirmed by pore profile measurements. In contrast, asymmetric 2 and 3 appear to be in an active state. However, it is crucial to acknowledge that, in the case of asymmetric 3, the exclusion of chain C from the pore bundle and the opening of the interface between chain D and chain E enable lipid molecules to enter and obstruct the receptor's pore. The opening of the interface is also supported by the lack of HSM at the chain D^{+}/E^{-} binding site (Fig. 5.3.1a) Consequently, even though the pore radius of asymmetric 3 is wide enough to permit the passage of chloride ions, it is actually occluded by lipid molecules (Fig. 5.3.2h-j), rendering this state non-conducting.

The mechanism of lipid block, a phenomenon not previously demonstrated for pLGICs, appears to represent a significant mechanism for channel closure. In electrophysiological experiments, this state would likely be categorized as short-lived desensitized, revealing a novel modulation mechanism within the Cys-loop receptor family. This further reinforces the importance of the lipid environment, as discussed in Chapter III.

To better understand the conformations taking place during the gating cycle of the β3 homomer, I conducted an analysis of the Cα RMSDs between subsequent states (Fig. 5.3.3). During the transition from the pre-active to asymmetric 1, chain C undergoes the largest

conformational change (Fig. 5.3.3a), which in turn pushes the M2-M3 loop of the neighboring chain B subunit downwards.

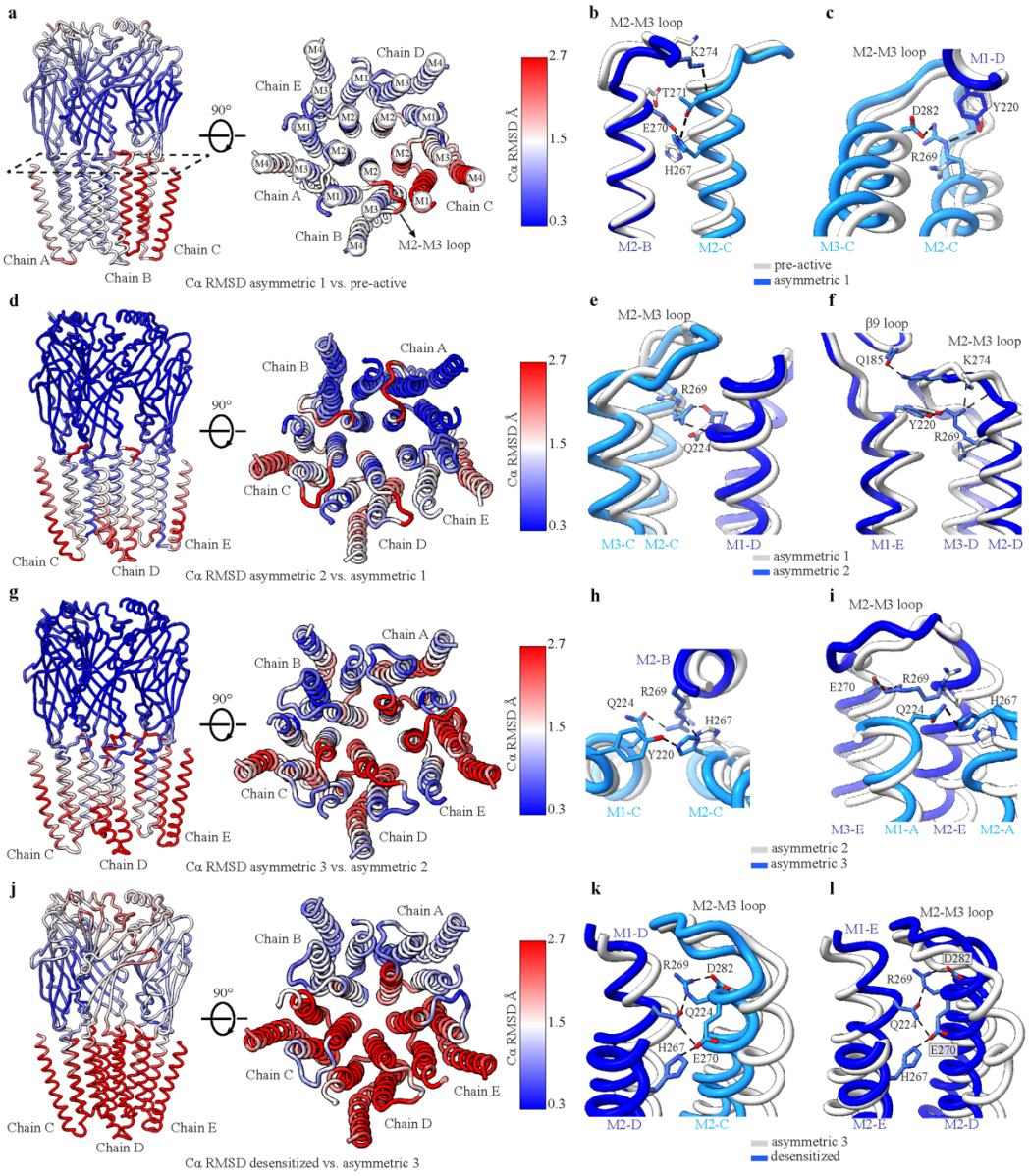


Fig 5.3.3 - The β3 homomer gates via an intersubunit conformational wave

a) *Cα RSMDs between asymmetric1 and pre-active.* ***b-c)*** *Conformational changes and hydrogen bond interactions that stabilize asymmetric 1 when compared to pre-active.* ***d)*** *Cα RSMDs between asymmetric 2 and asymmetric 1.* ***e-f)*** *Conformational changes and hydrogen bond interactions that stabilize asymmetric 2 when compared to asymmetric 1.* ***g)*** *Cα RSMDs between asymmetric 3 and asymmetric 2.* ***h-i)*** *Conformational changes and hydrogen bond interactions that stabilize asymmetric 3 when compared to asymmetric 2.* ***j)*** *Cα RSMDs between desensitized and asymmetric 3.* ***k-l)*** *Conformational changes and hydrogen bond interactions that stabilize the desensitized state when compared to asymmetric 3.*

The new state is stabilized by hydrogen bond interactions from Lys 274.B to the backbone of chain C's M2 helix. Furthermore, His 267.C flips out and now forms a hydrogen bond network with Thr 271.C and Glu 270.B (Fig. 5.3.3b). Notably, Lys 274 is critical for the transitions through the gating cycle as mutations to the equivalent GlyR α1 Lys276Glu lead to much slower gating (Lape et al., 2012). The novel conformation of chain C is further stabilized by a hydrogen bond network formed from Arg 269.C, Asp 282.C and Tyr 220.D (Fig. 5.3.3c). The critical significance of Arg 269 in the β3 subunits has been well-established, and it is worth noting that substitutions of the equivalent Arg 271 in GlyR α1 are the most prevalent cause of hyperekplexia. Furthermore, the disease mutations Arg271Leu or Arg271Gln in the GlyR lead to the uncoupling of the ECD and TMD further highlighting the importance of this residue during gating (Rajendra et al., 1995). The trigger for this stems from the β3-D^+/β3-E^- ECD interface which leads to the counter-clockwise rotation of their TMDs and in turn pushes the β3-C subunit clockwise by 3.3 Å (Fig. 5.3.3.a). This implies that the gating mechanism of the β3 homomer involves an intersubunit conformational wave previously proposed to exist for nAChRs (Grosman et al., 2000). In the proposed nAChR mechanism, opening occurs during the conformational wave from the resting to the desensitized states. However, for the β3 homomer, I determined distinct states corresponding to closed and open receptors. Notably, gating is initiated by agonist binding to the ECD between adjacent subunits (β3-D^+/β3-E^-) thus triggering the motion of the subunit immediately clockwise to the ECD interface that gets activated - β3-C. This gives rise to a stable short-lived asymmetric intermediate pre-active state (Fig. 5.3.3a).

In the transition from asymmetric 1 to asymmetric 2, noteworthy conformational changes are observed predominantly in chains C, D, and E (Fig. 5.3.3d). Interestingly, asymmetric 2 features stabilization through a hydrogen bond network involving Arg 269.C and Gln 224.D (Fig. 5.3.3e). Chain D's stability in the asymmetric conformation is further supported by hydrogen bonds formed between Arg 269.D, the M2-M3 loop backbone, and Tyr 220.E. This interaction pushes the M2-M3 loop upward, facilitating the interaction between Lys 274.D and Gln 185.E, a component of the β9 ECD loop (Fig. 5.3.3f). In the case of asymmetric 3, chain C is entirely displaced from the pore bundle, opening the interface between chains D and E for lipid entry, effectively blocking the pore and rendering the receptor non-conductive (Fig. 5.3.3g). The stability of this state is established through a hydrogen bond network featuring Arg 269.B, Gln 224.C, Tyr 220.C, and His 267.C (as Fig. 5.3.3h). Simultaneously, chain E is drawn closer to chain A, with conformational stability

notably reinforced by hydrogen bonds formed between Arg 269.E and Glu 270.E, as well as His 267.A and Gln 224.A (Fig. 5.3.3i). As the gating cycle progresses towards the final deep desensitized state, chains C, D, and E undergo substantial movements, while chains A and B are already close to a desensitized conformation (Fig. 5.3.3j). This desensitized state derives stability from an extensive hydrogen bond network established at the TMD interfaces between His 267, Gln 224, and Glu 270, Arg 269, as well as Asp 282 of adjacent subunits (Fig. 5.3.3k-l).

Taken together, the β3 homomer exhibits an intriguing asymmetric gating cycle, a remarkable departure from the perfect five-fold symmetry observed in its apo and desensitized states. This asymmetry in the gating cycle is orchestrated through an intersubunit conformational wave, triggered by the binding of agonists to an adjacent ECD interface (Fig. 5.3.3a). Notably, the receptor's five identical agonist binding sites allow for the occurrence of an occasional rotation of one of the five subunits, initiating the breakdown of symmetry, followed by two subsequent asymmetric states before the receptor ultimately desensitizes. These transitions are predominantly driven by the formation of newly established hydrogen bond networks, involving key residues such as the M2-M3 loop Lys 274 as well as key M2 residues His 267, Glu 270, and Arg 269. Additionally, I have uncovered a novel mechanism of receptor modulation through lipid block, rendering the asymmetric 3 state non-conductive and therefore assigning it as short-lived desensitized. Interestingly, the gating of the β3 homomer is primarily driven by the subunit in position C. To explore the effect of this position on the gating of the channel, I next explored the β3γ2 diheteromer comprised of four β3 subunits and one γ2 subunit which replaces the β3-C subunit on the homomer.

5.4 The β3γ2 diheteromer gating motion

The β3 homomer displays an asymmetric gating cycle, initiated by a single subunit that disrupts the five-fold symmetry observed in resting and pre-active states. To delve deeper into the function of this subunit, I replaced just one of the five β3 subunits with a γ2 subunit by expressing the β3 and γ2 subunits in a lenti viral generated cell pool (Fig. 5.4a). In contrast to the homomer, this $GABA_A$ receptor assembly features only three agonist binding sites due to the presence of three $\beta3^+/\beta3^-$ interfaces. To elucidate the gating dynamics of this receptor, I employed a 300mM GABA spray. While low concentrations of GABA lack the potency to affect the $\beta3^+/\beta3^-$ interfaces like HSM, higher GABA concentrations of 10mM or greater leads to channel opening (Miller and Aricescu, 2014).

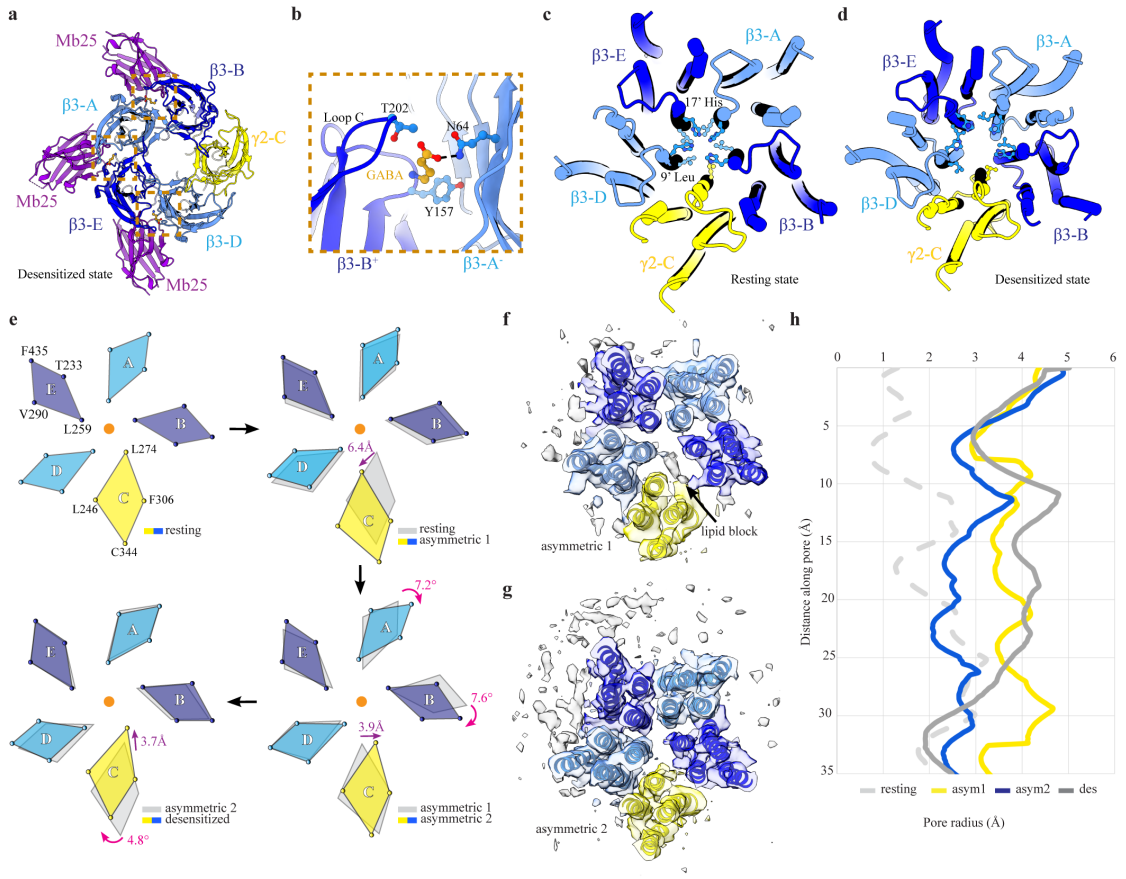


Figure 5.4 – The activation and desensitization of the β3γ2 diheteromer

a) *View from the ECD of the desensitized β3γ2 diheteromer highlighting the three copies of Mb25 bound to each of the β3⁻/β3⁺ interfaces as well as GABA bound under loop C.* ***b)*** *GABA is stabilized under loop C by a hydrogen bond interaction with Asn64.* ***c)*** *View of the TMD of the resting state of β3γ2 highlighting the closed 17' His267 and 9' Leu gates.* ***d)*** *View of the TMD of the desensitized state of β3γ2 highlighting the open 17' His267 and 9' Leu gates.* ***e)*** *The gating cycle of the β3γ2 depicted in tetragons generated from Cα atoms of the highlighted residues for the resting state. The orange circle depicts the center of the pore of the resting state. In all figures the grey tetragons represent the previous state of the cycle whereas the coloured tetragons the current state of the gating cycle. For all panels rotations were measured by calculating the angle between the M4's Cα atoms and the center of the pore of the pre-active state whereas translations were measured by determining the distance between the M2's Cα atoms. Cryo-EM map density of* ***f)*** *asymmetric 1 and* ***g)*** *asymmetric 2.* ***h)*** *Pore profiles of the resting, asymmetric 1, asymmetric 2 and desensitized states of the β3γ2 diheteromer.*

The decision to use GABA instead of HSM was motivated by the desire to validate the calculations regarding agonist diffusion discussed in Chapter 5.2. As estimated in Fig. 5.2.2, the agonist concentration is approximately ~0.1xC_0, translating to 30mM GABA, depending on the size of the droplet. Notably, GABA binding at the orthosteric ligand site was observed, leading to the closure of loop C and the formation of a crucial hydrogen bond with

β3Asn64 (Fig. 5.4b). Since the $\beta3^{+}/\beta3^{-}$ interfaces do not bind GABA below 10mM, it becomes evident that the estimations discussed earlier are indeed accurate, and the GABA concentration approximates 30mM in the vicinity of the ligand droplet.

Once again, from this dataset I could separate two pseudo-symmetric states – a resting state with no agonist present under the orthosteric binding site and a desensitized state. In the case of the resting state, both 17' His267 and 9' Leu gates are closed rendering the channel non-conducting (Fig. 5.4c. h). On the other hand, in the desensitized state both 17' and 9' gates open whereas the channel is closed by the -2' gate at the intracellular end of the TMD (Fig.5.4d, h).

Alongside these two states, however, I also distinguished two asymmetric states. Notably, during the activation of the β3γ2 diheteromer, akin to the β3 homomer, one subunit breaks the symmetry. In asymmetric 1, however, it is the γ2 subunit that notably translates away from the center of the pore (Fig. 5.4e). Surprisingly, the remaining β3 subunits do not undergo substantial motion and largely maintain their positions from the resting state.

During the transition from asymmetric 1 to asymmetric 2, the γ2 subunit translates and rotates, accompanied by significant clockwise rotations of the β3-A and β3-B subunits, bringing them closer to a desensitized-like conformation. Comparing the desensitized state with asymmetric 2 reveals that the β3 subunits in asymmetric 2 are already close to a desensitized state, requiring only the rotation and translation of the γ2 subunit for the receptor to desensitize (Fig. 5.4e). This highlights a difference in the gating cycle between the β3 homomer and the β3γ2 diheteromer. For the β3 homomer, one subunit initiates the gating cycle by breaking the pore's symmetry, with the rest of the subunits also undergoing significant rotation and translation during gating. In contrast, the β3γ2 receptor gates predominantly through the γ2 subunit, dictating the transition of the cycle. Nevertheless, similarities exist between the gating of these receptors. Like the β3 homomer, the β3γ2 receptor is highly sensitive to the lipid environment, with lipids playing a crucial role in its gating. In asymmetric 1, a distinct lipid density obstructs the pore, rendering the channel non-conducting (Fig. 5.4f), despite its pore profile supporting the passage of chloride ions (Fig. 5.4h). Conversely, asymmetric 2 features an unobstructed pore (Fig. 5.4g), with a pore profile exhibiting a minimum radius of 2 Å, meeting the criteria for an open channel pore. Importantly, the pore constricts to 2 Å at the level of the 6' Thr gate which provides a hydrophilic environment and facilitates the passage of chloride ions.

Taken together, the β3γ2 diheteromer, just like the β3 homomer, also gates via an asymmetric gating cycle with short-lived intermediate open and non-conducting states with lipids playing a key role in blocking the pore. Crucially, in both cases the gating cycle is initiated by one subunit breaking the symmetry of the pore in the resting state. Interestingly, however, replacing just one of the β3 subunits in the homomer with a γ2 subunit, dramatically changes the landscape of gating motions.

In the β3γ2 receptor, the primary driving force behind the gating cycle is the γ2 subunit, whereas the remaining subunits undergo minimal motion, contrasting with the homomer's gating behavior. This disparity likely stems from the weaker interfaces of the γ2 subunit compared to β3. This observation finds further support in studies demonstrating the γ2 subunit's susceptibility to collapse when exposed to harsh detergents like DDM (Zhu et al., 2018), a phenomenon not observed in the β3 homomer (Miller and Aricescu, 2014). Additionally, the γ2 subunit's collapse within the pore in Saposin A nanodiscs (Chapter III) underscores its frail interface contacts which is likely the reason for the differences observed in the gating cycles of these two assemblies.

Nevertheless, it is essential to underscore the need for a comparison between the gating cycle of homomers and diheteromers with three or more agonist binding sites and that of di- and triheteromers, where only two agonist binding sites are present, and significantly, these two binding sites are not identical. This divergence may introduce further complexity into the gating cycle. To explore this, I shifted my focus to the α1β3 diheteromer and the α1β3γ2 triheteromer.

5.5 PIP_2 controls the opening of full-length α1β3 and α1β3γ2 receptors

In the instance of the full-length (FL) α1β3 diheteromer and the FL α1β3γ2 triheteromer, in contrast to the β3 homomer and the β3γ2 diheteromer, only two orthosteric ligand binding sites are present, located at the $\beta3^+/\alpha1^-$ ECD interface (Fig. 5.5.1b-c, e-g). This observation implies a potential divergence in their gating mechanism compared to receptors with three or five agonist binding sites. To unravel their gating cycle, I sprayed 300mM GABA and 300mM HSM to the α1β3 receptor. HSM is a recognized PAM for receptors containing the $\beta3^+/\beta3^-$ interface, that also functions as an agonist for β3 homomers (Kasaragod et al., 2022). Including HSM in the spraying mix aimed to maximize the open probability (P_{open}) of the receptor. However, contrary to expectations, the FL α1β3 receptor did not open despite exposure to millisecond-scale ligand application.

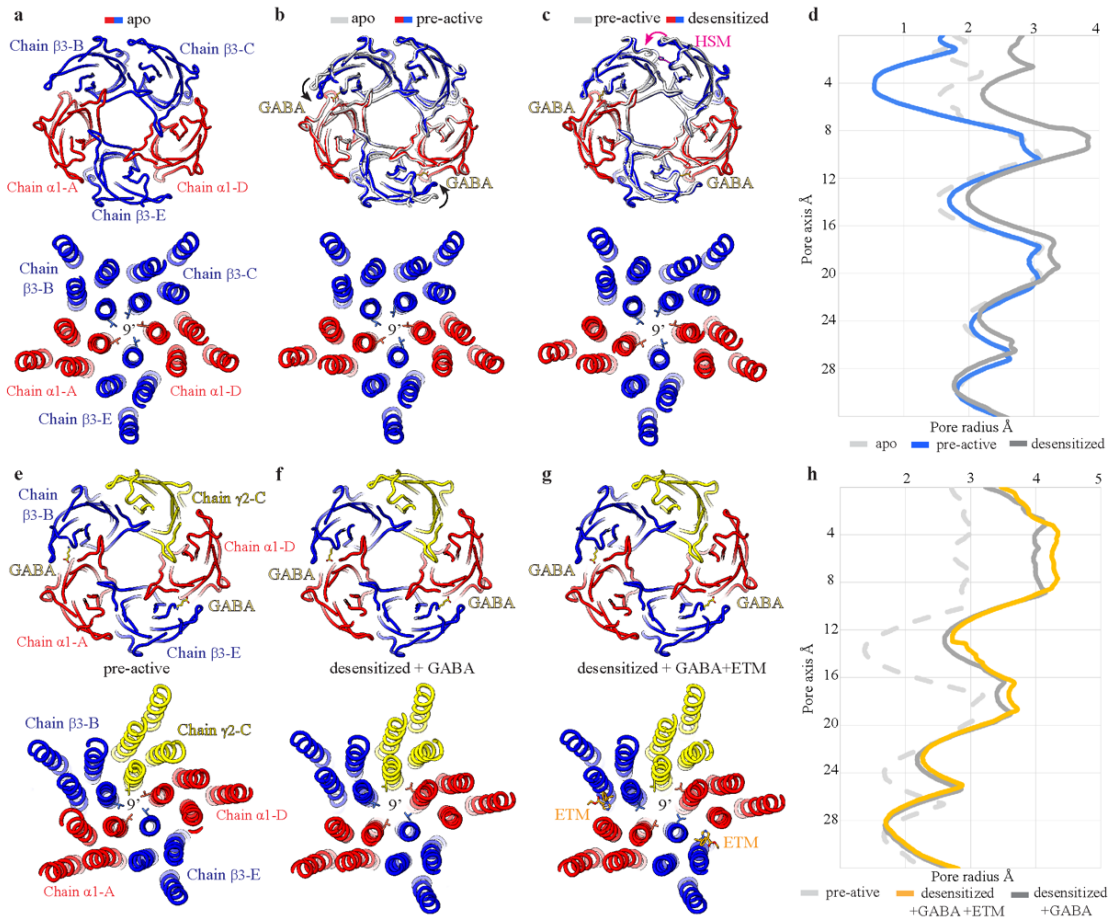


Figure 5.5.1 – FL α1β3 and FL α1β3γ2 do not undergo gating

*The FL α1β3 receptor assumes three pseudo-symmetric states – **a)** apo, **b)** pre-active and **c)** desensitized upon 300mM GABA and 300mM HSM spray. **d)** Pore profile of the α1β3 states. The FL α1β3γ2 like the FL α1β3 does not undergo gating when sprayed with 100mM GABA and 7mM ETM and assumes three states – **e)** pre-active state, **d)** desensitized state with GABA bound and **g)** desensitized state with GABA and ETM bound. **h)** Pore profile of the α1β3γ2 states.*

I could separate three distinct states in this dataset – namely apo, pre-active and desensitized. In the case of the pre-active state, only GABA was bound to the ECD region. Upon desensitization, however, density for HSM was observed at the β3/β3 ECD interface (Fig. 5.5.1a-c). These states are all pseudo-symmetric and cannot be assigned as open states based on their pore profiles (Fig. 5.5.1d). Nevertheless, α1β3 diheteromers are categorized as extrasynaptic receptors and have a lower P_{open} even at saturating agonist concentrations when compared to synaptic $GABA_A$ receptors (Smart, 1992). Therefore, these receptors may have a very small population in the open state even when ligand exposure is limited to less than 15ms and at saturating concentration. To test this, I further sprayed the synaptic FL α1β3γ2 with 100mM GABA and 7mM ETM. The α1β3γ2 will have a $P_{open} = 1$ at saturating GABA concentrations but to further make sure that the receptor will open upon spraying, I

also added 7mM Etomidate to the spraying mixture. At this concentration ETM will serve the role of a PAM and hence further shift the equilibrium towards an open state (Yang and Uchida, 1996). Surprisingly, yet again I could not classify an open state. Only three states were present in this dataset, namely pre-active with GABA bound to the ECD and the TMD still in the resting state (Fig. 5.5.1 e), desensitized with only GABA bound (Fig. 5.5.1 f) and desensitized with both GABA and ETM bound (Fig. 5.5.1 g). All of these states are however pseudo-symmetric and non-conducting based on their pore profiles (Fig. 5.5.1 h). I further collected two more separate datasets on the FL α1β3γ2 sprayed with 100mM GABA. On both occasions, however, only the pre-active and desensitized state could be separated.

It therefore becomes evident that unlike the β3 homomer and the β3γ2 diheteromer, FL α1-containing di- and triheteromers cannot undergo gating. What is the reason for this inhibition however remains unclear. In order to determine a factor that could play a role in inhibiting the receptor I turned my attention to the SMALPs dataset discussed in detail in Chapter III.

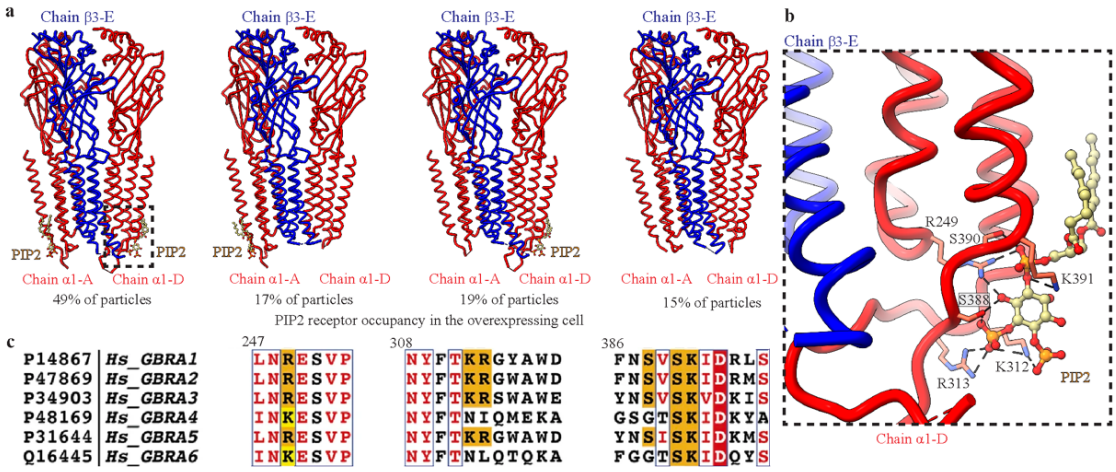


Figure 5.5.2 – PIP_2 modulation of FL α1β3γ2 in a native lipid context

a) *The PIP_2 $GABA_A$ receptor occupancy in the overexpressing cell. Roughly half of the receptors have 2 PIP_2 molecules bound. The remaining 50% have either one PIP_2 bound to one of the binding sites or none PIP_2 bound.* ***b)*** *The binding site of PIP_2 stabilizes the ICL M3-M4 loop of α1 as well as the ICL of the neighboring β3.* ***c)*** *Sequence alignments between the human α1 subunit and the rest of the GABAA receptor α subunit. The residues coloured in orange for the α1 subunit form hydrogen bonds with PIP_2. The conserved residues in other subunits are also coloured in orange if identical or yellow if similar. The image was adapted from (Laverty et al., 2019).*

Despite the fact that $GABA_A$ receptors cannot undergo desensitization and gating in SMALPs and collapse upon GABA exposure, the apo state is still intact and may shed light

into the inhibition mechanism since the receptor in SMALPs is purified directly in a native membrane context.

Strikingly, upon careful classification of the particles in the apo state, I could separate four distinct classes with different occupancy of PIP_2. Half of the particles have two PIP_2 molecules bound to each α1 subunit. Nevertheless, I could also separate classes with only one PIP_2 bound to each α1 subunit as well as receptors without PIP_2 (Fig. 5.5.2 a). PIP_2 binds the α1 subunit towards the end of the TMD region and its inositol headgroup structures the α1 ICD (Laverty et al., 2019). This in turn also stabilizes the neighboring β3 subunit's ICL essentially gluing the two subunits together (Fig. 5.5.2 b). Therefore, it seems that when PIP_2 is present, the receptor cannot undergo gating and enters the desensitized state immediately. Currents recorded by electrophysiology may therefore be generated from receptors that have one or none PIP_2 bound which amounts to a half of all receptors.

What is more, the PIP_2 binding residues of the α1 subunit are also shared among other members of the family based on their sequence alignments (Fig. 5.5.2 c). In fact, α2, α3 and α5 subunits will also be able to bind PIP_2 (structures of the FL α2β3γ2 and FL α3β3γ2 have been solved by other members of the Aricescu lab with PIP_2 present, unpublished data). α4 and α6 subunits on the other hand will not be able to. This is evident in α4β3δ triheteromers that lack PIP_2 (Sente et al., 2022). It therefore appears that α subunits which are associated predominantly with synaptic $GABA_A$ receptor assemblies – α1, α2, α3 and α5 - will have PIP_2 bound, whereas α subunits that are present in extrasynaptic ensembles – α4 and α6 - will not. The inhibition mechanism will be thus important for shaping the GABAergic signalling. Synaptic plasticity is known to be modulated by the probability of neurotransmitter release as well as the number of activatable receptors present at the synapse (Citri and Malenka, 2008). The inhibition by PIP_2, however, introduces another layer of complexity to synaptic communication and emerges as an additional mechanism through which synaptic plasticity is modulated. The strength of the GABAergic synapse will thus be dependent not only on the number of receptors present and neurotransmitter release but also on the number of activatable receptors that lack PIP_2.

Further evidence for the involvement of PIP_2 in the gating of the receptor was discussed in Chapter IV. The β-lactam Nafcillin stabilized an asymmetric state in the FL α1β3γ2, where one β3/α1 module was displaced away from the pore. Notably, the absence of PIP_2 was observed in the α1 subunit undergoing motion. Such receptors, however, were just a small

fraction. Furthermore, electrophysiological experiments with the PIP_2 scavenger poly-L-lysine resulted in an increase in the peak-current amplitudes upon the addition of etomidate (Hille et al., 2015, Laverty et al., 2019). Collectively, these findings underscore the significant role of PIP_2 in GABAergic signalling. However, the precise mechanism of PIP_2 cleavage and removal from $GABA_A$ receptors in the synapse remains elusive. Nonetheless, previous studies have explored the oscillations of PIP_2 levels in neurons. Activation of muscarinic acetylcholine (mAChR) or group I metabotropic glutamate (mGluRI) receptors in CA1 hippocampal neurons induces transient depletion of PIP_2 in both the soma and dendritic tree *in situ*. This process is facilitated through the activation of the $G\alpha_q$ G-protein, which directly activates PLCβ, leading to a reduction in PIP_2 levels (Hackelberg and Oliver, 2018). PLCβ is activated and sequestered to the plasma membrane by the activated G-protein which also orients its active site for optimal PIP_2 cleavage (Falzone and MacKinnon, 2023). Significantly, the major $GABA_A$ subunits expressed in CA1 neurons are the PIP_2-sensitive α1, α2, α3, and α5, along with β3 and γ2 (Palpagama et al., 2019). This highlights the potential for a feedback loop between metabotropic and electrical neuronal activity, as the reduction of PIP_2 levels would also enhance GABAergic signalling.

To experimentally assess the impact of PIP_2 on receptor gating, my focus turned to α1 mutations designed to prevent PIP_2 binding to the receptor. The necessity for generating mutants arose from the prevalent presence of PIP_2 in nearly all receptors reconstituted in a nanodisc. This prevalence likely stems from the addition of bovine brain extract during disc formation, which however is required as it supplements the receptor with essential lipids needed for the binding newly formed interfaces or to block the pore and might be lost during solubilization. In the case of SMALPs reconstitution, 50% of receptors lack one or two PIP_2 molecules. However, when reconstituted in the MSP2N2 disc, virtually all receptors have PIP_2 bound. The nafcillin dataset revealed that out of 700,000 desensitized receptors, only 18,000 were in the asymmetric state with only one PIP_2 site occupied—constituting 2.5% of all receptors. None of these receptors lacked two PIP_2 molecules. Therefore, to achieve high-resolution structure determination with a time-resolved approach, it is essential to have receptors that are consistently PIP_2-less. To achieve this, I generated the K312N/R313I/S388G α1 mutant, introducing mutations in all PIP_2-contacting amino acids to match those present in the α4 subunit, which does not bind PIP_2 (Fig. 5.5.2). Unfortunately, the expression of this mutant proved significantly poor, hindering its structure determination. This was also the case for a second mutation, α1R249E, which

exhibited insufficient expression. The diminished expression could be attributed to the unstructured state of the intracellular loop, preventing pentamer assembly and leading to subunit degradation in the endoplasmic reticulum.

To overcome this, my focus shifted to the previously described truncated α1 subunit which lacks the PIP_2 binding region (Kasaragod et al., 2022). Attempting to replicate wild-type receptor conditions as closely as possible, I co-expressed the full-length β3 subunit with the truncated α1 subunit to eliminate PIP_2 stabilization of the ICD loops. The expression of such mixed receptors, combining a full-length and truncated subunit, was again very poor, precluding the acquisition of their structures via cryo-EM. Therefore, I redirected my attention to the truncated β3 subunit, building on previous success where the truncated α1 subunit was expressed alongside a β3 subunit lacking its ICD. Notably, receptors incorporating the truncated α1 and β3 subunits maintained electrophysiological properties akin to WT receptors (Kasaragod et al., 2022), which likely fire only in the absence of PIP_2. This was also the case for α1β3γ2 with truncated subunits which showed gating kinetics similar to non-mutant receptors (Phulera et al., 2018, Zhu et al., 2018).

5.6 α1β3 receptors gate via two branches

To unravel the gating cycle of PIP_2-less diheteromers, I exposed the double-truncated α1β3 receptor to a 300mM GABA spray, limiting ligand application to less than 10ms. Surprisingly, analysis of this dataset revealed nine distinct states with resolutions ranging from 3.4 Å to 2.5 Å. Importantly, spraying PBS alone, as a control, did not result in the emergence of any other state other than the apo state indicating that the states observed are a result of GABA spraying on the millisecond timescale. The removal of PIP_2 evidently unleashed the receptor's gating cycle. Intriguingly, the α1β3 combination exhibited two distinct gating branches, a departure from the β3 homomer and the β3γ2 diheteromer, which featured a linear gating cycle initiated by the break of symmetry from one subunit (Fig. 5.6.1, Fig. 5.3.1). This disparity likely arises because the α1β3 receptor possesses two inequivalent agonist binding sites that can dictate the branch through which the receptor gates. Despite this, however, in all resolved structures, GABA was bound to both orthosteric binding sites (Fig. 5.6.1a), including the pre-active state likely due to the saturating agonist concentration. Given the receptor's full occupancy by GABA, the likelihood of entering either branch would be dependent on the specific GABA interface. The particle numbers in the reconstructions, however, suggest an equal probability of gating through either branch upon GABA exposure. Nevertheless, the emergence of two gating branches may hold

significance for the actions of PAMs and NAMs, which could modulate the receptor by potentially favoring one of these branches.

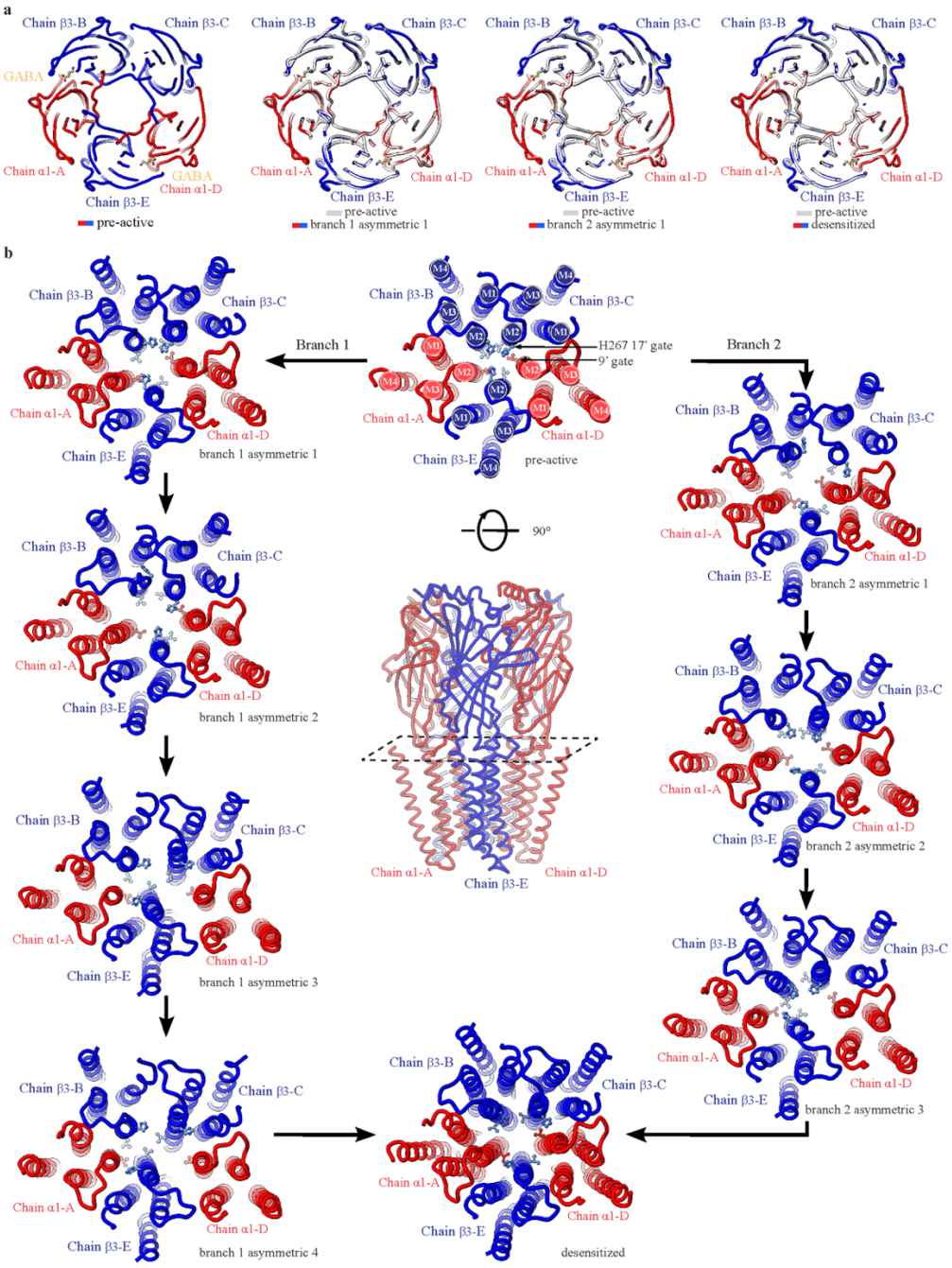


Figure 5.6.1 - α1β3 $GABA_A$ receptors gate via two branches

a) *View of the ECD domains of 4 different states showing GABA is bound to the two β3+/α1- interfaces. No major differences can be observed at the level of ECD when comparing branch 1 asymmetric 1, branch2 asymmetric2 and desensitized to pre-active.* ***b)*** *The α1β3 receptor gates via two branches with major conformational changes in the TMD. Branch1 has 4 asymmetric states, whereas branch 2 has 3 asymmetric states. Both branches emerge from the pseudo-symmetric pre-active state and ultimately converge into the pseudo-symmetric desensitized state.*

Interestingly, the emergence of these distinct branches is orchestrated by the β3 subunit in position C, positioned adjacent to the two GABA binding sites. In α1β3γ2 triheteromeric synaptic receptors, this position is occupied by the γ2 subunit. In the first branch, the initial asymmetric state unfolds as chain C β3 undergoes an outward drift. This drift weakens the α1-D/β3-C interface, with β3-C primarily interacting with the TMD of β3-B. Consequently, the states in branch 1 likely stem from GABA binding at the β3-E/α1-D interface. Four asymmetric states are observed in branch 1 before the receptor ultimately transitions into the pseudo-symmetric desensitized state.

Similarly, in branch 2, β3-C is the first subunit to break symmetry. However, in this branch, the β3-B^+/β3-C^- interface weakens, and β3-C predominantly interacts with α1-D. Thus, in contrast to branch 1, branch 2 originates from GABA binding to the other orthosteric site, specifically the β3-B^+/α1-A^- interface. Three distinct states can be seen for branch 2 before the receptor undergoes desensitization, leading to the same pseudo-symmetric desensitized state as in branch 1. Moreover, the final asymmetric states in both branches exhibit notable differences. In asymmetric state 4 of branch 1, chain α1-D is displaced from the TMD bundle, resulting in a pore formed from only four subunits, similar to the β3 homomer. Conversely, in asymmetric state 3 of branch 2, chain α1-A is pushed away, forming a pore from the remaining four subunits. This observation further supports the hypothesis that the receptor gates through two distinct branches, and that the α1 subunit that determines which branch the receptor will select, ultimately gets displaced from the bundle (Fig. 5.6.1b).

The high resolution of the reconstructions not only facilitates the precise categorization of states as conducting or non-conducting but also reveals that, akin to the β3 homomer, the α1β3 undergoes modulation through lipid blocks in both branches of its cycle. In branch 1, three states—branch 1 asymmetric 1, branch 1 asymmetric 2, and branch 1 asymmetric 4—display evident lipid densities within the pore, hence can be assigned as transient desensitized states. Notably, branch 1 asymmetric 3 exhibits a clear, unobstructed pore and, accordingly, can be identified as open and conductive, supported by the pore profile (Fig. 5.6.2a, e). Similarly, branch 2 mirrors this behavior, as branch 2 asymmetric 1 and branch 2 asymmetric 3 are obstructed by lipids. In contrast, branch 2 asymmetric 2 features an unobstructed pore with a radius exceeding 2 Å, designating it as a conducting state (Fig. 5.6.2a, e). However, the involvement of key lipid molecules extends beyond mere pore blockade; they play a crucial role in facilitating the transitions between asymmetric states. Throughout the gating process, subunits undergo drifting and rotation, exposing

hydrophobic cavities to the environment. Specific lipids stabilize these cavities at the interfaces between moving subunits, exemplified by branch 1 asymmetric 2, where an unidentified lipid stabilizes the β3-B^{+}/α1-A^{-} TMD interface.

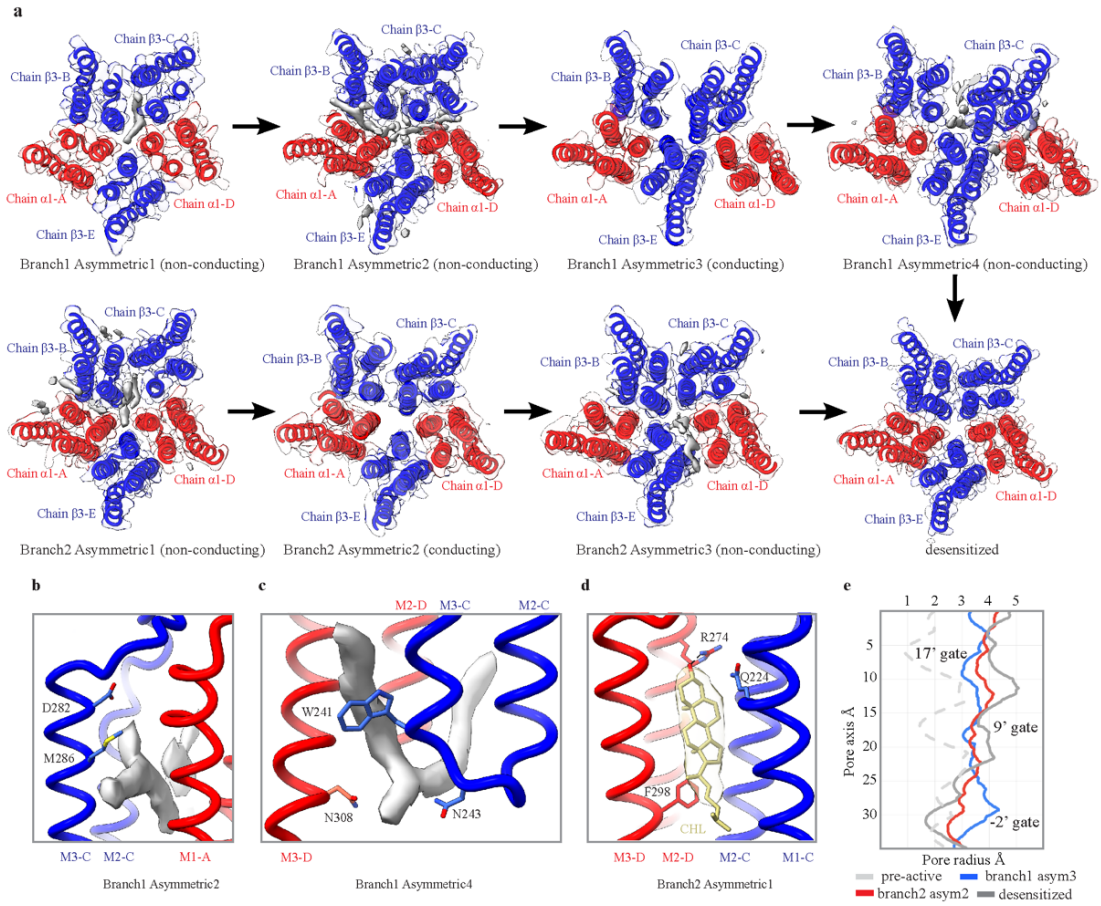


Figure 5.6.2 – Lipids orchestrate the transitions of the α1β3 gating cycle

a) *Cross-section at the level of the 9' activation gate of the maps with fitted models for all asymmetric states and the desensitized state highlighting the lipid blocks in five out of the seven asymmetric states.* ***b)*** *An unidentified lipid stabilizes the α1-D^{+}/β3-C^{-} interface of branch 1 asymmetric 2.* ***c)*** *An unidentified lipid stabilizes the α1-D^{+}/β3-C^{-} interface of branch 1 asymmetric 4.* ***d)*** *Cholesterol stabilizes the α1-D^{+}/β3-C^{-} of branch 2 asymmetric 1.* ***e)*** *Pore profiles of the pre-active, desensitized, branch 1 asymmetric 3 and branch 2 asymmetric 2 states.*

Importantly, this interface serves as the binding site for two widely used clinical anaesthetics, propofol and etomidate. Thus, anaesthetics may be able to modulate the receptor by stabilizing the newly formed interfaces during the gating cycle. In addition, an unidentified phospholipid provides stability to the α1-D^{+}/β3-C^{-} interface in branch 1 asymmetric 4 (Fig. 5.6.c). Notably, I observed a distinct density corresponding to cholesterol at the α1-D^{+}/β3-C^{-} interface in branch 2 asymmetric 1 (Fig. 5.6.2d). As previously discussed in Chapter III, cholesterol is recognized for its significance in receptor gating, and depleting

cholesterol from the membrane results in the uncoupling of the ECD from the TMD. The presence of cholesterol proves essential for the gating process, as the emergence of branch 2 asymmetric 1 would not be feasible without cholesterol in the membrane (Fig. 5.6.2d). Collectively, membrane lipids assume a dual role in the $GABA_A$ receptor's gating cycle. They are indispensable for the transitions between asymmetric states stabilizing new hydrophobic cavities that arise during the asymmetric motions, essentially functioning as grease in a machine engine, thereby positively modulating the receptor. However, lipids also play a pivotal role in closing the receptor by obstructing the pore in six out of the eight asymmetric states, thereby finely tuning the channel's open times of the channel.

The sequential progression of events within the gating cycle of the α1β3 diheteromer, akin to the β3 homomer and the β3γ2 diheteromer, is characterized by coordinated movements of subunits. In branch 1, the conformational change induced by GABA binding to the ECD β3-E^+/α1-D^- interface results in an overall translation of β3-E and a clockwise rotation of α1-D. Consequently, the interface between α1-D^+/β3-C^- weakens, prompting β3-C to rotate counter-clockwise, predominantly interacting with β3-B. As the branch transitions to its second state, β3-B undergoes an outward drift, while α1-D is carried away, rotating further counter-clockwise, intensifying the asymmetry of the pore. The shift from branch 1 asymmetric 2 to branch 1 asymmetric 3 involves the collective translation and rotation of β3-B, α1-A, and β3-E as a bundle. Meanwhile, β3-C experiences a substantial counter-clockwise rotation of 14.8°. This collective movement leads to the translation and rotation of α1-D, which is now excluded from the pore. In branch 1 asymmetric 4, β3-B rotates counter-clockwise, and β3-E translates away from α1-D, further excluding it from the pore. Consequently, the pore in this state is formed by only four subunits: α1-A, β3-B, β3-C, and β3-E. During the deep desensitization of branch 1, chains α1-A, β3-B, α1-D, and β3-E undergo significant conformational changes, whereas chain β3-C is already in a state close to desensitized (Fig. 5.6.3a).

In contrast to branch 1, where the conformational wave is initiated by GABA binding to the ECD of the β3-E^+/α1-D^- interface, the gating of branch 2 commences with GABA binding to the ECD β3-B^+/α1-A^- interface. This initiates the clockwise rotation of α1-A TMD and a significant outward drift, accompanied by the counter-clockwise rotation of β3-C TMD.

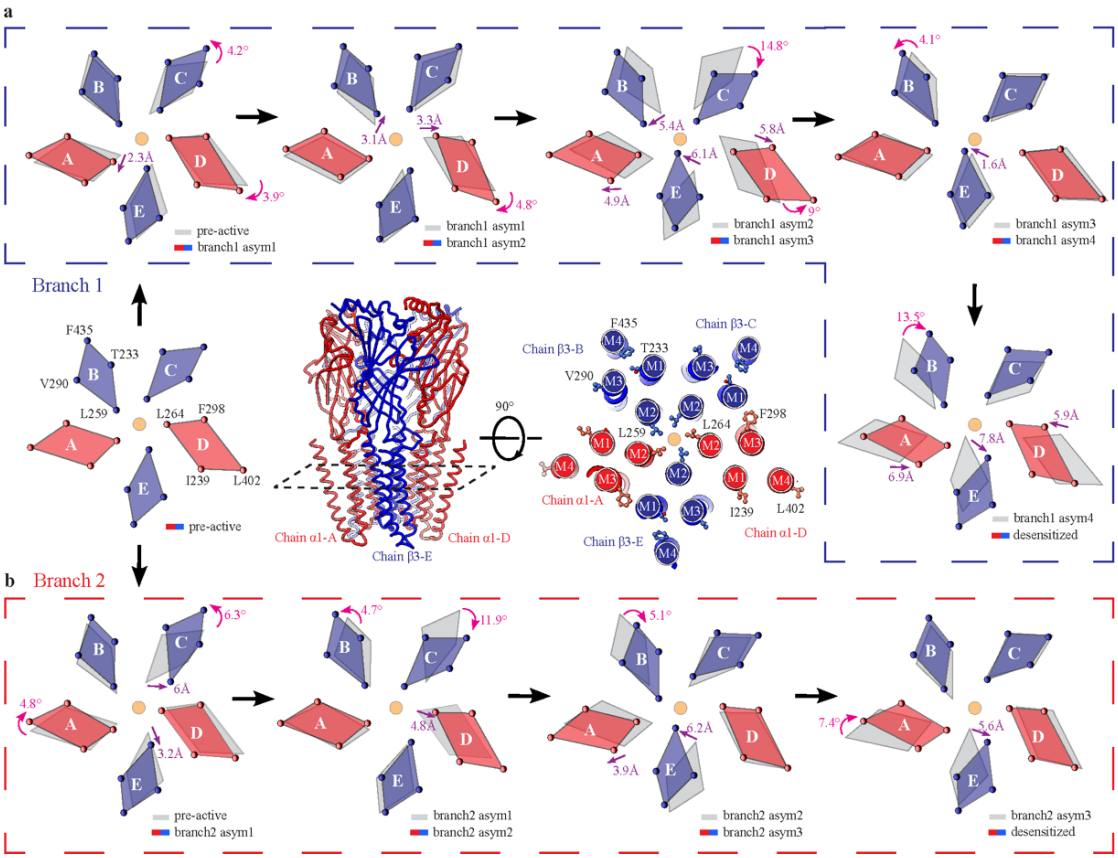


Figure 5.6.3 – α1β3 receptors gate via a dual-branch conformational wave

A cross section at the level of the TMD of the pre-active state highlighting the Cα atoms of the residues used to generate the tetragons used thereafter. The orange circle depicts the center of the pore of the pre-active state. In all figures the grey tetragons represent the previous state of the cycle whereas the coloured tetragons the current state of the gating cycle. For all panels rotations were measured by calculating the angle between the M4's Cα atoms and the center of the pore of the pre-active state whereas translations were measured by determining the distance between the M2's Cα atoms. ***a)*** *Branch 1 of the α1β3 gating cycle starting from the pseudo-symmetric pre-active and finishing with the pseudo-symmetric desensitized state showing the motions that take place.* ***b)*** *The motions and states of branch 2 starting and ending with the same pre-active and desensitized states as branch 1.*

This movement nearly completely disrupts the interactions between β3-C^+/β3-B^- transmembrane domains, with β3-C now predominantly interacting with the α1-D TMD, supported by the presence of cholesterol (Fig. 5.6.2d). During the second stage of branch 2, α1-D moves away from the pore, while β3-C undergoes a substantial clockwise rotation, bringing it closer to the centroid of the pre-active state. In branch 2 asymmetric 3, β3-E drifts significantly toward the center of the pore, alongside β3-B. This results in the overall drift of α1-A away from the bundle, and the pore is now formed by the remaining four subunits.

Throughout the desensitization of branch 2, β3-E translates, while α1-A rotates counter-clockwise.

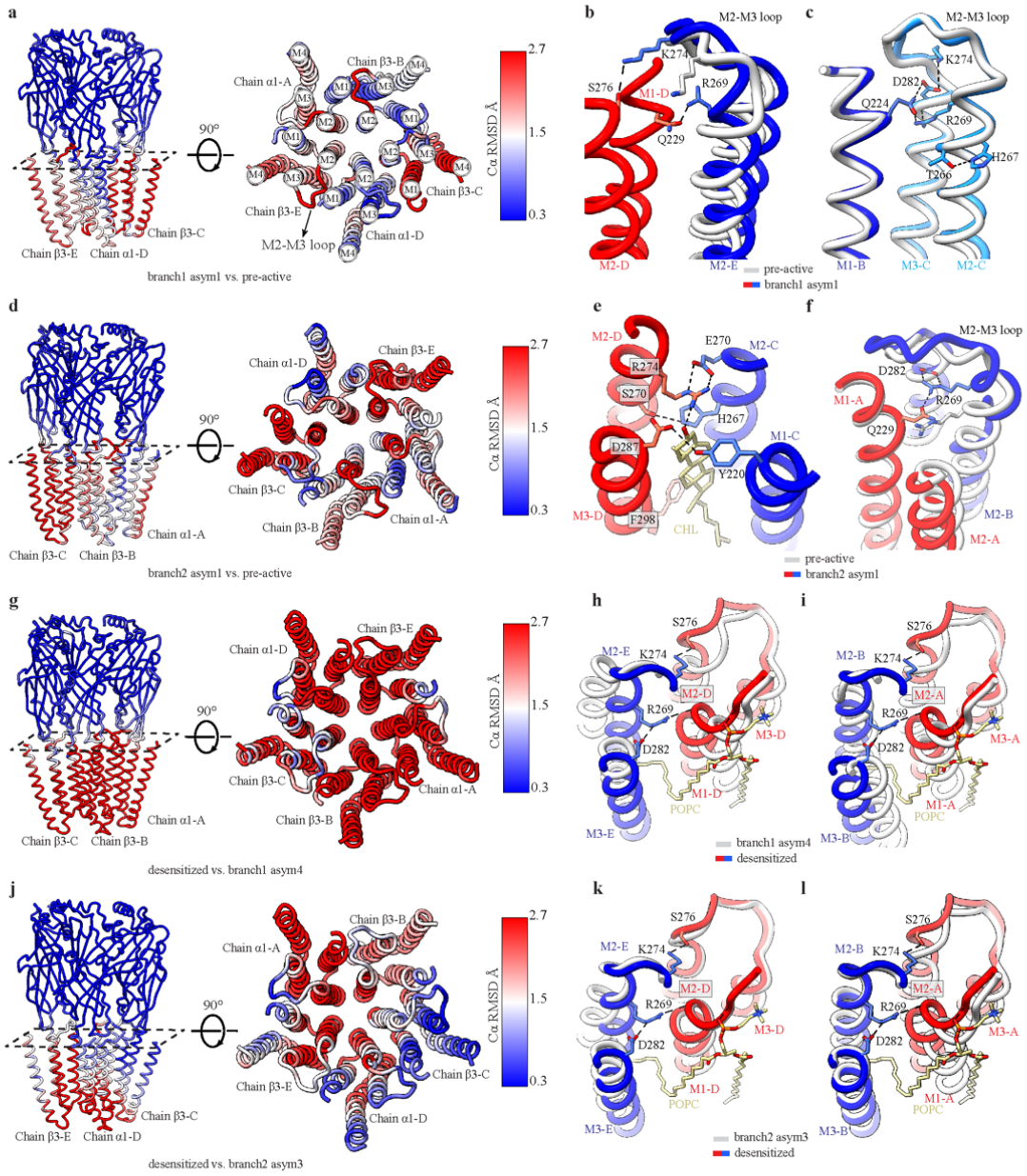


Figure 5.6.5 – The activation and desensitization of α1β3 receptors

a) *Cα RMSDs between branch1 asymmetric1 and pre-active.* ***b-c)*** *Conformational changes and hydrogen bond interactions that stabilize branch1 asymmetric 1 when compared to pre-active.* ***d)*** *Cα RMSDs between branch2 asymmetric1 and pre-active.* ***e-f)*** *Conformational changes and hydrogen bond interactions that stabilize branch2 asymmetric1 when compared to pre-active.* ***g)*** *Cα RMSDs between branch1 asymmetric4 and desensitized.* ***h-i)*** *Conformational changes and hydrogen bond interactions that stabilize the desensitized state when compared to branch1 asymmetric4.* ***j)*** *Cα RMSDs between branch2 asymmetric3 and desensitized.* ***k-l)*** *Conformational changes and hydrogen bond interactions that stabilize the desensitized state when compared to branch2 asymmetric3.*

The other three subunits are already close to the desensitized state and therefore do not undergo substantial conformational changes. Taken together, the gating via the two asymmetric branches ultimately converges to the same pseudo-symmetric desensitized state. Importantly, the entry into either of the branches is dictated by a conformational wave triggered by GABA binding specifically to one of the two orthosteric sites. The analysis of the Cα RMSDs between pre-active and branch 1 asymmetric 1 further highlights the effect of GABA binding to the β3-E^+/α1-D^- interface during the initial steps of activation of branch 1 (Fig. 5.6.5a). Upon GABA binding, the β3-E M2-M3 loop moves upwards allowing Lys 274 to form a hydrogen bond with α1Ser276-D. Furthermore, the displacement of the β3-E M2 helix brings Arg 269 in proximity to α1Gln229-D further stabilizing the newly formed interface (Fig. 5.6.5b). Due to the increased contacts between β3-E and α1-D and overall translation of the two subunits, the TMD interface between β3-C and α1-D weakens allowing β3-C to rotate away from the pore and hence to form new interaction with β3-B stabilized by a hydrogen bond network comprising β3His267-C, β3Thr266-C, β3Gln224-B, β3Arg269-C, β3Asp282-C and β3Lys274-C (Fig. 5.6.5c).

In contrast to branch 1, branch 2 enters the asymmetric cycle via GABA binding to the β3-B^+/α1-A^- interface. This pushes β3-C towards α1-D, which is exactly opposite to what happens during the transition into branch 1 where β3-C rotates away from α1-D (Fig. 5.6.5d). The newly formed interaction between β3-C and α1-D is notably stabilized by the critical insertion of cholesterol at the interface which makes a hydrogen bond with α1Arg274 as well as van der Waals interactions with Phe398. The interface is further stabilized by a hydrogen bond network formed between β3Tyr220 and α1Asp287, β3His267 and α1Ser270 as well as β3Glu270 and α1Arg274 (Fig. 5.6.5e). GABA binding to the β3-B^+/α1-A^- interface, on the other hand leads, to the rotation of β3-B thus weakening its contacts to β3-C. The new conformation is stabilized by a hydrogen bond network formed by α1Gln229, β3Arg269 and β3Asp282 (Fig. 5.6.5f). The pivotal role of β3Arg269 and α1Gln229 was further shown in disulfide crosslinking experiments (Bali and Akabas, 2012). By expressing the α1I228Cβ3R269Cγ2 receptor, the authors of the study report robust initial GABA-induced currents. Interestingly, however, the observed currents decreased upon GABA reapplication which was fully reversed by the application of the reducing agent DTT This strongly suggests that upon GABA binding, residue Arg269 and Ile228 get in close proximity. This is also the case in the activation for both branches (Fig. 5.6.5a-b). Nevertheless, β3Arg269 and α1Ile228 are also close to each other in the desensitized state,

thus, the crosslinking observed between the two residues may happen during both the activation as well as during the deep desensitized state.

The desensitization of the receptor is intricately influenced by hydrogen bond interactions and lipid molecules, which play a crucial role in stabilizing the TMD interfaces between β3 and α1 subunits. Specifically, β3Arg269 establishes hydrogen bonds with the α1 M1 helix and β3Asp282, contributing to the desensitization process. Additionally, the pivotal residue of the β3 M2-M3 loop, Lys274, interacts with α1Ser270, thereby stabilizing the position of the α1 M2 helix. The state is further fortified by the presence of POPC, forming hydrogen bonds with the α1 subunit. Notably, one of its lipid tails extends between the $\beta3^{+}/\alpha1^{-}$ interfaces, providing stabilization for the binding pocket where etomidate and propofol interact (Fig. 5.6.5 g-l).

Crucial dynamics unfold during the transition to the desensitized state. Notably, in branch 1 asymmetric 4, the two $\beta3^{+}/\alpha1^{-}$ interfaces exhibit distinct and contrasting movements. The β3-E subunit undergoes an outward motion relative to the pore, while β3-B moves inward. Concurrently, in both interfaces, the α1-A subunit exhibits an inward movement (Fig. 5.6.5h-i). In contrast to branch 1 asymmetric 4, branch 2 asymmetric 3 is closer to a desensitized state, evident from the Cα RMSDs (Fig. 5.6.5g, j). During this transition, the β3-E subunit undergoes an outward motion relative to the pore, whereas α1-D adopts a conformation closer to desensitized (Fig. 5.6.5k). Conversely, in the other interface, the β3-B subunit is close to desensitized, while the α1-A subunit moves inward (Fig. 5.6.5l).

Collectively, the removal of PIP_2 from the α1β3 receptor gave rise to a nine-state dual branch gating cycle with both branches emerging from and converging into the same pseudo-symmetric state. The initiation of one of the branches is notably triggered by GABA binding to one of the two orthosteric binding sites, inducing a break in symmetry. I further establish the manifestation of two open states in each of the branches. This falls well in line with single-channel electrophysiology experiments which demonstrate that two open states with different duration times could be detected. Short and long open dwell times (termed τ_{O1} and τ_{O2} respectively) were approximately τ_{O1} = 0.65 ms and τ_{O2} = 4.3 ms in duration (Kasaragod et al., 2022). However, based on the data presented here, it is not possible to assign which branch has the short duration open state and which one has the long duration open state.

Importantly, the entry into the asymmetric gating cycle is consistently manifested by the β3-C subunit which is also the case for β3γ2 receptors where γ2-C initiates the gating cycle.

Notably, this position in the tri-heteromeric α1β3γ2 receptors is also a γ2 subunit. This substitution could be a crucial determinant for the occurrence of different open or short-lived desensitized asymmetric states, adding a layer of complexity to the gating process. What is more, similar to the β3 homomer and β3γ2 diheteromers, lipids emerge as pivotal players in the gating dynamics of α1β3 receptors. Beyond acting as pore blockers to finely tune channel open times, lipids are indispensable for facilitating transitions between asymmetric states. This is exemplified in branch 2 asymmetric 1, where cholesterol is identified at the α1-D^{+}/β3-C^{-} interface thus stabilizing it (Fig. 5.6.5c).

5.7 Positive allosteric modulators and general anaesthetics may tune α1β3 $GABA_A$ receptors by branch selection

While the emergence of a dual branch gating cycle adds complexity to the gating mechanism, it may also hold significance for the modulation of the receptor through PAMs. In an effort to elucidate the mechanism of action of positive allosteric modulation, I directed my attention towards histamine, which has been demonstrated to increase the amplitude of α1β3 currents when co-administered with GABA (Kasaragod et al., 2022). I also specifically focused on elucidating the mechanism of direct activation of the receptor by the general anaesthetic propofol.

Upon spraying the α1β3 receptor with a combination of 300mM GABA and 300mM Histamine (HSM), the receptor once again gated, however, in contrast to the GABA only spray where the manifestation of two branches was observed, in the presence of the PAM HSM the receptor gated only through branch 1 (Fig. 5.7.1a). The mechanism for this modulation likely stems from the fact that HSM stabilizes the β3-C^{+}/β3-B^{-} subunit pair, thus the only TMD interface that can break to initiate gating is α1-D^{+}/β3-C^{-} thereby allowing only branch 1 to manifest. This implies that the emergence of two branches is also critical for the modulation of the receptor by PAMs.

Furthermore, when 200mM of the general anaesthetic propofol (PPF) was sprayed on the receptor once again one branch was selected over the other. At higher concentration PPF can act as an agonist itself (Fig. 3.4.2) therefore GABA was not added to the spraying mixture. This aimed to determine the effect of agonist binding to the TMD rather than the ECD orthosteric site. In contrast to HSM, however, PPF selects branch 2 with prominent PPF densities in branch 2 asymmetric 1 and the desensitized state. The other two asymmetric states had a lower resolution in the TMD region and no unambiguous density for PPF could

be observed. There could be two explanations for this. Either PPF is bound but cannot be resolved due to the limited interpretability of the map or PPF only binds initially thus pushing the receptor to enter branch 2 by stabilizing branch 2 asymmetric 1 and lowering the activation energy barrier. The progression through the branch then can happen independently from PPF and it is not required to be bound in the following states in the branch. Once the receptor desensitizes, propofol can then bind to the last state of the cycle (Fig. 5.7.1b). Interestingly, this is also the case for HSM. Its density could not be observed for branch 1 asymmetric 3 (Fig. 5.7.1a) further highlighting that the branch is selected by the initial state and progression through the branch then becomes independent of the PAM or agonist present.

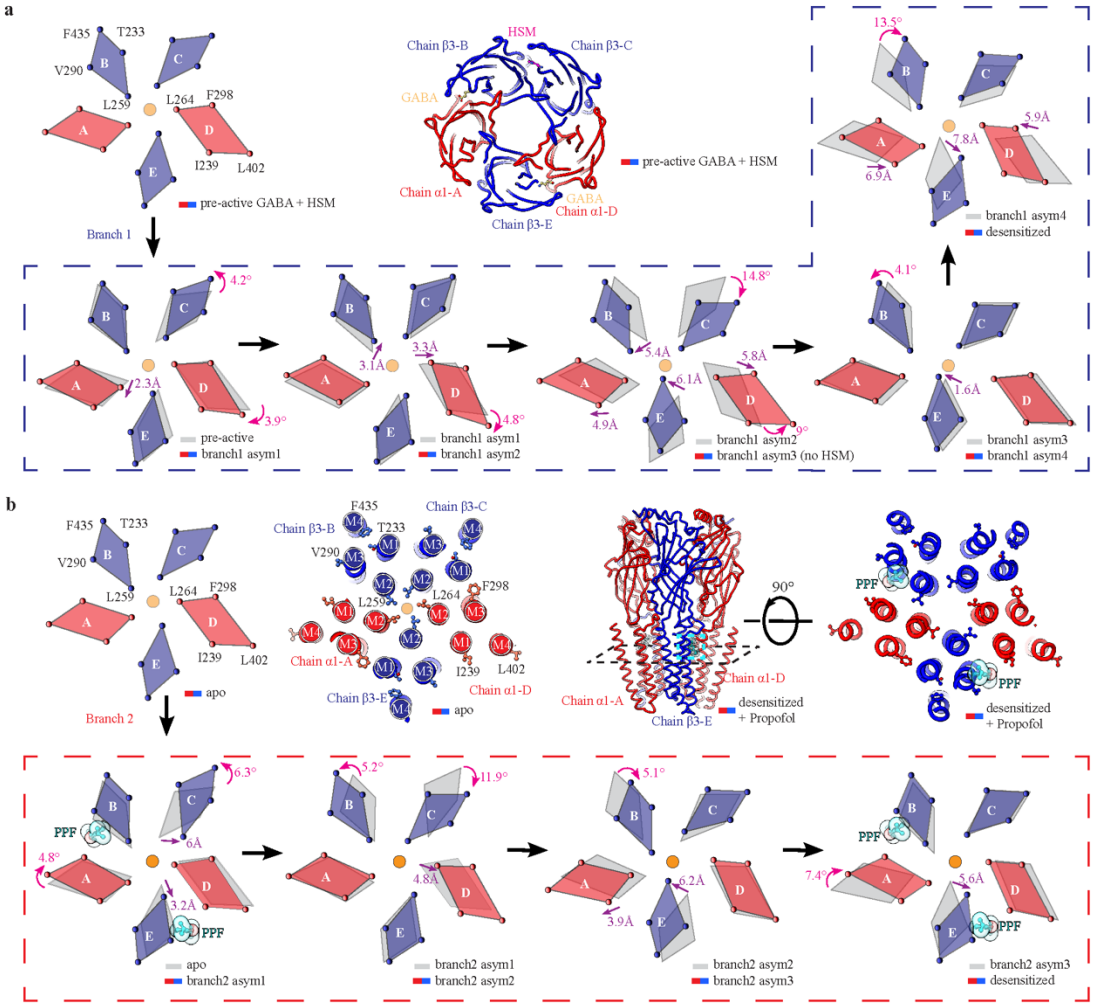


Figure 5.7.1 – Histamine and propofol modulate the receptor by branch selection

a) *In the presence of GABA and HSM the α1β3 receptor gates only via branch 1. Notably, branch1 asymmetric3 has no density for HSM present indicating that branch selection happens during the first state of the cycle.* ***b)*** *When PPF is used as an agonist for the receptor only branch 2 emerges. PPF is bound to branch2 asymmetric1 and desensitized state but not to the two other states.*

Importantly, in both GABA/HSM and PPF spray, the states are essentially identical to the states observed when GABA alone is sprayed as judged by the Cα RMSDs which are below 0.7 Å. Therefore, it becomes clear that regardless of the agonist or modulator present, the receptor undergoes the same gating cycle. It is hence likely that once a PAM is added, the duration of the open states increases in order to account for the increase in current amplitude and slower rates of desensitization. Alternatively, the duration of the open times can remain the same but the number of events i.e. the number of times the receptor enters the open state could increase. Importantly, however, when PPF is used as an agonist, the activation of the receptor is suboptimal when compared to 1mM GABA, but the rate of desensitization is slower (Chapter III, Fig. 3.4.2). This is also the case for ETM suggesting PPF and ETM exert their effects by a shared structural mechanism. The lower conductivity levels likely stem from the fact that branch2 is the lesser conducting branch and perhaps branch 2 asymmetric 2 is the short-lived open state. Nevertheless, to fully interpret the branch and state separation, it will be crucial to perform single-channel recordings with propofol or GABA plus HSM and determine the open state duration of each condition, the number of open states detected as well as the number of times the receptor opens. With this in hand it will be possible to unequivocally assign branch 1 asymmetric 3 and branch 2 asymmetric 2 as the short or long lived open states (Kasaragod et al., 2022).

Moreover, it becomes evident that modulators and agonists favoring branch 2 over branch 1 are particularly influenced by the cholesterol levels in membranes, as exemplified by propofol. Notably, studies indicate that depleting membrane cholesterol in dissociated hippocampal neurons moderately diminished the potentiation of GABA by PPF, albeit not to a significant extent (Sooksawate and Simmonds, 2001). This could be attributed to the high affinity for cholesterol in the newly formed interface. In contrast, increasing the cholesterol content significantly enhanced the potentiation of GABA by PPF. This reinforces the observation that PPF selects branch 2 over branch 1 and that the cholesterol level in the membrane is critical for the action of propofol on the receptor and for the transition of the states in branch 2. Thus, propofol may have a larger impact on receptors embedded in membranes with higher cholesterol content further increasing the scope of anaesthetics modulation.

Chapter VI

Conclusion and outlook

6.1 Conclusion

In this thesis I discussed in detail the structural effects of the environment surrounding the receptor on its gating cycle. A systematic exploration was undertaken to evaluate the influence of different scaffolding proteins within the nanodisc environment on the $GABA_A$ receptor. The findings underscore the significance of MSP2N2 nanodiscs, revealing they most faithfully preserve the physiological conformations and desensitization capabilities of the receptor. Notably, Saposin A and SMALPs discs on the other hand induced non-physiological states, particularly impacting the γ2 subunit and disrupting essential domain contacts leading to the uncoupling of the ECD and TMD. Expanding the investigation, I delved into the impact of altering disc thickness by modifying the acyl-chain length of incorporated lipids during nanodisc reconstitution. Surprisingly, this manipulation did not yield notable changes in the receptor's structure, pointing toward the likelihood that a significant proportion of the lipids originates directly from the cell. Mass spectrometry analysis provided additional support for this conclusion. Furthermore, an examination of the influence of membrane rigidity was conducted by enriching nanodiscs with approximately 50 mol% cholesterol, however, no structural impact was observed on the resting and desensitized state. Nevertheless, the presence of cholesterol in the disc is essential for gating as it orchestrates the entry into branch 2 of the gating cycle for α1β3 receptors by stabilizing the first asymmetric state.

Having established an accurate lipid environment replicating the *in situ* context of the receptor most accurately, my focus shifted to unveiling the mechanism through which β-lactam antibiotics interfere with the $GABA_A$ receptor gating and function as channel blockers. This study investigated the binding modes of four distinct β-lactams in the presence of GABA on the synaptic α1β3γ2L $GABA_A$ receptor. Remarkably, all four β-lactams employ the same inhibition mechanism, binding to the pore and obstructing chloride ion influx. Despite this commonality, however, they exhibit diverse binding modes, influenced by the variable groups attached to the penicillin ring. Interestingly, while PenG and PenV reveal a single clear density in the channel's pore, piperacillin has three binding sites, completely obstructing the channel pore from the 2’ to the 20’ levels. Expanding the analysis, I determined the structure of the α1β3γ2L $GABA_A$ receptor bound to nafcillin and GABA, revealing two distinct states – asymmetrically and symmetrically desensitized. What is more, nafcillin binds to the benzodiazepine pocket and pockets usually occupied by general anaesthetics, implying a dual allosteric role, simultaneously potentiating and

inhibiting the receptor. The asymmetric state exhibits a significant motion at the β3-B^+/α1-A^- subunit module, suggesting this state represents an intermediate stage in the gating cycle. Notably, PIP_2 is no longer resolved in the asymmetric α1-A subunit, hinting at a potential role in receptor gating, consistent with its known modulation of ion channels (Suh and Hille, 2008). However, the emergence of this state may be influenced by the deep β-lactam binding pocket, potentially interfering with the β3-B^+/α1-A^- pair and inducing the observed conformational change. To comprehensively interpret these findings, I moved on to determine the gating cycle of the receptor on the millisecond timescale.

To unveil the entirety of the receptor's gating cycle in the presence of agonist alone, I employed the time-resolved cryo-EM strategy pioneered by Berriman and Unwin in 1994 (Berriman and Unwin, 1994). Utilizing a manual plunger and a ligand deposition spraying nozzle, this technique enables the structural investigation of the receptor with millisecond-scale time intervals between activation and plunge freezing. This approach allowed the exploration of the orchestrated motions involved in receptor activation and desensitization, including side chain and secondary structure rearrangements in both homomeric and heteromeric receptors.

I determined that the first step of receptor activation is agonist binding to the ECD thus priming the receptor. The TMD, however, is still in the symmetric resting state meaning that these states are pre-active (Fig. 6.1). I further revealed that the gating cycle progresses through asymmetric intermediate states and the entry into the gating cycle is initiated by a single subunit in position C breaking the symmetry of the pore for all $GABA_A$ receptor subtypes. This was also observed for the *Torpedo* nAChR in a native membrane (Unwin and Fujiyoshi, 2012). The displacement of the first chain from the bundle is triggered by agonist to the adjacent ECD interface. This weakens the interaction with the subunit in position C thus allowing it to rotate and break the TMD interface. Subunit C at the level of the TMD then interacts mainly with the other neighbouring subunit (Fig. 6.1). I also showed that the open states for homomeric and diheteromeric receptors are always asymmetric with unobstructed pores (Fig. 6.1).

Surprisingly, lipids were identified as crucial modulators throughout the receptor's gating cycle in both homomeric and heteromeric receptors. Remarkably, these lipids were observed binding in the pore thus obstructing the chloride ion flow—a previously undocumented phenomenon in pLGICs. This lipid block mechanism represents a significant means of

channel closure, categorizing such states as short-lived desensitized/closed in electrophysiological experiments, unveiling a novel modulation mechanism within the Cys-loop receptor family (Fig. 6.1). For all receptors, the last long-lived desensitized state transitions back to be pseudo-symmetric/symmetric (Fig. 6.1).

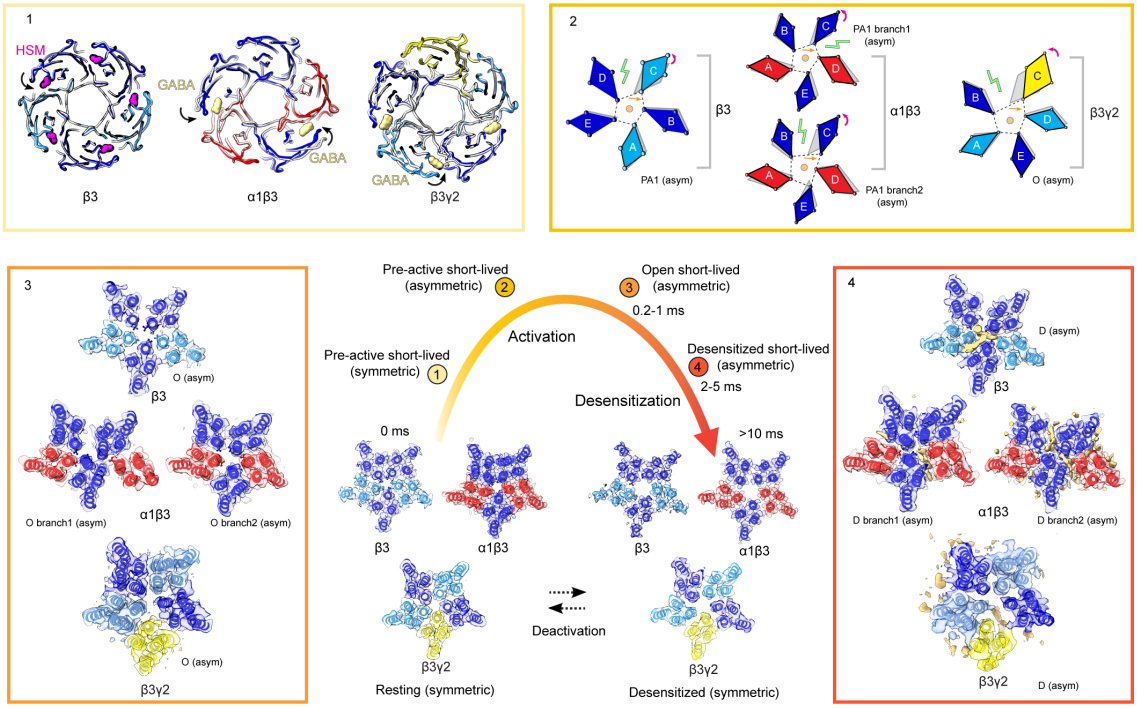


Figure 6.1 – Diverse assemblies of human $GABA_A$ receptors gate by a shared structural mechanism

The first step of the gating cycle of the $GABA_A$ receptor is the binding of the agonist to the ECD as depicted in 1). In this state the ECD is primed and the loop Cs are closed, however, the conformational change has not reached the TMD yet and it is in the resting state. 2) During activation, initially only one subunit breaks the asymmetry of the receptor and this is triggered by agonist binding to the ECD interface immediately next to subunit C. The interfaces with weakened contacts are highlighted with a green crossed line 3) All open states of diverse $GABA_A$ receptor assemblies are asymmetric with clear pores. 4) Lipids play a key role in shutting the receptor by blocking the pore leading to the emergence of short-lived closed/desensitized asymmetric states.

Additionally, I demonstrated that in the presence of PIP_2, which binds to α1,2,3, and 5 subunits typically associated with synaptic receptors, the full-length α1β3 and α1β3γ2 receptors failed to undergo gating. Strikingly, upon PIP_2 removal through subunit truncation, the receptor could undergo asymmetric gating. In the case of the truncated α1β3 diheteromer, a single dataset revealed a gating cycle comprising nine distinct structural states at spatial resolutions from 3.5 Å to 2.4 Å and temporal resolution less than 10 milliseconds. Notably, the diheteromer gates by two branches, with entry into either branch facilitated by structural

changes triggered from one of the two orthosteric GABA binding sites (Fig. 6.1). Furthermore, I demonstrated that positive allosteric modulators and general anaesthetics can fine-tune the receptor by selecting one branch over the other. In the case of HSM and GABA spray on α1β3 receptors, only branch 1 is present since HSM stabilizes the β3-B^+/β3-C^- interface, not allowing it to be disrupted which is required for entry into branch 2. On the other hand, the α1-D^+/β3-C^- is not stabilized and can be disrupted to initiate branch 1. In contrast, when I sprayed PPF at high concentrations to act as an agonist, only branch 2 was manifested. The exact mechanism for this selection, however, remains unclear. Branch selection is hence an important mechanism for modulation of the receptor and may be shared with other members of the pLGICs and more complex $GABA_A$ receptor assemblies.

6.2 Outlook and future directions

6.2.1 The gating cycle of triheteromeric receptors

I determined that the gating cycle of both homomeric and heteromeric receptors consists of asymmetric intermediate states. Additionally, the transitions between these states involve an orchestrated motion, notably triggered by the displacement of one subunit to initially break the pseudo-symmetry of the receptor. Interestingly, in the α1β3 diheteromer, the subunit initiating the gating cycle in both branches is β3-C, which is substituted by the γ2 subunit in the triheteromeric α1β3γ2 synaptic receptors. This is also the case for the β3γ2 diheteromer where the γ2-C subunit is the driving force of the gating cycle of the receptor. This implies that the complexity and number of states in the gating cycle are influenced by the interface contacts of the subunit in this position. Notably, the γ2 subunit in this position exhibits weaker interface contacts than β3, as evidenced by the propensity of γ2 to collapse in SMALPs and in Saposin A, as discussed in Chapter III. What is more, when α1β3γ2 receptors are solubilized with harsh detergents such as DM or DDM, the γ2 collapses inside the pore of the resting receptor and the ECD/TMD coupling is completely lost (Phulera et al., 2018, Zhu et al., 2018), which is not the case for the β3 homomer in DDM for example (Miller and Aricescu, 2014). This complexity is further underscored by single-channel electrophysiology recordings, which indicate that, unlike α1β3 receptors, the α1β3γ2 receptor enters the longer-lived open state more frequently and has a higher open probability (Kasaragod et al., 2022).

To elucidate the gating of triheteromeric receptors, I purified the PIP_2-less truncated α1β3γ2 (Miller et al., 2018). Due to the lack of ICD density in the truncated receptor, breaking the

pseudo-symmetry computationally posed a challenge. To address this, Nb38 was added to the receptor (Fig. 6.2.1a). Upon reconstructing a trial cryo-EM dataset, however, I determined that the cell pool generated consists of two different receptor ensembles: α1-A/β3-B/γ2-C/α1-D/β3-E and α1-A/β3-B/γ2-C/β3-D/β3-E. The latter, however, will not be gated by GABA at lower concentration as it lacks one of the orthosteric binding sites. This was evident from the weaker density of the α1.D subunit and specific β3 markers in this position, such as His267 pointing towards the pore and density for the β3-specific Asn149 glycan (Fig. 6.2.1b,c). To resolve this issue, β3/β3 interface-specific Mb25 will be added in order to separate the α1-A/β3-B/γ2-C/β3-D/β3-E class *in silico*, focusing on the remaining α1-A/β3-B/γ2-C/α1-D/β3-E assembly. This dataset should reveal whether α1β3γ2 receptors also gate via a dual-branch gating cycle and determine the order of its progressions, possibly also involving short-lived asymmetric intermediates.

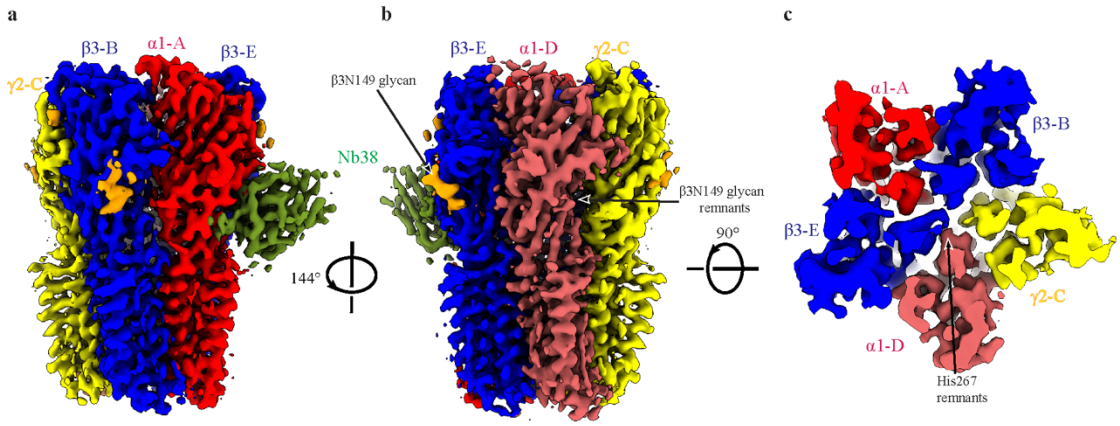


Figure 6.2.1 – Truncated α1β3γ2 receptor cryo-EM reconstruction

a) *Side view of the receptor highlighting Nb38 bound to the α1-A^{+}/β3-B^{-} interface. The α1-A has no features of other subunits present and the density is not fragmented.* ***b)*** *Side view of the receptor highlighting the α1-D subunit (purple). The density for this subunit is fragmented towards the ECD and some features of the β3-specific Asn149 glycan are present suggesting this position is a mixture of α1 and β3.* ***c)*** *Slice at the level of the TMD showing remnants of the β3-specific His267 density emerging from the α1-D subunit.*

6.2.2 Allosteric modulation of triheteromeric receptors

With the activation and desensitization mechanism of α1β3γ2 receptor in hand, it will be important to establish the structural mechanism of action of different classes of allosteric modulators on the $GABA_A$ receptor. As discussed in this thesis, for α1β3 receptors the positive allosteric modulator histamine was shown to modulate the receptor via branch selection and selected branch 1 over branch 2. On the other hand, when the general

anaesthetic propofol was used as an agonist, it selected branch 2 over branch 1. It therefore appears that different allosteric modulators can select one branch over the other thus modulating the mean-open times on the level of single channels or their burst frequency and duration.

In the case of the triheteromeric α1β3γ2 receptors, however, many more allosteric ligands are known to modulate the receptor. One such class of ligands are the benzodiazepines that bind to the ECD (Fig. 6.2.2a) which alone cannot gate the receptor at clinically relevant concentrations but can potentiate the GABA response. In general, benzodiazepines fall into three categories. Classical benzodiazepines such as Valium or Xanax are positive allosteric modulators which shift the GABA response curve to the left and increase the mean open times of the channel (Twyman et al., 1989). On the other hand, other benzodiazepines like flumazenil do not affect the GABA curve and are therefore called 'benzodiazepine pocket antagonists' (Corda et al., 1989). The third class of molecules are the benzodiazepine pocket inverse agonists. One such drug is Ro15-4513 which shifts the GABA response curve to the right thus lowering the effect of GABA on the receptor (Corda et al., 1989). Despite the diversity in benzodiazepine classes, the exact mechanism of their modulation remains unknown. Notably, structural analyses involving compounds such as diazepam, flumazenil, Ro15-4513, and α5-specific benzodiazepine NAMs and PAMs reveal no major structural conformational changes in both the resting and deep desensitized states (Phulera et al., 2018, Masiulis et al., 2019, Kasaragod et al., 2023, Sente et al., 2022). This observation suggests that these molecules likely modulate the receptor only during channel activation and millisecond-scale desensitization. They may selectively influence one branch over the others, stabilize specific states of the gating cycle, or potentiate different open states than those observed with GABA alone. The complex details of these modulatory effects, however, require further investigation.

Moreover, just like homomeric and diheteromeric receptors, the triheteromeric α1β3γ2 can also be influenced by small molecules binding to its TMD region. A specific class of such molecules are the anaesthetics, which, as previously discussed, can function as both modulators and agonists. Notably, in the α1β3γ2 receptor, two new interfaces emerge on either side of the γ2 subunit, offering additional targets alongside the remaining interfaces which are also present in the α1β3 receptor. For instance, 4-benzoyl-propofol can activate the receptor directly by binding to the $\alpha1^{+}/\gamma2^{-}$ and $\alpha1^{+}/\beta3^{-}$ TMD interfaces. In contrast, pentobarbital can bind to four different interfaces, including the $\gamma2^{+}/\alpha1^{-}$ interface. This raises

the question of how different anaesthetics modulate the receptor, especially when compared to compounds like propofol and etomidate, which bind the $\beta3^{+}/\alpha1^{-}$ interface (Fig. 6.2.2b). Furthermore, the impact on the gating cycle remains unclear when multiple anaesthetics targeting distinct interfaces are used simultaneously. Will there be synergy and additivity between the two drugs, or will one predominantly drive the transitions during activation and desensitization? This aspect of receptor modulation and the interplay between various anaesthetics targeting different interfaces will be a key in understanding their mechanism of action.

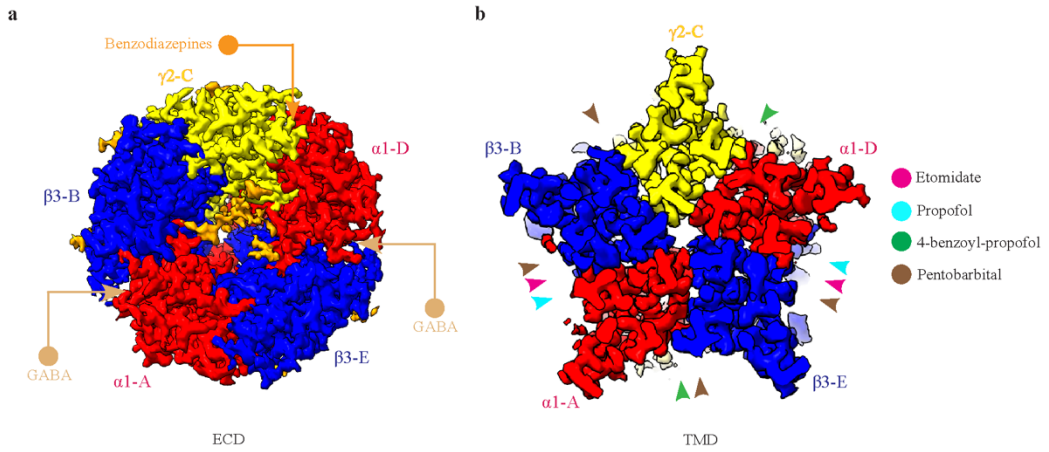


Figure 6.2.2 – Allosteric modulation of the α1β3γ2 receptor

a) *View of the extracellular domain indicating the benzodiazepine and GABA binding pockets.* ***b)*** *View of the transmembrane domain showing the binding sites between subunit interfaces for a diverse set of anaesthetics including etomidate, propofol, 4-benzoyl-propofol and pentobarbital*

Furthermore, the TMD region can also be targeted by yet another class of potentiators – the neurosteroids (Hosie et al., 2006). Neurosteroids, just like benzodiazepines can function both as PAMs e.g allopregnanolone (Diviccaro et al., 2022) and NAMs e.g pregnenolone sulfate (Akk et al., 2001). How would these molecules compare to ligands modulating the receptor via the ECD or to anaesthetics that also function through the TMD?

6.2.3 The mechanism of $GABA_A$ receptor deactivation

In this thesis, I have extensively explored the mechanism of $GABA_A$ receptor activation and desensitization triggered by GABA and small molecules upon application on the millisecond timescale. However, to complete the full gating cycle, it is imperative for the receptor to deactivate—releasing GABA from the orthosteric binding site and transitioning from the desensitized to the resting state.

The process of deactivation in the synaptic environment is complex and primarily driven by the rapid reuptake of GABA through GAT1 transporters in presynaptic terminals and adjacent glial cells (Lavoie et al., 1997). Unfortunately, structurally characterizing the deactivation process requires GABA to be released from the receptor, which is impossible to achieve on the cryo-EM grid. To address this challenge, I employed the GABA competitive antagonist Bicuculline (BCC). It has been demonstrated that, in the presence of BCC, recorded currents fully deactivate even when GABA is still present in the solution (Lavoie et al., 1997).

To validate this hypothesis, I used the α1β3 receptor fully desensitized by a 2-hour incubation with 0.5 µM GABA. Subsequently, 100 µM (-) BCC methiodide was added to the receptor and incubated for an additional 2 hours, aiming to return all particles to the resting state. Upon reconstruction of this dataset, density for BCC can be seen under both orthosteric binding sites (Fig. 6.2.3a-b). Just as for the α1β3γ2 reported previously. BCC binding under loop C flips it out thereby stabilizing the resting state. Additionally, it is evident that the receptor has indeed reverted to the resting state, with both 17' His and 9' Leu gates fully closed (Fig. 6.2.3c). Comparing the pore profiles between the apo state, BCC-bound state and desensitized state further confirms that the receptor has transitioned back to the resting state (Fig. 6.2.3d).

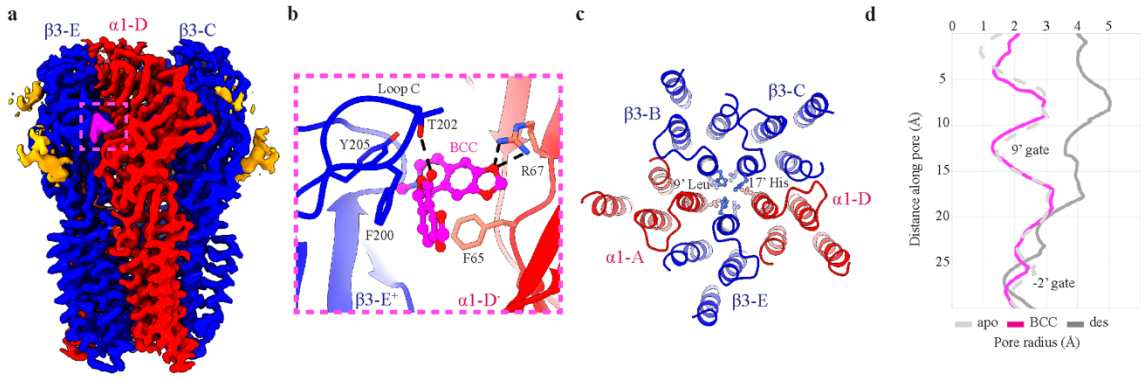


Figure 6.2.3 – Deactivation of α1β3 by bicuculline

a) *Side view of the cryo-EM map highlighting the density for BCC under loop C.* ***b)*** *BCC stabilizes loop C in an outward conformation by a hydrogen bond network as well as π-π interactions.* ***c)*** *View of the TMD regions highlighting that the 17' and 9' gates are closed.* ***d)*** *Pore profiles of the apo state, BCC-bound state and desensitized state*

Notably, however, no intermediate states could be classified at this timescale. This is well in line with electrophysiology recordings which show that the transitions during deactivation

also occur on the millisecond timescale (Lavoie et al., 1997). To address this limitation, my plan is to spray BCC on receptors desensitized by prolonged GABA incubations limiting the BCC application to ~40ms, capturing the millisecond-scale dynamics of deactivation. This approach aims to provide a comprehensive structural model of the complete $GABA_A$ receptor gating cycle.

6.2.4 Updated model for $GABA_A$ receptor gating

In this thesis, I have demonstrated that the $GABA_A$ receptor gating cycle on the millisecond timescale involves transient asymmetric states, both conducting and non-conducting, each of short duration. What is more, the gating of the $GABA_A$ receptor is always initiated by the subunit in position C of the bundle that breaks the symmetry of the pore. Notably, the influence of lipids emerges as a crucial factor, finely regulating receptor open times by blocking the pore as well as stabilizing newly formed interfaces. Furthermore, all open states of the receptors are asymmetric with unobstructed pores (Fig. 6.1). The groundbreaking time-resolved methodology pioneered by Berriman and Unwin in 1994 has been instrumental in unraveling the details of the gating cycle. This not only enhances our understanding of the receptor's dynamics but also opens up new avenues for exploring the interactions and modulation of the $GABA_A$ receptor by clinically relevant drugs as well as for the development of novel therapeutics.

It is crucial to note, however, that the study discussed herein is based on *in vitro* reconstituted receptors. A comprehensive understanding of the $GABA_A$ receptor's gating cycle within the brain remains a crucial next step. While recent advances in cryo-electron tomography represent a significant step toward achieving this goal, it is essential to acknowledge that, to date, no membrane protein has been resolved by cryo-ET to high enough resolution required to study the dynamics of the receptor. The promise of unveiling the nuanced details at the secondary structure and side chain levels of the receptor's gating cycle within the brain relies on crucial advancements in microscope hardware and processing software in the coming decades. As technology progresses, the potential to achieve higher resolution becomes increasingly attainable, paving the way for a more comprehensive understanding of the receptor's dynamics within its native neural environment.

References

AFONINE, P. V., POON, B. K., READ, R. J., SOBOLEV, O. V., TERWILLIGER, T. C., URZHUMTSEV, A. & ADAMS, P. D. 2018. Real-space refinement in PHENIX for cryo-EM and crystallography. *Acta Crystallogr D Struct Biol,* 74**,** 531-544.

AKK, G., BRACAMONTES, J. & STEINBACH, J. H. 2001. Pregnenolone sulfate block of GABA(A) receptors: mechanism and involvement of a residue in the M2 region of the alpha subunit. *J Physiol,* 532**,** 673-84.

ALLEN, J. A., HALVERSON-TAMBOLI, R. A. & RASENICK, M. M. 2007. Lipid raft microdomains and neurotransmitter signalling. *Nat Rev Neurosci,* 8**,** 128-40.

ARICESCU, A. R., LU, W. & JONES, E. Y. 2006. A time- and cost-efficient system for high-level protein production in mammalian cells. *Acta Crystallogr D Biol Crystallogr,* 62**,** 1243-50.

BAI, D., PENNEFATHER, P. S., MACDONALD, J. F. & ORSER, B. A. 1999a. The general anesthetic propofol slows deactivation and desensitization of GABA(A) receptors. *J Neurosci,* 19**,** 10635-46.

BAI, D., PENNEFATHER, P. S., MACDONALD, J. F. & ORSER, B. A. 1999b. The general anesthetic propofol slows deactivation and desensitization of GABAA receptors. *Journal of Neuroscience,* 19**,** 10635-10646.

BALI, M. & AKABAS, M. H. 2007. The location of a closed channel gate in the GABAA receptor channel. *J Gen Physiol,* 129**,** 145-59.

BALI, M. & AKABAS, M. H. 2012. Gating-induced conformational rearrangement of the γ-aminobutyric acid type A receptor β-α subunit interface in the membrane-spanning domain. *J Biol Chem,* 287**,** 27762-70.

BARBERIS, A., MOZRZYMAS, J. W., ORTINSKI, P. I. & VICINI, S. 2007. Desensitization and binding properties determine distinct alpha1beta2gamma2 and alpha3beta2gamma2 GABA(A) receptor-channel kinetic behavior. *Eur J Neurosci,* 25**,** 2726-40.

BEPLER, T., MORIN, A., RAPP, M., BRASCH, J., SHAPIRO, L., NOBLE, A. J. & BERGER, B. 2019. Positive-unlabeled convolutional neural networks for particle picking in cryo-electron micrographs. *Nat Methods,* 16**,** 1153-1160.

BERA, A. K., CHATAV, M. & AKABAS, M. H. 2002. GABAA receptor M2–M3 loop secondary structure and changes in accessibility during channel gating. *Journal of Biological Chemistry,* 277**,** 43002-43010.

BERRIMAN, J. & UNWIN, N. 1994. Analysis of transient structures by cryo-microscopy combined with rapid mixing of spray droplets. *Ultramicroscopy,* 56**,** 241-252.

BHARAT, T. A., RICHES, J. D., KOLESNIKOVA, L., WELSCH, S., KRÄHLING, V., DAVEY, N., PARSY, M. L., BECKER, S. & BRIGGS, J. A. 2011. Cryo-electron tomography of Marburg virus particles and their morphogenesis within infected cells. *PLoS Biol,* 9**,** e1001196.

BIANCHI, M. T., BOTZOLAKIS, E. J., HAAS, K. F., FISHER, J. L. & MACDONALD, R. L. 2007. Microscopic kinetic determinants of macroscopic currents: insights from coupling and uncoupling of GABAA receptor desensitization and deactivation. *J Physiol,* 584**,** 769-87.

BIDAUT, M. 1980. Pharmacological dissection of pyloric network of the lobster stomatogastric ganglion using picrotoxin. *J Neurophysiol,* 44**,** 1089-1101.

BOCQUET, N., NURY, H., BAADEN, M., LE POUPON, C., CHANGEUX, J. P., DELARUE, M. & CORRINGER, P. J. 2009. X-ray structure of a pentameric ligand-gated ion channel in an apparently open conformation. *Nature,* 457**,** 111-4.

BOUZAT, C. 2012. New insights into the structural bases of activation of Cys-loop receptors. *J Physiol Paris,* 106**,** 23-33.

BREJC, K., VAN DIJK, W. J., KLAASSEN, R. V., SCHUURMANS, M., VAN DER OOST, J., SMIT, A. B. & SIXMA, T. K. 2001. Crystal structure of an ACh-binding protein reveals the ligand-binding domain of nicotinic receptors. *Nature,* 411**,** 269-76.

BRICKLEY, S. G. & MODY, I. 2012. Extrasynaptic GABA(A) receptors: their function in the CNS and implications for disease. *Neuron,* 73**,** 23-34.

CASCIO, M. 2006. Modulating inhibitory ligand-gated ion channels. *Aaps j,* 8**,** E353-61.

CASPAR, D. L. D. & KIRSCHNER, D. A. 1971. Myelin Membrane Structure at 10 Å Resolution. *Nature New Biology,* 231**,** 46-52.

CHAKRAPANI, S. & AUERBACH, A. 2005. A speed limit for conformational change of an allosteric membrane protein. *Proc Natl Acad Sci U S A,* 102**,** 87-92.

CHANGEUX, J. P. 2014. Protein dynamics and the allosteric transitions of pentameric receptor channels. *Biophys Rev,* 6**,** 311-321.

CHEN, V. B., ARENDALL, W. B., 3RD, HEADD, J. J., KEEDY, D. A., IMMORMINO, R. M., KAPRAL, G. J., MURRAY, L. W., RICHARDSON, J. S. & RICHARDSON, D. C. 2010. MolProbity: all-atom structure validation for macromolecular crystallography. *Acta Crystallogr D Biol Crystallogr,* 66**,** 12-21.

CHOII, G. & KO, J. 2015. Gephyrin: a central GABAergic synapse organizer. *Exp Mol Med,* 47**,** e158.

CHOW, P. & MATHERS, D. 1986. Convulsant doses of penicillin shorten the lifetime of GABA-induced channels in cultured central neurones. *Br J Pharmacol,* 88**,** 541-7.

CITRI, A. & MALENKA, R. C. 2008. Synaptic Plasticity: Multiple Forms, Functions, and Mechanisms. *Neuropsychopharmacology,* 33**,** 18-41.

CLOUGH, G. & MICHEL, C. C. 1981. The role of vesicles in the transport of ferritin through frog endothelium. *J Physiol,* 315**,** 127-42.

CORDA, M. G., GIORGI, O., LONGONI, B. & BIGGIO, G. 1989. Ro 15-4513, a partial inverse agonist for benzodiazepine recognition sites, has proconflict and proconvulsant effects in the rat. *Eur J Pharmacol,* 159**,** 233-9.

COTMAN, C., BLANK, M. L., MOEHL, A. & SNYDER, F. 1969. Lipid composition of synaptic plasma membranes isolated from rat brain by zonal centrifugation. *Biochemistry,* 8**,** 4606-12.

CRAIG, A. M. & KANG, Y. 2007. Neurexin-neuroligin signaling in synapse development. *Curr Opin Neurobiol,* 17**,** 43-52.

CRANK, J. 1979. *The mathematics of diffusion*, Oxford university press.

CRIADO, M., EIBL, H. & BARRANTES, F. J. 1982. Effects of lipids on acetylcholine receptor. Essential need of cholesterol for maintenance of agonist-induced state transitions in lipid vesicles. *Biochemistry,* 21**,** 3622-9.

DÄMGEN, M. A. & BIGGIN, P. C. 2021. State-dependent protein-lipid interactions of a pentameric ligand-gated ion channel in a neuronal membrane. *PLoS Comput Biol,* 17**,** e1007856.

DARLISON, M. G. 1992. Invertebrate GABA and glutamate receptors: molecular biology reveals predictable structures but some unusual pharmacologies. *Trends Neurosci,* 15**,** 469-74.

DAVIES, P. A., WANG, W., HALES, T. G. & KIRKNESS, E. F. 2003. A novel class of ligand-gated ion channel is activated by Zn2+. *J Biol Chem,* 278**,** 712-7.

DICKERSON, J. L., LU, P. H., HRISTOV, D., DUNIN-BORKOWSKI, R. E. & RUSSO, C. J. 2022. Imaging biological macromolecules in thick specimens: The role of inelastic scattering in cryoEM. *Ultramicroscopy,* 237**,** 113510.

DIVICCARO, S., CIOFFI, L., FALVO, E., GIATTI, S. & MELCANGI, R. C. 2022. Allopregnanolone: An overview on its synthesis and effects. *J Neuroendocrinol,* 34**,** e12996.

DÖRR, J. M., SCHEIDELAAR, S., KOORENGEVEL, M. C., DOMINGUEZ, J. J., SCHÄFER, M., VAN WALREE, C. A. & KILLIAN, J. A. 2016. The styrene-maleic acid copolymer: a versatile tool in membrane research. *Eur Biophys J,* 45**,** 3-21.

DOSTALOVA, Z., LIU, A., ZHOU, X., FARMER, S. L., KRENZEL, E. S., AREVALO, E., DESAI, R., FEINBERG-ZADEK, P. L., DAVIES, P. A., YAMODO, I. H., FORMAN, S. A. & MILLER, K. W. 2010. High-level expression and purification of Cys-loop ligand-gated ion channels in a tetracycline-inducible stable mammalian cell line: GABAA and serotonin receptors. *Protein Sci,* 19**,** 1728-38.

DOSTALOVA, Z., ZHOU, X., LIU, A., ZHANG, X., ZHANG, Y., DESAI, R., FORMAN, S. A. & MILLER, K. W. 2014. Human α1β3γ2L gamma-aminobutyric acid type A receptors: High-level production and purification in a functional state. *Protein Sci,* 23**,** 157-66.

ELEGHEERT, J., BEHIELS, E., BISHOP, B., SCOTT, S., WOOLLEY, R. E., GRIFFITHS, S. C., BYRNE, E. F. X., CHANG, V. T., STUART, D. I., JONES, E. Y., SIEBOLD, C. & ARICESCU, A. R. 2018. Lentiviral transduction of mammalian cells for fast, scalable and high-level production of soluble and membrane proteins. *Nat Protoc,* 13**,** 2991-3017.

ELENES, S. & AUERBACH, A. 2002. Desensitization of diliganded mouse muscle nicotinic acetylcholine receptor channels. *J Physiol,* 541**,** 367-83.

EMSLEY, P., LOHKAMP, B., SCOTT, W. G. & COWTAN, K. 2010. Features and development of Coot. *Acta Crystallogr D Biol Crystallogr,* 66**,** 486-501.

FALZONE, M. E. & MACKINNON, R. 2023. Gβγ activates PIP2 hydrolysis by recruiting and orienting PLCβ on the membrane surface. *Proc Natl Acad Sci U S A,* 120**,** e2301121120.

FARRANT, M. & NUSSER, Z. 2005. Variations on an inhibitory theme: phasic and tonic activation of GABAA receptors. *Nature Reviews Neuroscience,* 6**,** 215-229.

FIELD, M., DOROVYKH, V., THOMAS, P. & SMART, T. G. 2021. Physiological role for GABAA receptor desensitization in the induction of long-term potentiation at inhibitory synapses. *Nature Communications,* 12**,** 2112.

FLAYHAN, A., MERTENS, H. D. T., URAL-BLIMKE, Y., MARTINEZ MOLLEDO, M., SVERGUN, D. I. & LÖW, C. 2018. Saposin Lipid Nanoparticles: A Highly Versatile and Modular Tool for Membrane Protein Research. *Structure,* 26**,** 345-355.e5.

FONG, T. M. & MCNAMEE, M. G. 1986. Correlation between acetylcholine receptor function and structural properties of membranes. *Biochemistry,* 25**,** 830-40.

FORMAN, S. A. & MILLER, K. W. 2011. Anesthetic sites and allosteric mechanisms of action on Cys-loop ligand-gated ion channels. *Can J Anaesth,* 58**,** 191-205.

FUJIMOTO, M., MUNAKATA, M. & AKAIKE, N. 1995. Dual mechanisms of GABAA response inhibition by beta-lactam antibiotics in the pyramidal neurones of the rat cerebral cortex. *Br J Pharmacol,* 116**,** 3014-20.

GE, Y., KANG, Y., CASSIDY, R. M., MOON, K. M., LEWIS, R., WONG, R. O. L., FOSTER, L. J. & CRAIG, A. M. 2018. Clptm1 Limits Forward Trafficking of GABA(A) Receptors to Scale Inhibitory Synaptic Strength. *Neuron,* 97**,** 596-610.e8.

GEMMER, M., CHAILLET, M. L., VAN LOENHOUT, J., CUEVAS ARENAS, R., VISMPAS, D., GRÖLLERS-MULDERIJ, M., KOH, F. A., ALBANESE, P., SCHELTEMA, R. A., HOWES, S. C., KOTECHA, A., FEDRY, J. & FÖRSTER, F. 2023. Visualization of translation and protein biogenesis at the ER membrane. *Nature,* 614**,** 160-167.

GENTET, L. J., STUART, G. J. & CLEMENTS, J. D. 2000. Direct measurement of specific membrane capacitance in neurons. *Biophys J,* 79**,** 314-20.

GIELEN, M. & CORRINGER, P. J. 2018. The dual-gate model for pentameric ligand-gated ion channels activation and desensitization. *J Physiol,* 596**,** 1873-1902.

GONZALEZ-GUTIERREZ, G., LUKK, T., AGARWAL, V., PAPKE, D., NAIR, S. K. & GROSMAN, C. 2012. Mutations that stabilize the open state of the Erwinia chrisanthemi

ligand-gated ion channel fail to change the conformation of the pore domain in crystals. *Proc Natl Acad Sci U S A,* 109**,** 6331-6.

GONZALEZ-GUTIERREZ, G., WANG, Y., CYMES, G. D., TAJKHORSHID, E. & GROSMAN, C. 2017. Chasing the open-state structure of pentameric ligand-gated ion channels. *J Gen Physiol,* 149**,** 1119-1138.

GRENNINGLOH, G., GUNDELFINGER, E., SCHMITT, B., BETZ, H., DARLISON, M. G., BARNARD, E. A., SCHOFIELD, P. R. & SEEBURG, P. H. 1987. Glycine vs GABA receptors. *Nature,* 330**,** 25-6.

GRINKOVA, Y. V., DENISOV, I. G. & SLIGAR, S. G. 2010. Engineering extended membrane scaffold proteins for self-assembly of soluble nanoscale lipid bilayers. *Protein Eng Des Sel,* 23**,** 843-8.

GROSMAN, C., ZHOU, M. & AUERBACH, A. 2000. Mapping the conformational wave of acetylcholine receptor channel gating. *Nature,* 403**,** 773-6.

GUITCHOUNTS, G., STEWART, D. S. & FORMAN, S. A. 2012. Two etomidate sites in α1β2γ2 γ-aminobutyric acid type A receptors contribute equally and noncooperatively to modulation of channel gating. *Anesthesiology,* 116**,** 1235-44.

HACKELBERG, S. & OLIVER, D. 2018. Metabotropic Acetylcholine and Glutamate Receptors Mediate PI(4,5)P2 Depletion and Oscillations in Hippocampal CA1 Pyramidal Neurons in situ. *Scientific Reports,* 8**,** 12987.

HAMMOND, J. R. & MARTIN, I. L. 1987. Modulation of [3H]flunitrazepam binding to rat cerebellar benzodiazepine receptors by phosphatidylserine. *Eur J Pharmacol,* 137**,** 49-58.

HAMOUDA, A. K., SANGHVI, M., SAULS, D., MACHU, T. K. & BLANTON, M. P. 2006. Assessing the lipid requirements of the Torpedo californica nicotinic acetylcholine receptor. *Biochemistry,* 45**,** 4327-37.

HAN, W., SHEPARD, R. D. & LU, W. 2021. Regulation of GABA(A)Rs by Transmembrane Accessory Proteins. *Trends Neurosci,* 44**,** 152-165.

HANNAN, S., MINERE, M., HARRIS, J., IZQUIERDO, P., THOMAS, P., TENCH, B. & SMART, T. G. 2020. GABA(A)R isoform and subunit structural motifs determine synaptic and extrasynaptic receptor localisation. *Neuropharmacology,* 169**,** 107540.

HANSEN, S. B., SULZENBACHER, G., HUXFORD, T., MARCHOT, P., TAYLOR, P. & BOURNE, Y. 2005. Structures of Aplysia AChBP complexes with nicotinic agonists and antagonists reveal distinctive binding interfaces and conformations. *Embo j,* 24**,** 3635-46.

HARVEY, R. J., VREUGDENHIL, E., ZAMAN, S. H., BHANDAL, N. S., USHERWOOD, P. N., BARNARD, E. A. & DARLISON, M. G. 1991. Sequence of a functional invertebrate GABAA receptor subunit which can form a chimeric receptor with a vertebrate alpha subunit. *Embo j,* 10**,** 3239-45.

HIBBS, R. E. & GOUAUX, E. 2011. Principles of activation and permeation in an anion-selective Cys-loop receptor. *Nature,* 474**,** 54-60.

HILF, R. J. & DUTZLER, R. 2008. X-ray structure of a prokaryotic pentameric ligand-gated ion channel. *Nature,* 452**,** 375-9.

HILF, R. J. & DUTZLER, R. 2009. Structure of a potentially open state of a proton-activated pentameric ligand-gated ion channel. *Nature,* 457**,** 115-8.

HILLE, B., DICKSON, E. J., KRUSE, M., VIVAS, O. & SUH, B. C. 2015. Phosphoinositides regulate ion channels. *Biochim Biophys Acta,* 1851**,** 844-56.

HOSIE, A. M., WILKINS, M. E., DA SILVA, H. M. & SMART, T. G. 2006. Endogenous neurosteroids regulate GABAA receptors through two discrete transmembrane sites. *Nature,* 444**,** 486-9.

INGÓLFSSON, H. I., CARPENTER, T. S., BHATIA, H., BREMER, P. T., MARRINK, S. J. & LIGHTSTONE, F. C. 2017. Computational Lipidomics of the Neuronal Plasma Membrane. *Biophys J,* 113**,** 2271-2280.

JAYAKAR, S. S., ZHOU, X., CHIARA, D. C., JARAVA-BARRERA, C., SAVECHENKOV, P. Y., BRUZIK, K. S., TORTOSA, M., MILLER, K. W. & COHEN, J. B. 2019. Identifying Drugs that Bind Selectively to Intersubunit General Anesthetic Sites in the α1β3γ2 GABA(A)R Transmembrane Domain. *Mol Pharmacol,* 95**,** 615-628.

KAILA, K., LAMSA, K., SMIRNOV, S., TAIRA, T. & VOIPIO, J. 1997. Long-lasting GABA-mediated depolarization evoked by high-frequency stimulation in pyramidal neurons of rat hippocampal slice is attributable to a network-driven, bicarbonate-dependent K+ transient. *J Neurosci,* 17**,** 7662-72.

KASARAGOD, V. B., MALINAUSKAS, T., WAHID, A. A., LENGYEL, J., KNOFLACH, F., HARDWICK, S. W., JONES, C. F., CHEN, W. N., LUCAS, X., EL OMARI, K., CHIRGADZE, D. Y., ARICESCU, A. R., CECERE, G., HERNANDEZ, M. C. & MILLER, P. S. 2023. The molecular basis of drug selectivity for α5 subunit-containing GABA(A) receptors. *Nat Struct Mol Biol,* 30**,** 1936-1946.

KASARAGOD, V. B., MORTENSEN, M., HARDWICK, S. W., WAHID, A. A., DOROVYKH, V., CHIRGADZE, D. Y., SMART, T. G. & MILLER, P. S. 2022. Mechanisms of inhibition and activation of extrasynaptic αβ GABAA receptors. *Nature,* 602**,** 529-533.

KIM, J. J., GHARPURE, A., TENG, J., ZHUANG, Y., HOWARD, R. J., ZHU, S., NOVIELLO, C. M., WALSH, R. M., LINDAHL, E. & HIBBS, R. E. 2020. Shared structural mechanisms of general anaesthetics and benzodiazepines. *Nature,* 585**,** 303-308.

KIMANIUS, D., DONG, L., SHAROV, G., NAKANE, T. & SCHERES, S. H. W. 2021. New tools for automated cryo-EM single-particle analysis in RELION-4.0. *Biochem J,* 478**,** 4169-4185.

KINDE, M. N., CHEN, Q., LAWLESS, M. J., MOWREY, D. D., XU, J., SAXENA, S., XU, Y. & TANG, P. 2015. Conformational Changes Underlying Desensitization of the Pentameric Ligand-Gated Ion Channel ELIC. *Structure,* 23**,** 995-1004.

KRISHEK, B. J., MOSS, S. J. & SMART, T. G. 1996. Homomeric beta 1 gamma-aminobutyric acid A receptor-ion channels: evaluation of pharmacological and physiological properties. *Mol Pharmacol,* 49**,** 494-504.

LAHA, K. T., GHOSH, B. & CZAJKOWSKI, C. 2013. Macroscopic kinetics of pentameric ligand gated ion channels: comparisons between two prokaryotic channels and one eukaryotic channel. *PLoS One,* 8**,** e80322.

LAPE, R., PLESTED, A. J., MORONI, M., COLQUHOUN, D. & SIVILOTTI, L. G. 2012. The α1K276E startle disease mutation reveals multiple intermediate states in the gating of glycine receptors. *J Neurosci,* 32**,** 1336-52.

LAVERTY, D., DESAI, R., UCHAŃSKI, T., MASIULIS, S., STEC, W. J., MALINAUSKAS, T., ZIVANOV, J., PARDON, E., STEYAERT, J., MILLER, K. W. & ARICESCU, A. R. 2019. Cryo-EM structure of the human α1β3γ2 GABA(A) receptor in a lipid bilayer. *Nature,* 565**,** 516-520.

LAVOIE, A. M., TINGEY, J. J., HARRISON, N. L., PRITCHETT, D. B. & TWYMAN, R. E. 1997. Activation and deactivation rates of recombinant GABA(A) receptor channels are dependent on alpha-subunit isoform. *Biophys J,* 73**,** 2518-26.

LEE, W. Y., FREE, C. R. & SINE, S. M. 2009. Binding to gating transduction in nicotinic receptors: Cys-loop energetically couples to pre-M1 and M2–M3 regions. *Journal of Neuroscience,* 29**,** 3189-3199.

LEGENDRE, P., MULLER, E., BADIU, C. I., MEIER, J., VANNIER, C. & TRILLER, A. 2002. Desensitization of homomeric alpha1 glycine receptor increases with receptor density. *Mol Pharmacol,* 62**,** 817-27.

LIAO, Y., LIU, X., JOUNAIDI, Y., FORMAN, S. A. & FENG, H. J. 2019. Etomidate Effects on Desensitization and Deactivation of α4β3δ GABA(A) Receptors Inducibly Expressed in HEK293 TetR Cells. *J Pharmacol Exp Ther,* 368**,** 100-105.

LIN, C. S., CHENG, C. J., CHOU, C. H. & LIN, S. H. 2007. Piperacillin/tazobactam-induced seizure rapidly reversed by high flux hemodialysis in a patient on peritoneal dialysis. *Am J Med Sci,* 333**,** 181-4.

LIU, X., KRAUSE, W. C. & DAVIS, R. L. 2007. GABAA receptor RDL inhibits Drosophila olfactory associative learning. *Neuron,* 56**,** 1090-102.

LIU, X. & WANG, W. 2023. Asymmetric gating of a human hetero-pentameric glycine receptor. *Nature Communications,* 14**,** 6377.

LIU, Y. T., TAO, C. L., ZHANG, X., XIA, W., SHI, D. Q., QI, L., XU, C., SUN, R., LI, X. W., LAU, P. M., ZHOU, Z. H. & BI, G. Q. 2020. Mesophasic organization of GABA(A) receptors in hippocampal inhibitory synapses. *Nat Neurosci,* 23**,** 1589-1596.

LONGSWORTH, L. G. 1953. Diffusion Measurements, at 25°, of Aqueous Solutions of Amino Acids, Peptides and Sugars. *Journal of the American Chemical Society,* 75**,** 5705-5709.

LÜSCHER, B. P., BAUR, R., GOELDNER, M. & SIGEL, E. 2012. Influence of GABA(A) receptor α subunit isoforms on the benzodiazepine binding site. *PLoS One,* 7**,** e42101.

LYNCH, J. W. 2004. Molecular structure and function of the glycine receptor chloride channel. *Physiol Rev,* 84**,** 1051-95.

MACDONALD, R. L., ROGERS, C. J. & TWYMAN, R. E. 1989. Kinetic properties of the GABAA receptor main conductance state of mouse spinal cord neurones in culture. *J Physiol,* 410**,** 479-99.

MALANGA, C. J., KOKONTIS, L. & MAUZY, S. 1997. Piperacillin-induced seizures. *Clin Pediatr (Phila),* 36**,** 475-8.

MAN, B. L. & FU, Y. P. 2015. Piperacillin/tazobactam-induced myoclonic jerks in a man with chronic renal failure. *BMJ Case Rep,* 2015.

MARKRAM, H., MULLER, E., RAMASWAMY, S., REIMANN, M. W., ABDELLAH, M., SANCHEZ, C. A., AILAMAKI, A., ALONSO-NANCLARES, L., ANTILLE, N., ARSEVER, S., KAHOU, G. A., BERGER, T. K., BILGILI, A., BUNCIC, N., CHALIMOURDA, A., CHINDEMI, G., COURCOL, J. D., DELALONDRE, F., DELATTRE, V., DRUCKMANN, S., DUMUSC, R., DYNES, J., EILEMANN, S., GAL, E., GEVAERT, M. E., GHOBRIL, J. P., GIDON, A., GRAHAM, J. W., GUPTA, A., HAENEL, V., HAY, E., HEINIS, T., HERNANDO, J. B., HINES, M., KANARI, L., KELLER, D., KENYON, J., KHAZEN, G., KIM, Y., KING, J. G., KISVARDAY, Z., KUMBHAR, P., LASSERRE, S., LE BÉ, J. V., MAGALHÃES, B. R., MERCHÁN-PÉREZ, A., MEYSTRE, J., MORRICE, B. R., MULLER, J., MUÑOZ-CÉSPEDES, A., MURALIDHAR, S., MUTHURASA, K., NACHBAUR, D., NEWTON, T. H., NOLTE, M., OVCHARENKO, A., PALACIOS, J., PASTOR, L., PERIN, R., RANJAN, R., RIACHI, I., RODRÍGUEZ, J. R., RIQUELME, J. L., RÖSSERT, C., SFYRAKIS, K., SHI, Y., SHILLCOCK, J. C., SILBERBERG, G., SILVA, R., TAUHEED, F., TELEFONT, M., TOLEDO-RODRIGUEZ, M., TRÄNKLER, T., VAN GEIT, W., DÍAZ, J. V., WALKER, R., WANG, Y., ZANINETTA, S. M., DEFELIPE, J., HILL, S. L., SEGEV, I. & SCHÜRMANN, F. 2015. Reconstruction and Simulation of Neocortical Microcircuitry. *Cell,* 163**,** 456-92.

MARTIN, C. & LOWERY, D. 2018. Selective GABAA receptor modulators: intellectual property landscape. *Nature Reviews Drug Discovery,* 17**,** 778-778.

MASIULIS, S., DESAI, R., UCHAŃSKI, T., SERNA MARTIN, I., LAVERTY, D., KARIA, D., MALINAUSKAS, T., ZIVANOV, J., PARDON, E., KOTECHA, A., STEYAERT, J., MILLER, K. W. & ARICESCU, A. R. 2019. GABA(A) receptor signalling mechanisms revealed by structural pharmacology. *Nature,* 565**,** 454-459.

MCCORMACK, T. J., MELIS, C., COLÓN, J., GAY, E. A., MIKE, A., KAROLY, R., LAMB, P. W., MOLTENI, C. & YAKEL, J. L. 2010. Rapid desensitization of the rat α7 nAChR is

facilitated by the presence of a proline residue in the outer β-sheet. *J Physiol,* 588**,** 4415-29.

MCMULLAN, G., NAYDENOVA, K., MIHAYLOV, D., YAMASHITA, K., PEET, M. J., WILSON, H., DICKERSON, J. L., CHEN, S., CANNONE, G., LEE, Y., HUTCHINGS, K. A., GITTINS, O., SOBHY, M. A., WELLS, T., EL-GOMATI, M. M., DALBY, J., MEFFERT, M., SCHULZE-BRIESE, C., HENDERSON, R. & RUSSO, C. J. 2023. Structure determination by cryoEM at 100 keV. *Proc Natl Acad Sci U S A,* 120**,** e2312905120.

MENG, E. C., GODDARD, T. D., PETTERSEN, E. F., COUCH, G. S., PEARSON, Z. J., MORRIS, J. H. & FERRIN, T. E. 2023. UCSF ChimeraX: Tools for Structure Building and Analysis. *Protein Sci***,** e4792.

MEYER, M. A. 2014. Myoclonic jerks secondary to piperacillin and nafcillin. *Neurol Int,* 6**,** 5349.

MILLER, P. S. & ARICESCU, A. R. 2014. Crystal structure of a human GABAA receptor. *Nature,* 512**,** 270-5.

MILLER, P. S., MASIULIS, S., MALINAUSKAS, T., KOTECHA, A., RAO, S., CHAVALI, S., COLIBUS, L. D., PARDON, E., HANNAN, S., SCOTT, S., SUN, Z., FRENZ, B., KLESSE, G., LI, S., DIPROSE, J. M., SIEBERT, C. A., ESNOUF, R. M., DIMAIO, F., TUCKER, S. J., SMART, T. G., STEYAERT, J., BABU, M. M., SANSOM, M. S. P., HUISKONEN, J. T. & ARICESCU, A. R. 2018. Heteromeric GABA_A receptor structures in positively-modulated active states. *bioRxiv***,** 338343.

MILLER, P. S. & SMART, T. G. 2010. Binding, activation and modulation of Cys-loop receptors. *Trends Pharmacol Sci,* 31**,** 161-74.

MODY, I. & PEARCE, R. A. 2004. Diversity of inhibitory neurotransmission through GABA(A) receptors. *Trends Neurosci,* 27**,** 569-75.

MONOD, J., WYMAN, J. & CHANGEUX, J. P. 1965. ON THE NATURE OF ALLOSTERIC TRANSITIONS: A PLAUSIBLE MODEL. *J Mol Biol,* 12**,** 88-118.

MORTENSEN, M., KRISTIANSEN, U., EBERT, B., FRØLUND, B., KROGSGAARD-LARSEN, P. & SMART, T. G. 2004. Activation of single heteromeric GABA(A) receptor ion channels by full and partial agonists. *J Physiol,* 557**,** 389-413.

MOZRZYMAS, J. W., BARBERIS, A., MERCIK, K. & ZARNOWSKA, E. D. 2003a. Binding sites, singly bound states, and conformation coupling shape GABA-evoked currents. *J Neurophysiol,* 89**,** 871-83.

MOZRZYMAS, J. W., ZARNOWSKA, E. D., PYTEL, M. & MERCIK, K. 2003b. Modulation of GABA(A) receptors by hydrogen ions reveals synaptic GABA transient and a crucial role of the desensitization process. *J Neurosci,* 23**,** 7981-92.

MUNJOMA, N., ISAAC, G., MUAZZAM, A., CEXUS, O., AZHAR, F., PANDHA, H., WHETTON, A. D., TOWNSEND, P. A., WILSON, I. D., GETHINGS, L. A. & PLUMB, R. S. 2022. High Throughput LC-MS Platform for Large Scale Screening of Bioactive Polar Lipids in Human Plasma and Serum. *J Proteome Res,* 21**,** 2596-2608.

NAKANE, T., KOTECHA, A., SENTE, A., MCMULLAN, G., MASIULIS, S., BROWN, P., GRIGORAS, I. T., MALINAUSKAITE, L., MALINAUSKAS, T., MIEHLING, J., UCHAŃSKI, T., YU, L., KARIA, D., PECHNIKOVA, E. V., DE JONG, E., KEIZER, J., BISCHOFF, M., MCCORMACK, J., TIEMEIJER, P., HARDWICK, S. W., CHIRGADZE, D. Y., MURSHUDOV, G., ARICESCU, A. R. & SCHERES, S. H. W. 2020. Single-particle cryo-EM at atomic resolution. *Nature,* 587**,** 152-156.

NOTHDURFTER, C., TANASIC, S., DI BENEDETTO, B., UHR, M., WAGNER, E. M., GILLING, K. E., PARSONS, C. G., REIN, T., HOLSBOER, F., RUPPRECHT, R. & RAMMES, G. 2013. Lipid raft integrity affects GABAA receptor, but not NMDA receptor modulation by psychopharmacological compounds. *Int J Neuropsychopharmacol,* 16**,** 1361-71.

NOVIELLO, C. M., GHARPURE, A., MUKHTASIMOVA, N., CABUCO, R., BAXTER, L., BOREK, D., SINE, S. M. & HIBBS, R. E. 2021. Structure and gating mechanism of the α7 nicotinic acetylcholine receptor. *Cell,* 184**,** 2121-2134.e13.

NUSSER, Z., SIEGHART, W. & SOMOGYI, P. 1998. Segregation of different GABAA receptors to synaptic and extrasynaptic membranes of cerebellar granule cells. *J Neurosci,* 18**,** 1693-703.

OLSEN, R. W. 2018. GABA(A) receptor: Positive and negative allosteric modulators. *Neuropharmacology,* 136**,** 10-22.

ORSER, B. A., MCADAM, L. C., RODER, S. & MACDONALD, J. F. 1998. General anaesthetics and their effects on GABA(A) receptor desensitization. *Toxicol Lett,* 100-101**,** 217-24.

PALPAGAMA, T. H., SAGNIEZ, M., KIM, S., WALDVOGEL, H. J., FAULL, R. L. & KWAKOWSKY, A. 2019. GABA(A) Receptors Are Well Preserved in the Hippocampus of Aged Mice. *eNeuro,* 6.

PAPADOPOULOS, T. & SOYKAN, T. 2011. The role of collybistin in gephyrin clustering at inhibitory synapses: facts and open questions. *Front Cell Neurosci,* 5**,** 11.

PHULERA, S., ZHU, H., YU, J., CLAXTON, D. P., YODER, N., YOSHIOKA, C. & GOUAUX, E. 2018. Cryo-EM structure of the benzodiazepine-sensitive α1β1γ2S tri-heteromeric GABAA receptor in complex with GABA. *eLife,* 7**,** e39383.

PITHADIA, A. B. & JAIN, S. M. 2009. 5-Hydroxytryptamine Receptor Subtypes and their Modulators with Therapeutic Potentials. *J Clin Med Res,* 1**,** 72-80.

POSTIS, V., RAWSON, S., MITCHELL, J. K., LEE, S. C., PARSLOW, R. A., DAFFORN, T. R., BALDWIN, S. A. & MUENCH, S. P. 2015. The use of SMALPs as a novel membrane protein scaffold for structure study by negative stain electron microscopy. *Biochim Biophys Acta,* 1848**,** 496-501.

PUNJANI, A., RUBINSTEIN, J. L., FLEET, D. J. & BRUBAKER, M. A. 2017. cryoSPARC: algorithms for rapid unsupervised cryo-EM structure determination. *Nature Methods,* 14**,** 290-296.

RAJENDRA, S., LYNCH, J. W., PIERCE, K. D., FRENCH, C. R., BARRY, P. H. & SCHOFIELD, P. R. 1995. Mutation of an arginine residue in the human glycine receptor transforms beta-alanine and taurine from agonists into competitive antagonists. *Neuron,* 14**,** 169-75.

RITCHIE, T. K., GRINKOVA, Y. V., BAYBURT, T. H., DENISOV, I. G., ZOLNERCIKS, J. K., ATKINS, W. M. & SLIGAR, S. G. 2009. Chapter 11 - Reconstitution of membrane proteins in phospholipid bilayer nanodiscs. *Methods Enzymol,* 464**,** 211-31.

ROGER, C. & LOUART, B. 2021. Beta-Lactams Toxicity in the Intensive Care Unit: An Underestimated Collateral Damage? *Microorganisms,* 9.

ROHOU, A. & GRIGORIEFF, N. 2015. CTFFIND4: Fast and accurate defocus estimation from electron micrographs. *J Struct Biol,* 192**,** 216-21.

RORSMAN, P., BERGGREN, P. O., BOKVIST, K., ERICSON, H., MÖHLER, H., OSTENSON, C. G. & SMITH, P. A. 1989. Glucose-inhibition of glucagon secretion involves activation of GABAA-receptor chloride channels. *Nature,* 341**,** 233-6.

ROSSOKHIN, A. V., SHARONOVA, I. N., BUKANOVA, J. V., KOLBAEV, S. N. & SKREBITSKY, V. G. 2014. Block of GABA(A) receptor ion channel by penicillin: electrophysiological and modeling insights toward the mechanism. *Mol Cell Neurosci,* 63**,** 72-82.

ROTSTEIN, N. P., ARIAS, H. R., BARRANTES, F. J. & AVELDAÑO, M. I. 1987. Composition of lipids in elasmobranch electric organ and acetylcholine receptor membranes. *J Neurochem,* 49**,** 1333-40.

RUDOLPH, U. & MÖHLER, H. 2004. Analysis of GABAA receptor function and dissection of the pharmacology of benzodiazepines and general anesthetics through mouse genetics. *Annu Rev Pharmacol Toxicol,* 44**,** 475-98.

RUSAKOV, D. A., SAVTCHENKO, L. P., ZHENG, K. & HENLEY, J. M. 2011. Shaping the synaptic signal: molecular mobility inside and outside the cleft. *Trends Neurosci,* 34**,** 359-69.

SAKIMOTO, Y., KIDA, H. & MITSUSHIMA, D. 2019. Temporal dynamics of learning-promoted synaptic diversity in CA1 pyramidal neurons. *Faseb j,* 33**,** 14382-14393.

SALARI, R., MURLIDARAN, S. & BRANNIGAN, G. 2014. Pentameric Ligand-gated Ion Channels : Insights from Computation. *Mol Simul,* 40**,** 821-829.

SENTE, A., DESAI, R., NAYDENOVA, K., MALINAUSKAS, T., JOUNAIDI, Y., MIEHLING, J., ZHOU, X., MASIULIS, S., HARDWICK, S. W., CHIRGADZE, D. Y., MILLER, K. W. & ARICESCU, A. R. 2022. Differential assembly diversifies GABAA receptor structures and signalling. *Nature,* 604**,** 190-194.

SIEGHART, W. 2006. Structure, pharmacology, and function of GABAA receptor subtypes. *Adv Pharmacol,* 54**,** 231-63.

SIEGHART, W. & SAVIĆ, M. M. 2018. International Union of Basic and Clinical Pharmacology. CVI: GABA(A) Receptor Subtype- and Function-selective Ligands: Key Issues in Translation to Humans. *Pharmacol Rev,* 70**,** 836-878.

SIGEL, E. & STEINMANN, M. E. 2012. Structure, function, and modulation of GABA(A) receptors. *J Biol Chem,* 287**,** 40224-31.

SIMONS, K. & TOOMRE, D. 2000. Lipid rafts and signal transduction. *Nat Rev Mol Cell Biol,* 1**,** 31-9.

SMART, O. S., NEDUVELIL, J. G., WANG, X., WALLACE, B. A. & SANSOM, M. S. 1996. HOLE: a program for the analysis of the pore dimensions of ion channel structural models. *J Mol Graph,* 14**,** 354-60, 376.

SMART, T. G. 1992. A novel modulatory binding site for zinc on the GABAA receptor complex in cultured rat neurones. *J Physiol,* 447**,** 587-625.

SOLTANI, N., QIU, H., ALEKSIC, M., GLINKA, Y., ZHAO, F., LIU, R., LI, Y., ZHANG, N., CHAKRABARTI, R., NG, T., JIN, T., ZHANG, H., LU, W. Y., FENG, Z. P., PRUD'HOMME, G. J. & WANG, Q. 2011. GABA exerts protective and regenerative effects on islet beta cells and reverses diabetes. *Proc Natl Acad Sci U S A,* 108**,** 11692-7.

SOOKSAWATE, T. & SIMMONDS, M. A. 2001. Influence of membrane cholesterol on modulation of the GABA(A) receptor by neuroactive steroids and other potentiators. *Br J Pharmacol,* 134**,** 1303-11.

SÜDHOF, T. C. 2018. Towards an Understanding of Synapse Formation. *Neuron,* 100**,** 276-293.

SUGIMOTO, M., FUKAMI, S., KAYAKIRI, H., YAMAZAKI, S., MATSUOKA, N., UCHIDA, I. & MASHIMO, T. 2002. The beta-lactam antibiotics, penicillin-G and cefoselis have different mechanisms and sites of action at GABA(A) receptors. *Br J Pharmacol,* 135**,** 427-32.

SUGIMOTO, M., UCHIDA, I., MASHIMO, T., YAMAZAKI, S., HATANO, K., IKEDA, F., MOCHIZUKI, Y., TERAI, T. & MATSUOKA, N. 2003. Evidence for the involvement of GABA(A) receptor blockade in convulsions induced by cephalosporins. *Neuropharmacology,* 45**,** 304-14.

SUH, B. C. & HILLE, B. 2008. PIP2 is a necessary cofactor for ion channel function: how and why? *Annu Rev Biophys,* 37**,** 175-95.

SUN, C., ZHU, H., CLARK, S. & GOUAUX, E. 2023. Cryo-EM structures reveal native GABAA receptor assemblies and pharmacology. *Nature,* 622**,** 195-201.

TANG, A. H., CHEN, H., LI, T. P., METZBOWER, S. R., MACGILLAVRY, H. D. & BLANPIED, T. A. 2016. A trans-synaptic nanocolumn aligns neurotransmitter release to receptors. *Nature,* 536**,** 210-4.

TEGUNOV, D. & CRAMER, P. 2019. Real-time cryo-electron microscopy data preprocessing with Warp. *Nature Methods,* 16**,** 1146-1152.

THOMPSON, S. A., WHITING, P. J. & WAFFORD, K. A. 1996. Barbiturate interactions at the human GABAA receptor: dependence on receptor subunit combination. *Br J Pharmacol,* 117**,** 521-527.

TWYMAN, R. E., GREEN, R. M. & MACDONALD, R. L. 1992. Kinetics of open channel block by penicillin of single GABAA receptor channels from mouse spinal cord neurones in culture. *J Physiol,* 445**,** 97-127.

TWYMAN, R. E., ROGERS, C. J. & MACDONALD, R. L. 1989. Differential regulation of gamma-aminobutyric acid receptor channels by diazepam and phenobarbital. *Ann Neurol,* 25**,** 213-20.

UCHAŃSKI, T., MASIULIS, S., FISCHER, B., KALICHUK, V., LÓPEZ-SÁNCHEZ, U., ZARKADAS, E., WECKENER, M., SENTE, A., WARD, P., WOHLKÖNIG, A., ZÖGG, T., REMAUT, H., NAISMITH, J. H., NURY, H., VRANKEN, W., ARICESCU, A. R., PARDON, E. & STEYAERT, J. 2021. Megabodies expand the nanobody toolkit for protein structure determination by single-particle cryo-EM. *Nat Methods,* 18**,** 60-68.

UNWIN, N. 1993. Nicotinic acetylcholine receptor at 9 A resolution. *J Mol Biol,* 229**,** 1101-24.

UNWIN, N. 1995. Acetylcholine receptor channel imaged in the open state. *Nature,* 373**,** 37-43.

UNWIN, N. 1996. Projection structure of the nicotinic acetylcholine receptor: distinct conformations of the alpha subunits. *J Mol Biol,* 257**,** 586-96.

UNWIN, N. 2005. Refined structure of the nicotinic acetylcholine receptor at 4A resolution. *J Mol Biol,* 346**,** 967-89.

UNWIN, N. 2022. Structure of a cholinergic cell membrane. *Proc Natl Acad Sci U S A,* 119**,** e2207641119.

UNWIN, N. & FUJIYOSHI, Y. 2012. Gating movement of acetylcholine receptor caught by plunge-freezing. *J Mol Biol,* 422**,** 617-634.

VELISETTY, P. & CHAKRAPANI, S. 2012. Desensitization mechanism in prokaryotic ligand-gated ion channel. *J Biol Chem,* 287**,** 18467-77.

WALKER, A. E., JOHNSON, H. C. & KOLLROS, J. J. 1945. Penicillin convulsions; the convulsive effects of penicillin applied to the cerebral cortex of monkey and man. *Surg Gynecol Obstet,* 81**,** 692-701.

WIELAND, H. A., LÜDDENS, H. & SEEBURG, P. H. 1992. A single histidine in GABAA receptors is essential for benzodiazepine agonist binding. *J Biol Chem,* 267**,** 1426-9.

WISDEN, W., LAURIE, D. J., MONYER, H. & SEEBURG, P. H. 1992. The distribution of 13 GABAA receptor subunit mRNAs in the rat brain. I. Telencephalon, diencephalon, mesencephalon. *J Neurosci,* 12**,** 1040-62.

WOLSTENHOLME, A. J. 2012. Glutamate-gated chloride channels. *J Biol Chem,* 287**,** 40232-8.

XU, E., KUMAR, M., ZHANG, Y., JU, W., OBATA, T., ZHANG, N., LIU, S., WENDT, A., DENG, S., EBINA, Y., WHEELER, M. B., BRAUN, M. & WANG, Q. 2006. Intra-islet insulin suppresses glucagon release via GABA-GABAA receptor system. *Cell Metab,* 3**,** 47-58.

YAMASAKI, T., HOYOS-RAMIREZ, E., MARTENSON, J. S., MORIMOTO-TOMITA, M. & TOMITA, S. 2017. GARLH Family Proteins Stabilize GABA(A) Receptors at Synapses. *Neuron,* 93**,** 1138-1152.e6.

YANG, J. & UCHIDA, I. 1996. Mechanisms of etomidate potentiation of GABAA receptor-gated currents in cultured postnatal hippocampal neurons. *Neuroscience,* 73**,** 69-78.

YU, J., ZHU, H., LAPE, R., GREINER, T., DU, J., LÜ, W., SIVILOTTI, L. & GOUAUX, E. 2021. Mechanism of gating and partial agonist action in the glycine receptor. *Cell,* 184**,** 957-968.e21.

ZHANG, B., VOGELZANG, A., MIYAJIMA, M., SUGIURA, Y., WU, Y., CHAMOTO, K., NAKANO, R., HATAE, R., MENZIES, R. J., SONOMURA, K., HOJO, N., OGAWA, T., KOBAYASHI, W., TSUTSUI, Y., YAMAMOTO, S., MARUYA, M., NARUSHIMA, S., SUZUKI, K., SUGIYA, H., MURAKAMI, K., HASHIMOTO, M., UENO, H., KOBAYASHI, T., ITO, K., HIRANO, T., SHIROGUCHI, K., MATSUDA, F., SUEMATSU, M., HONJO, T. & FAGARASAN, S. 2021a. B cell-derived GABA elicits IL-10+ macrophages to limit anti-tumour immunity. *Nature,* 599**,** 471-476.

ZHANG, C., ATASOY, D., ARAÇ, D., YANG, X., FUCILLO, M. V., ROBISON, A. J., KO, J., BRUNGER, A. T. & SÜDHOF, T. C. 2010. Neurexins physically and functionally interact with GABA(A) receptors. *Neuron,* 66**,** 403-16.

ZHANG, Y., DIJKMAN, P. M., ZOU, R., ZANDL-LANG, M., SANCHEZ, R. M., ECKHARDT-STRELAU, L., KÖFELER, H., VOGEL, H., YUAN, S. & KUDRYASHEV, M. 2021b. Asymmetric opening of the homopentameric 5-HT(3A) serotonin receptor in lipid bilayers. *Nat Commun,* 12**,** 1074.

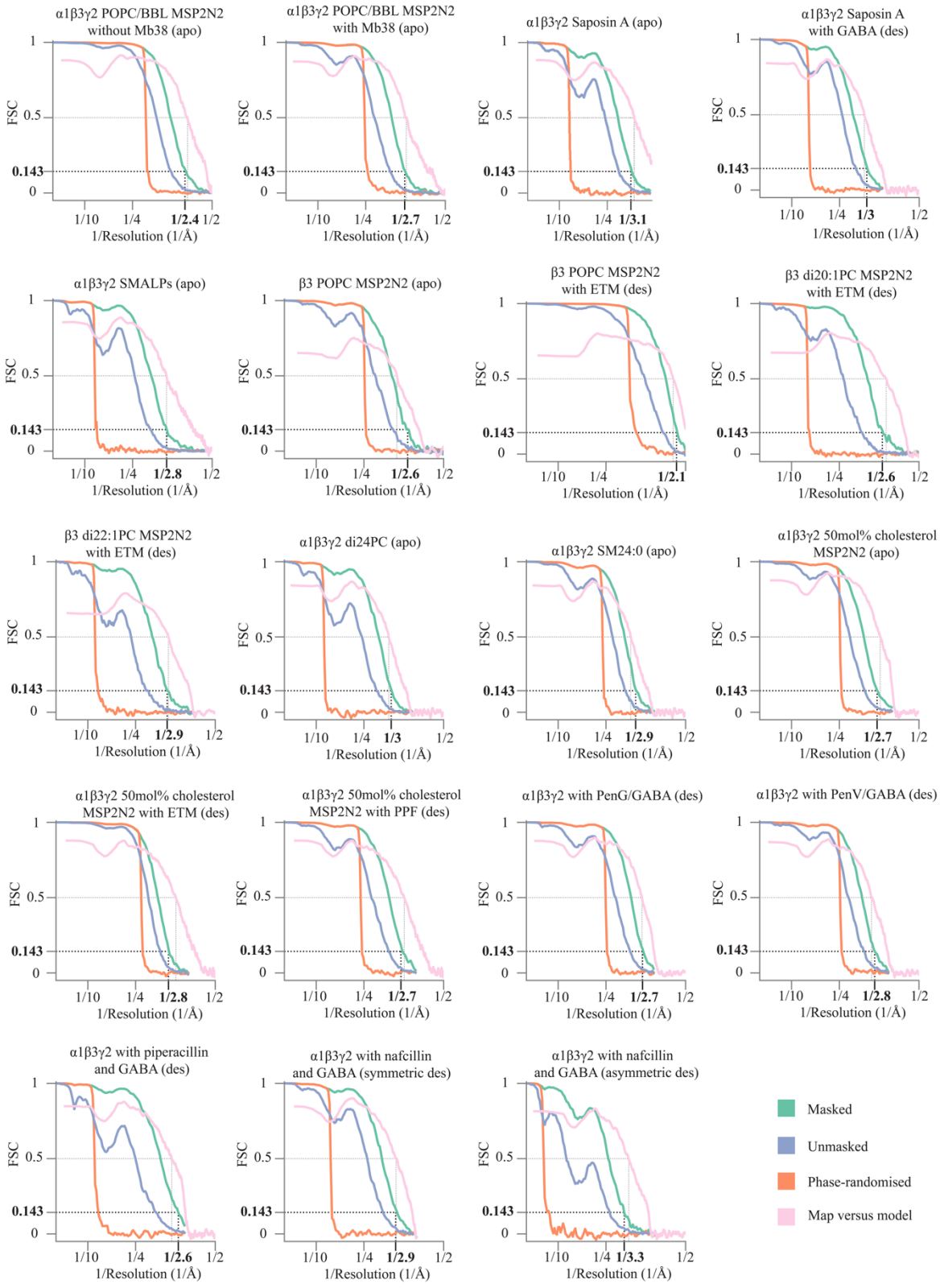
ZHENG, S. Q., PALOVCAK, E., ARMACHE, J. P., VERBA, K. A., CHENG, Y. & AGARD, D. A. 2017. MotionCor2: anisotropic correction of beam-induced motion for improved cryo-electron microscopy. *Nat Methods,* 14**,** 331-332.

ZHU, S., NOVIELLO, C. M., TENG, J., WALSH, R. M., JR., KIM, J. J. & HIBBS, R. E. 2018. Structure of a human synaptic GABA(A) receptor. *Nature,* 559**,** 67-72.

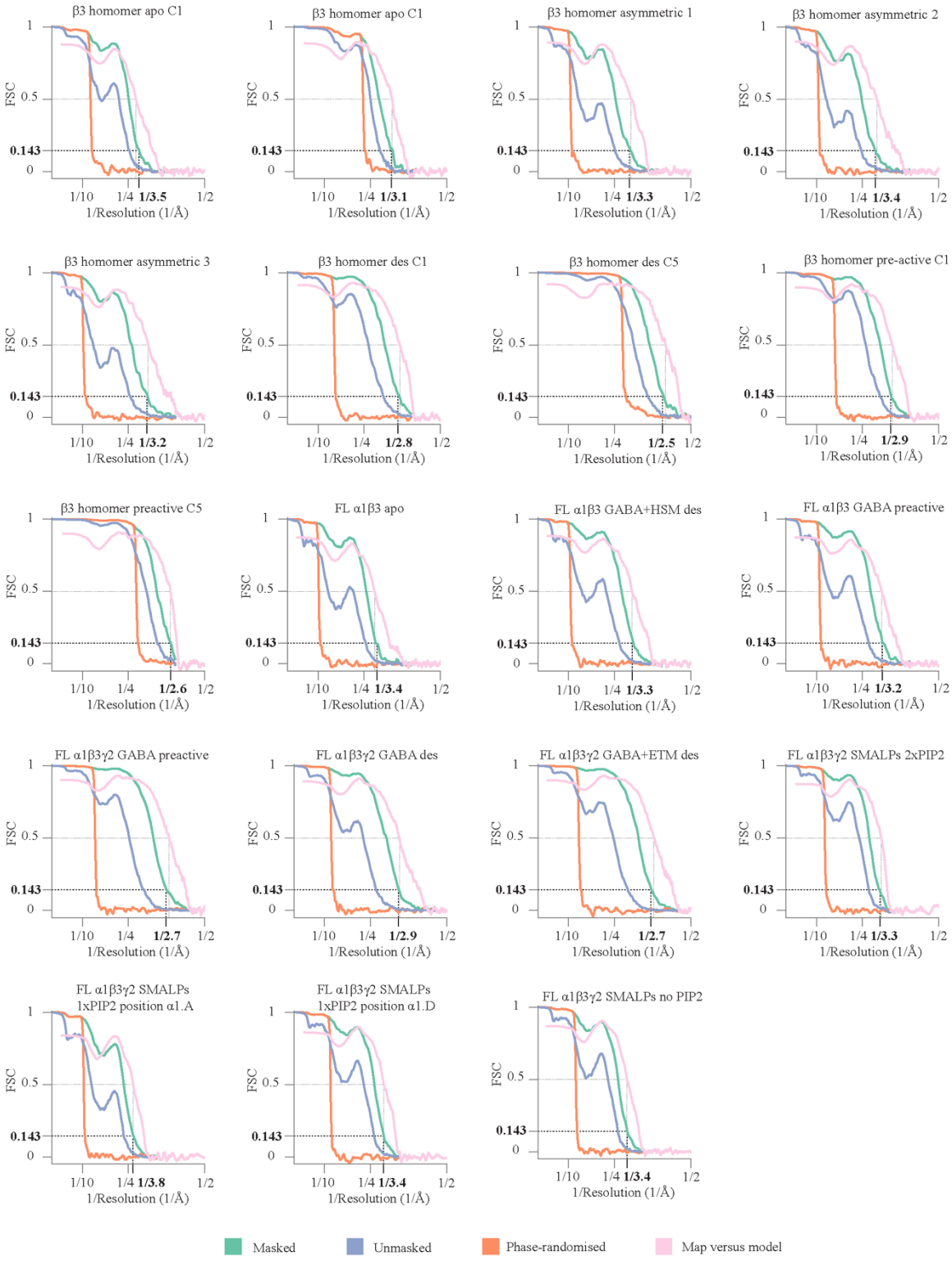
ZIDOVETZKI, R. & LEVITAN, I. 2007. Use of cyclodextrins to manipulate plasma membrane cholesterol content: evidence, misconceptions and control strategies. *Biochim Biophys Acta,* 1768**,** 1311-24.

ZIMMERMANN, I. & DUTZLER, R. 2011. Ligand activation of the prokaryotic pentameric ligand-gated ion channel ELIC. *PLoS Biol,* 9**,** e1001101.

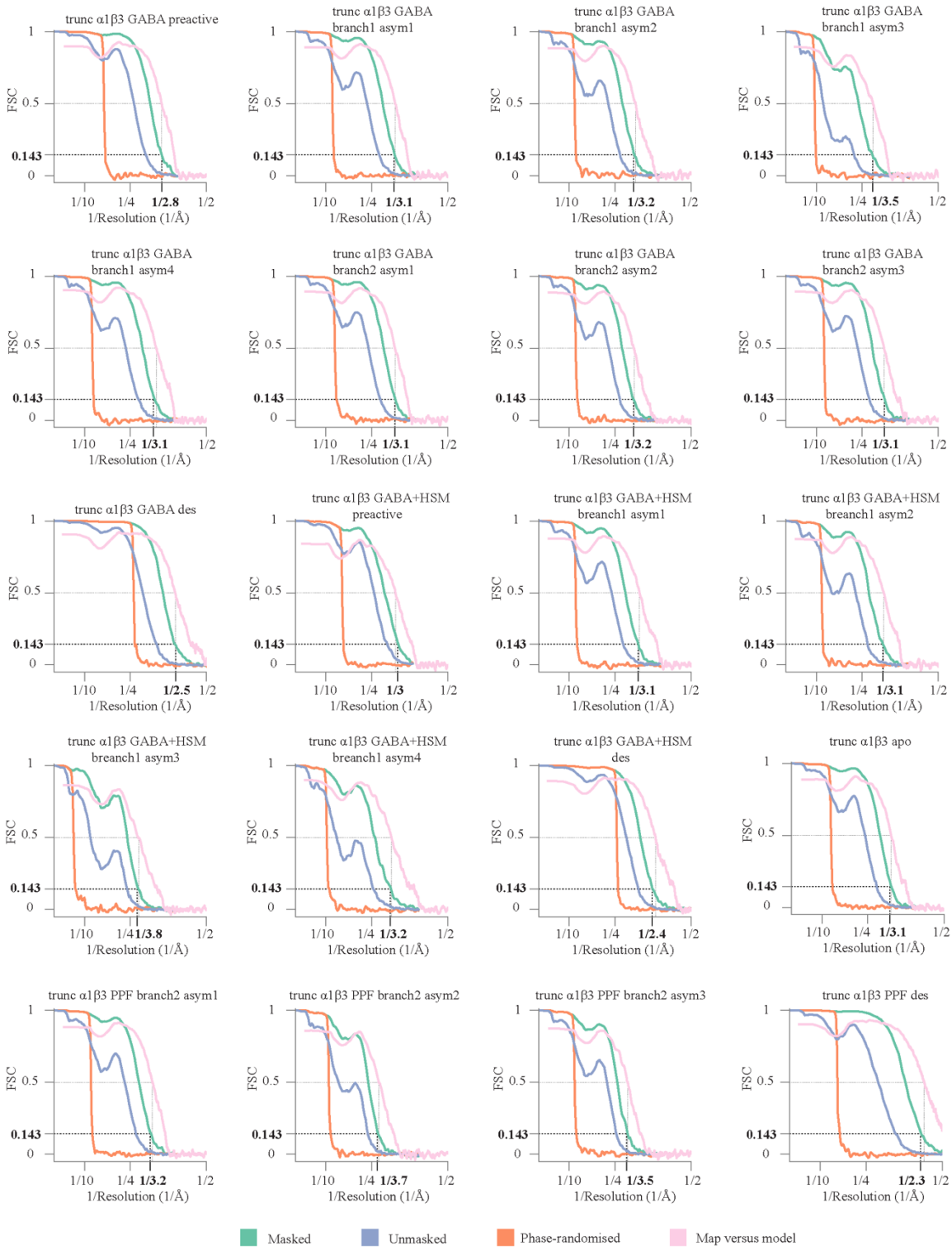
Appendix



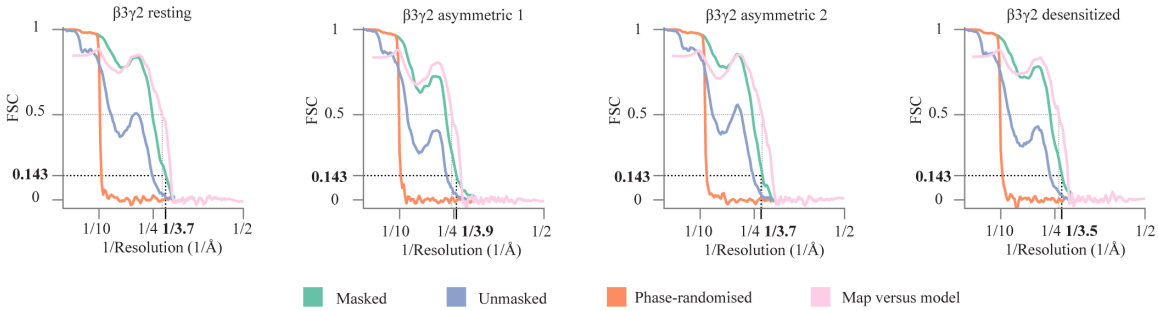
Appendix Figure 1 – FSC plots for structures discussed in Chapter III and IV. The plots were generated with a script written by Dr. Katerina Naydenova, MRC LMB



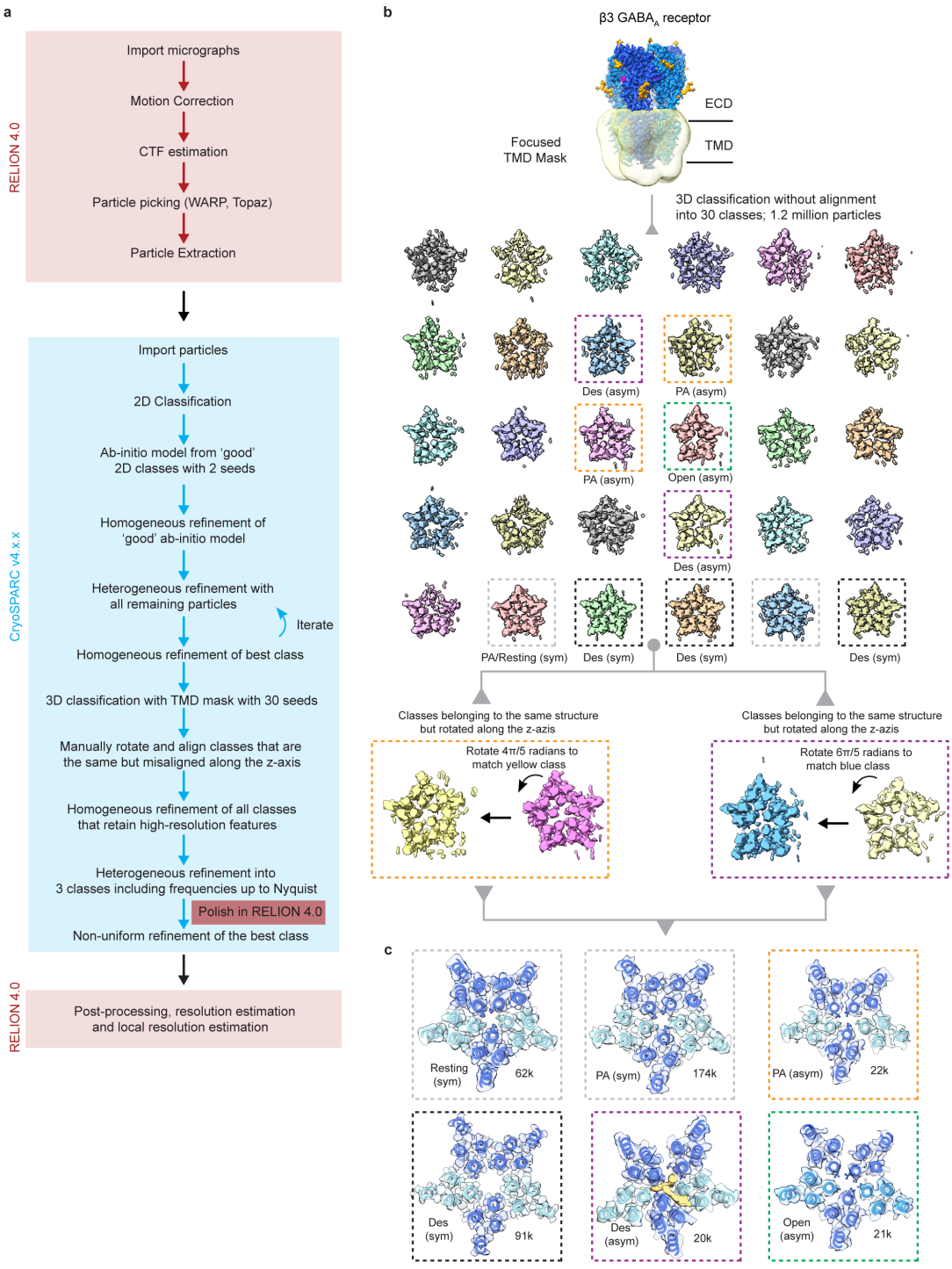
Appendix Figure 2 – FSC plots for structures discussed in Chapter V.



Appendix Figure 2 continued – FSC plots for structures discussed in Chapter V.

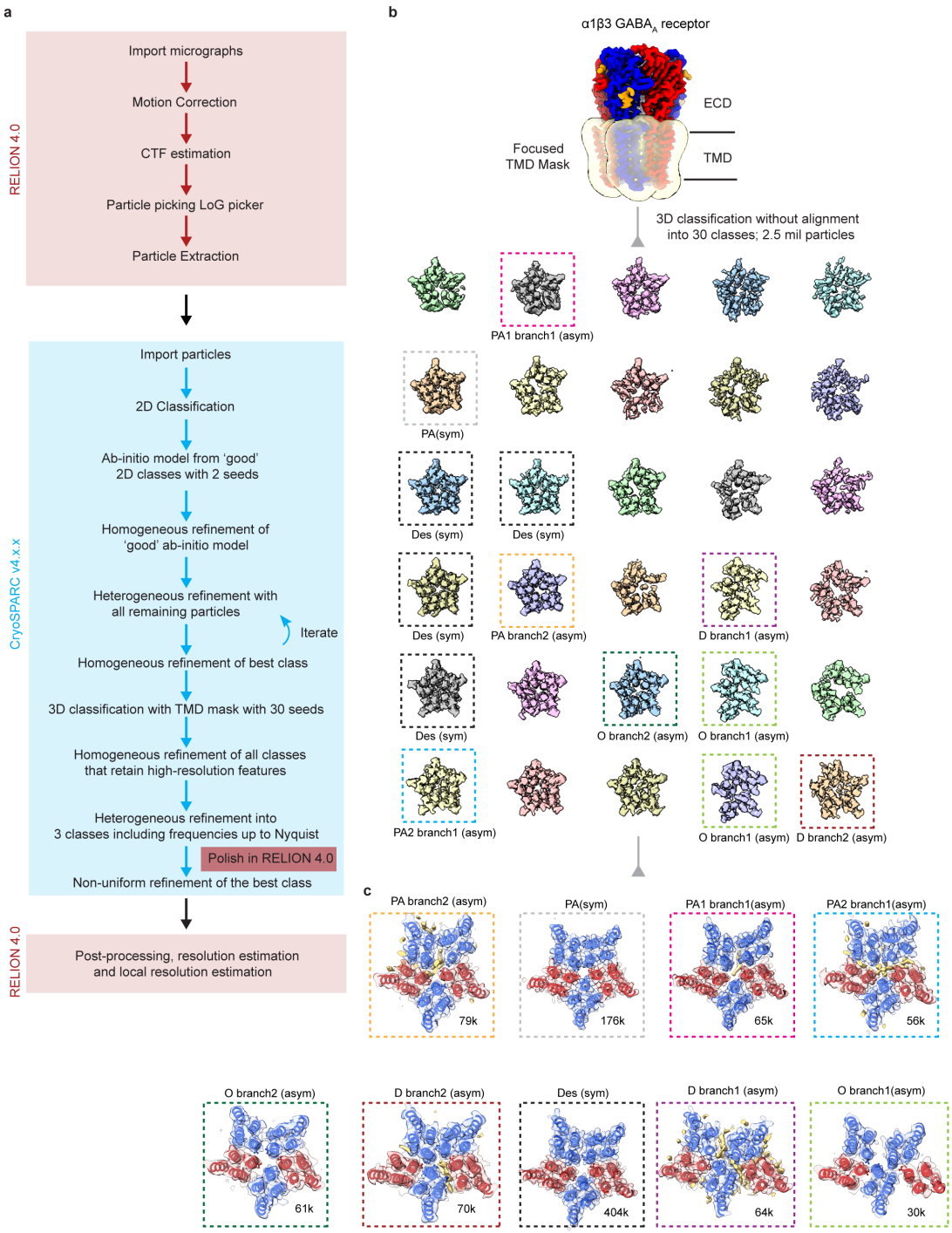


Appendix Figure 2 continued – FSC plots for structures discussed in Chapter V.



Appendix Figure 3 – Processing strategy for the β3 homomer sprayed dataset

a) *The detailed processing pipeline used for the β3 homomer.* ***b)*** *A soft TMD mask was used to classify the multiple states. In total 30 seeds were used. Classes with well-defined high-resolution features i.e. clear helical pitch were subjected to further refinement. Classes which are the same but rotated along the z-axis were manually aligned.* ***c)*** *Cross-sections at the level of the 9' activation gate for the final maps including the number of particles in the final reconstruction.*



Appendix Figure 4 – Processing strategy for the α1β3 homomer sprayed dataset

a) *The detailed processing pipeline used for the α1β3 diheteromer.* ***b)*** *A soft TMD mask was used to classify the multiple states. In total 30 seeds were used. Classes with well-defined high-resolution features i.e. clear helical pitch were subjected to further refinement.* ***c)*** *Cross-sections at the level of the 9' activation gate for the final maps including the number of particles in the final reconstruction.*

Constructs

1. Full length α1 $GABA_A$ receptor subunit FLAG tag

MKKSPGLSDYLWAWTLFLSTLTGRSYGDYKDDDDKQPSLQDELKDNTTVFTRIL
DRLLDGYDNRLRPGLGERVTEVKTDIFVTSFGPVSDHDMEYTIDVFFRQSWKDER
LKFKGPMTVLRLNNLMASKIWTPDTFFHNGKKSVAHNMTMPNKLLRITEDGTLL
YTMRLTVRAECPMHLEDFPMDAHACPLKFGSYAYTRAEVVYEWTREPARSVVV
AEDGSRLNQYDLLGQTVDSGIVQSSTGEYVVMTTHFHLKRKIGYFVIQTYLPCIMT
VILSQVSFWLNRESVPARTVFGVTTVLTMTTLSISARNSLPKVAYATAMDWFIAV
CYAFVFSALIEFATVNYFTKRGYAWDGKSVVPEKPKKVKDPLIKKNNTYAPTATS
YTPNLARGDPGLATIAKSATIEPKEVKPETKPPEPKKTFNSVSKIDRLSRIAFPLLFGI
FNLVYWATYLNREPQLKAPTPHQ

2. Full length β3 $GABA_A$ receptor subunit without tag

MCSGLLELLLPIWLSWTLGTRGSEPRSVNDPGNMSFVKETVDKLLKGYDIRLRPD
FGGPPVCVGMNIDIASIDMVSEVNMDYTLTMYFQQYWRDKRLAYSGIPLNLTLD
NRVADQLWVPDTYFLNDKKSFVHGVTVKNRMIRLHPDGTVLYGLRITTTAACM
MDLRRYPLDEQNCTLEIESYGYTTDDIEFYWRGGDKAVTGVERIELPQFSIVEHRL
VSRNVVFATGAYPRLSLSFRLKRNIGYFILQTYMPSILITILSWVSFWINYDASAAR
VALGITTVLTMTTINTHLRETLPKIPYVKAIDMYLMGCFVFVFLALLEYAFVNYIFF
GRGPQRQKKLAEKTAKAKNDRSKSESNRVDAHGNILLTSLEVHNEMNEVSGGIG
DTRNSAISFDNSGIQYRKQSMPREGHGRFLGDRSLPHKKTHLRRRSSQLKIKIPDLT
DVNAIDRWSRIVFPFTFSLFNLVYWLYYVN

3. Full length β3 $GABA_A$ receptor subunit with TwinStrep tag

MGILPSPGMPALLSLVSLLSVLLMGCVAEYPYDVPDYAGGSGGSGGSAWSHPQFE
KGGGSGGGSGGSAWSHPQFEKGGSTGQSVNDPGNMSFVKETVDKLLKGYDIRLR
PDFGGPPVCVGMNIDIASIDMVSEVNMDYTLTMYFQQYWRDKRLAYSGIPLNLTL
DNRVADQLWVPDTYFLNDKKSFVHGVTVKNRMIRLHPDGTVLYGLRITTTAACM
MDLRRYPLDEQNCTLEIESYGYTTDDIEFYWRGGDKAVTGVERIELPQFSIVEHRL
VSRNVVFATGAYPRLSLSFRLKRNIGYFILQTYMPSILITILSWVSFWINYDASAAR
VALGITTVLTMTTINTHLRETLPKIPYVKAIDMYLMGCFVFVFLALLEYAFVNYIFF
GRGPQRQKKLAEKTAKAKNDRSKSESNRVDAHGNILLTSLEVHNEMNEVSGGIG

DTRNSAISFDNSGIQYRKQSMPREGHGRFLGDRSLPHKKTHLRRRSSQLKIKIPDLT
DVNAIDRWSRIVFPFTFSLFNLVYWLYYVN

4. Full length γ2L $GABA_A$ receptor subunit 1D4 tag

MSSPNIWSTGSSVYSTPVFSQKMTVWILLLLSLYPGFTSQKSDDDYEDYASNKTW
VLTPKVPEGDVTVILNNLLEGYDNKLRPDIGVKPTLIHTDMYVNSIGPVNAINMEY
TIDIFFAQTWYDRRLKFNSTIKVLRLNSNMVGKIWIPDTFFRNSKKADAHWITTPN
RMLRIWNDGRVLYTLRLTIDAECQLQLHNFPMDEHSCPLEFSSYGYPREEIVYQW
KRSSVEVGDTRSWRLYQFSFVGLRNTTEVVKTTSGDYVVMSVYFDLSRRMGYFTI
QTYIPCTLIVVLSWVSFWINKDAVPARTSLGITTVLTMTTLSTIARKSLPKVSYVTA
MDLFVSVCFIFVFSALVEYGTLHYFVSNRKPSKDKDKKKKNPLLRMFSFKAPTIDI
RPRSATIQMNNATHLQERDEEYGYECLDGKDCASFFCCFEDCRTGAWRHGRIHIRI
AKMDSYARIFFPTAFCLFNLVYWVSYLYLGGSGGSGGSGKTETSQVAPA

5. Megabody 38

QVQLQESGGGLVQTKTTTSVIDTTNDAQNLLTQAQTIVNTLKDYCPILIAKSSSSN
GGTNNANTPSWQTAGGGKNSCATFGAEFSAASDMINNAQKIVQETQQLSANQPK
NITQPHNLNLNSPSSLTALAQKMLKNAQSQAEILKLANQVESDFNKLSSGHLKDYI
GKCDASAISSANMTMQNQKNNWGNGCAGVEETQSLLKTSAADFNNQTPQINQA
QNLANTLIQELGNNPFRASGGGSGGGGSGKLSDTYEQLSRLLTNDNGTNSKTSAQ
AINQAVNNLNERAKTLAGGTTNSPAYQATLLALRSVLGLWNSMGYAVICGGYTK
SPGENNQKDFHYTDENGNGTTINCGGSTNSNGTHSYNGTNTLKADKNVSLSIEQY
EKIHEAYQILSKALKQAGLAPLNSKGEKLEAHVTTSKYGSLRVSCAASGRTFTTYI
MAWFRQAPGKEREFLAAMDQGRIQYYGDSVRGRFTISRDYAKNSVDLQLDGLRP
EDTAVYYCAAGAGFWGLRTASSYHYWGQGTQVTVSSHHHHHHEPEA

6. Truncated α1 $GABA_A$ receptor subunit 1D4 tag

MGILPSPGMPALLSLVSLLSVLLMGCVAETGHASQDELKDNTTVFTRILDRLLDGY
DNRLRPGLGERVTEVKTDIFVTSFGPVSDHDMEYTIDVFFRQSWKDERLKFKGPM
TVLRLNNLMASKIWTPDTFFHNGKKSVAHNMTMPNKLLRITEDGTLLYTMRLTV
RAECPMHLEDFPMDAHACPLKFGSYAYTRAEVVYEWTREPARSVVVAEDGSRLN
QYDLLGQTVDSGIVQSSTGEYVVMTTHFHLKRKIGYFVIQTYLPCIMTVILSQVSF
WLNRESVPARTVFGVTTVLTMTTLSISARNSLPKVAYATAMDWFIAVCYAFVFSA

LIEFATVNYFTKSQPARAAKIDRLSRIAFPLLFGIFNLVYWATYLNREPQLKAPTPH
QGTTETSTQVAPA

7. Truncated α1 $GABA_A$ receptor subunit SBP tag

MGILPSPGMPALLSLVSLLSVLLMGCVAEMDEKTTGWRGGHVVEGLAGELEQLR
ARLEHHPQGQREPDYDIPTTENLYFQGTGQPSQDELKDNTTVFTRILDRLLDGYDN
RLRPGLGERVTEVKTDIFVTSFGPVSDHDMEYTIDVFFRQSWKDERLKFKGPMTV
LRLNNLMASKIWTPDTFFHNGKKSVAHNMTMPNKLLRITEDGTLLYTMRLTVRA
ECPMHLEDFPMDAHACPLKFGSYAYTRAEVVYEWTREPARSVVVAEDGSRLNQY
DLLGQTVDSGIVQSSTGEYVVMTTHFHLKRKIGYFVIQTYLPCIMTVILSQVSFWL
NRESVPARTVFGVTTVLTMTTLSISARNSLPKVAYATAMDWFIAVCYAFVFSALIE
FATVNYFTKSQPARAAKIDRLSRIAFPLLFGIFNLVYWATYLNREPQLKAPTPHQ

8. Truncated β3 $GABA_A$ receptor subunit SPB tag

MGILPSPGMPALLSLVSLLSVLLMGCVAEMDEKTTGWRGGHVVEGLAGELEQLR
ARLEHHPQGQREPDYDIPTTENLYFQGTGQSVNDPGNMSFVKETVDKLLKGYDIR
LRPDFGGPPVCVGMNIDIASIDMVSEVNMDYTLTMYFQQYWRDKRLAYSGIPLNL
TLDNRVADQLWVPDTYFLNDKKSFVHGVTVKNRMIRLHPDGTVLYGLRITTTAA
CMMDLRRYPLDEQNCTLEIESYGYTTDDIEFYWRGGDKAVTGVERIELPQFSIVEH
RLVSRNVVFATGAYPRLSLSFRLKRNIGYFILQTYMPSILITILSWVSFWINYDASA
ARVALGITTVLTMTTINTHLRETLPKIPYVKAIDMYLMGCFVFVFLALLEYAFVNY
IFFSQPARAAAIDRWSRIVFPFTFSLFNLVYWLYYVN

9. Truncated γ2L $GABA_A$ receptor subunit 1D4 tag

MGILPSPGMPALLSLVSLLSVLLMGCVAETGQKSDDDYEDYTSNKTWVLTPKVPE
GDVTVILNNLLEGYDNKLRPDIGVKPTLIHTDMYVNSIGPVNAINMEYTIDIFFAQT
WYDRRLKFNSTIKVLRLNSNMVGKIWIPDTFFRNSKKADAHWITTPNRMLRIWND
GRVLYTLRLTIDAECQLQLHNFPMDEHSCPLEFSSYGYPREEIVYQWKRSSVEVGD
TRSWRLYQFSFVGLRNTTEVVKTTSGDYVVMSVYFDLSRRMGYFTIQTYIPCTLIV
VLSWVSFWINKDAVPARTSLGITTVLTMTTLSTIARKSLPKVSYVTAMDLFVSVCF
IFVFSALVEYGTLHYFVSSQPARAAKMDSYARIFFPTAFCLFNLVYWVSYLYLGTG
GTTETSQVAPA

10. Megabody 25

QVQLVESGGGLVQTKTTTSVIDTTNDAQNLLTQAQTIVNTLKDYCPILIAKSSSSN
GGTNNANTPSWQTAGGGKNSCATFGAEFSAASDMINNAQKIVQETQQLSANQPK
NITQPHNLNLNSPSSLTALAQKMLKNAQSQAEILKLANQVESDFNKLSSGHLKDYI
GKCDASAISSANMTMQNQKNNWGNGCAGVEETQSLLKTSAADFNNQTPQINQA
QNLANTLIQELGNNTYEQLSRLLTNDNGTNSKTSAQAINQAVNNLNERAKTLAGG
TTNSPAYQATLLALRSVLGLWNSMGYAVICGGYTKSPGENNQKDFHYTDENGNG
TTINCGGSTNSNGTHSYNGTNTLKADKNVSLSIEQYEKIHEAYQILSKALKQAGLA
PLNSKGEKLEAHVTTSKYGSLRLSCAASGHTFNYPIMGWFRQAPGKEREFVGAIS
WSGGSTSYADSVKDRFTISRDNAKNTVYLEMNNLKPEDTAVYYCAAKGRYSGGL
YYPTNYDYWGQGTQVTVSSHHHHHHEPEA